THE STRUCTURAL PROTEOMICS OF S-NITROSYLATION: FROM GLOBAL IDENTIFICATION TO ELUCIDATING PROTEIN FUNCTION THROUGH STRUCTURAL BIOINFORMATICS

Jennifer L. Greene

A DISSERTATION

in

Biochemistry and Molecular Biophysics

Presented to the Faculties of the University of Pennsylvania

in Partial Fulfillment of the Requirements for the

Degree of Doctor of Philosophy

2011

_____

Supervisor of Dissertation: Harry Ischiropoulos, Ph.D., Research Professor of Pediatrics and Pharmacology

_____

Graduate Group Chairperson: Kathryn M. Ferguson, Ph.D., Associate Professor, Physiology

Dissertation Committee

Doron C. Greenbaum, Ph.D., Assistant Professor, Department of Pharmacology
Cecilia Tommos, Ph.D., Assistant Professor, Department of Biochemistry and Biophysics
Roland L. Dunbrack, Jr, Ph.D., Adjunct Associate Professor, Department of Biochemistry and Biophysics
Ian A. Blair, Ph.D., Professor, Department of Pharmacology
Gideon Dreyfuss, Ph.D., Professor, Department of Biochemistry and Biophysics
Andrew Gow, Ph.D., Associate Professor, Department of Pharmacology and Toxicology

THE STRUCTURAL PROTEOMICS OF S-NITROSYLATION: FROM GLOBAL IDENTIFICATION TO ELUCIDATING PROTEIN FUNCTION THROUGH STRUCTURAL BIOINFORMATICS

COPYRIGHT

"I was leaving the South to fling myself into the unknown. I was taking a part of the South to transplant in alien soil, to see if it could grow differently, if it could drink of new and cool rains, bend in strange winds, respond to the warmth of other suns, and, perhaps, to bloom."

-Richard Wright

To my grandparents, Flenard and Jessie, who planted the seed
and my mother, Melvelyn, who relentlessly nurtured it.

ACKNOWLEDGMENTS

I would first like to thank the entire Ischiropoulos Laboratory. I joined this lab at a time when I was unsure about my own future in science. The collaborative spirit and good nature of everyone in the lab, past and present, helped bring my scientific dreams back to life. I would like to thank my advisor, Dr. Harry Ischiropoulos, for his constant support and encouragement. Under his tutelage, I have become a far better scientist than I could have imagined. I would like to thank Richard Lightfoot, Drs. Margarita Tenopoulou and Paschalis-Thomas Doulias. Karthik Raju, Kristen Malkus, Marissa Martinez, and past members: Drs. Elpida Tsika, Todd Greco, and Christie Bruno. I would also like to thank the members of the Vanderkooi laboratory for being my lab home for my first 3 years here at Penn. I would like to thank the members of my committee for their advice and support. I'd also like to thank my friends and family, especially my mother Mel, my sister Nikoia, and my brother Bernard. And lastly, I'd like to thank my fiancé, Ebenezer. Without your love, I don't think I would have made it.

Sola fide

ABSTRACT

THE STRUCTURAL PROTEOMICS OF S-NITROSYLATION: FROM GLOBAL IDENTIFICATION TO ELUCIDATING PROTEIN FUNCTION THROUGH STRUCTURAL BIOINFORMATICS

Jennifer L. Greene

Harry Ischiropoulos, Ph.D.

S-nitrosylation is the covalent addition of nitric oxide to reduced cysteine residues on proteins. It has been well documented that not all proteins are S-nitrosylated and more specifically, not all cysteine residues within an S-nitrosylated protein are modified. Therefore, it is very important to determine how this specificity is derived. Additionally, the mechanism by which nitric oxide can modify cysteines is still unclear. Even with the discovery of functional consequences of S-nitrosylation, there are still large deficits in our understanding and validation that it is a newly identified means of nitric oxide signaling within the body.

These gaps in knowledge primarily exist due to a lack of tools necessary for identifying *in vivo* sites of S-nitrosylation. To this end, complementary mercury-based mass spectrometric approaches were developed for the identification of endogenous S-nitrosoproteomes. This resulted in the identification of 328 SNO-cysteines coordinated to 192 proteins in the mouse liver, 97% of which corresponded to novel targets of S-nitrosylation. Bioinformatic analysis of these targets then revealed that multiple mechanisms of S-nitrosylation may occur *in vivo*, one of which involving S-

nitrosoglutathione (GSNO). To test this hypothesis, the SNO-proteome of mice incapable of metabolizing GSNO was resolved. Quantum mechanics/molecular mechanics calculations coupled with molecular dynamics simulations proposed a novel GSNO-mediated mechanism of transnitrosation. Basic residues in the surrounding cysteine microenvironment were shown to catalyze the formation of protein S-nitrosocysteine residues. Collectively, these data suggest that the specificity of cysteines targeted for S-nitrosylation is driven by the surrounding protein microenvironment.

Additionally, with only 9 structures of S-nitrosylated proteins our present understanding of the structural consequences of S-nitrosylation is limited. Using an in vivo model, attempts were made to correlate changes in enzymatic activity as a function of S-nitrosylation. Normal mode analysis revealed local motions near the site of S-nitrosylation which may alter product release. In summary, this thesis utilized a global proteomic approach to craft a more targeted investigation into the specificity and molecular mechanism of S-nitrosylation.

TABLE OF CONTENTS

LIST OF TABLES

CHAPTER TWO

CHAPTER THREE

CHAPTER FOUR

LIST OF FIGURES

CHAPTER TWO

CHAPTER THREE

CHAPTER FOUR

CHAPTER ONE

1.1 Introduction

Nitric oxide (•NO) received the distinction of a signaling molecule in physiology when Furchgott, Ignarro, and Murad were awarded the 1998 Nobel Prize in Medicine & Physiology for their combined efforts in elucidating the role of •NO in vasodilation. It was concluded that •NO produced by endothelial cells can bind to the heme iron of soluble guanylate cyclase (sGC) thereby converting GTP to cGMP and resulting in a cascade of events leading to smooth muscle relaxation. Because it is well known that •NO can react with many intracellular targets, the mechanism by which •NO selectively reacted with sGC became of significance. Stamler et al. hypothesized that •NO could also propagate its signal by forming stable adducts with protein thiols that would then deliver nitric oxide to a specific target (Stamler et al. 1992). This study resulted in the first observation that nitric oxide could react with cysteine residues in proteins to form protein S-nitrosocysteine.

Over the past 2 decades, hundreds of proteins have been identified as being S-nitrosylated. S-nitrosylation is defined as the covalent addition of nitric oxide to selective protein cysteine residues that can regulate protein activity across a variety of organs and cellular systems. Their cellular functions have ranged from oxidoreductases to ion channels to histone deacetylases, suggesting that S-nitrosylation appears to be a widespread biological mechanism of nitric oxide signaling. Nevertheless, fundamental questions regarding this emerging posttranslational modification (PTM) still remain unanswered. It is difficult to convince the scientific community that upon generation of

this small highly reactive molecule, •NO selectively modifies a specific cysteine residue. The mechanism by which •NO can modify cysteines is still unclear. For other more characterized PTMs such as acetylation (which is of comparable relative size to •NO), specific enzymes are necessary to catalyze its reaction with its target protein. Therefore, with the unequivocal identification of such enzyme(s) for S-nitrosylation, it is difficult to ascertain how specificity is achieved. Answers to these pressing questions will expand our understanding of S-nitrosylation and offer insight as to how to better regulate this emerging posttranslational modification.

1.2 Nitric oxide

1.2.1 Chemical properties of nitric oxide

Nitric oxide (also known as nitrogen monoxide) is a colorless, diatomic gas composed of one nitrogen atom and one oxygen atom. It was first described as "nitrous air" in 1774 by Joseph Priestley in his book titled *Experiments and Observations on Different Kinds of Air, Vol. 1*. An uncharged free radical, nitric oxide has one unpaired electron. With an oil/water partition coefficient ~6.5 (K_{ow} measured at 37°C) and a low solubility in water, •NO is capable of easily diffusing through hydrophobic environments such as cell membranes (Balbatum et al. 2003). In aqueous solutions, nitric oxide reacts primarily with oxygen and its half-life is proportional to its concentration.

The half-life of •NO can be altered by its interactions with different targets. Nitric oxide can react with a wide range of molecules to form end products with various functions. Upon its reaction with molecular oxygen (O_2), nitric oxide is oxidized to form relative stable metabolites nitrite (NO_2^-) and nitrate (NO_3^-). Nitric oxide can also react

with free radicals such as superoxide ($O_2^{-\bullet}$) to generate the strong oxidant peroxynitrite ($ONOO^-$). This reaction has been observed to be near diffusion limited suggesting that it is only restricted by the ability of the molecules to come into contact with one another (Beckman et al. 1990; Koppenol, et al. 2001). The interaction of nitric oxide with lipid-derived radicals has also been characterized as being a diffusion-limited reaction (O'Donnell et al. 1997). $^{\bullet}$NO has been most classically described by its coordination to transition metals such as copper or iron to form M-NO (Wink et al. 1994; Wade & Castro 1990).

In general, the chemical reactivity of $^{\bullet}$NO is contingent upon its surrounding environment. Therefore, when attempting to understand the role of nitric oxide in biological processes, it is important to know when and where it is produced within the body.

1.2.2 Biological synthesis of nitric oxide

In 1916, Mitchell, Shonle, and Grindley first noticed that the amount of nitrates and nitrites excreted through urine from healthy subjects was more than the amount that could be ingested from the diet (Mitchell, et al. 1916). Using ^{15}N-labelled nitrate ($^{15}NO_3^-$), Tannenbaum et al. monitored nitrate metabolism and quantified an excess of excreted nitrates in human urine compared to dietary intake, supporting this 65-year old observation (Tannenbaum, et al. 1978; Green et al. 1981, *PNAS*). These experiments allowed them to conclude that an endogenous metabolic process was responsible for forming nitrogen oxides. Over the following decade, an elegant series of experiments

across different research groups biochemically characterized this mechanism and its necessary components (Stuehr & Marletta 1985; Hibbs et al. 1987; Iyengar et al. 1987; Marletta et al. 1988). It was discovered that the radical nitric oxide is an endogenously synthesized intermediate generated during the process of nitrite and nitrate formation (Ignarro et al. 1987a; Ignarro et al. 1987b; Palmer et al. 1987; Palmer et al. 1988).

•NO is synthesized from L-arginine and oxygen by the enzyme nitric oxide synthase (NOS) (Moncada & Higgs, 1993). Nitric oxide synthases are 150 kiloDaltons and composed of a homodimer containing an oxygenase domain and a reductase domain that are linked by a calmodulin recognition site. The oxygenase domain contains binding sites for the cofactors tetrahydrobiopterin (BH_4), protoporphyrin IX haem, and L-arginine while the reductase domain contains binding sites for the electron carriers FAD & FMN, and the reductant NADPH (Ghosh & Stuehr 1995). In summary, electrons supplied by NADPH are shuttled across the reductase domain by FAD and FMN to the heme iron of the oxygenase domain where they can oxidize L-arginine. A guanidino nitrogen of L-arginine undergoes a 5-electron oxidation via two mono-oxygenation steps to form •NO and L-citrulline (Marletta et al. 1993; White & Marletta et al. 1992; Mayer et al. 1991; Bredt & Snyder 1990; Bredt et al. 1991). Binding of calmodulin is required for the flow of electrons from the reductase domain to the oxygenase domain.

Three nitric oxide synthase isoforms exist: neuronal nitric oxide synthase (nNOS; NOS1), inducible nitric oxide synthase (iNOS; NOS2), and endothelial nitric oxide synthase (eNOS; NOS3). They differ in their regulation, quantity, and location of •NO production. Neuronal NOS was the first isoform to be purified and cloned (Bredt & Snyder 1990) using extracts from rat cerebellum (Bredt et al. 1991). It is expressed in the

brain and skeletal muscle (Salter et al. 1991; Nakane et al. 1993). Endothelial NOS is found in endothelial cells, cardiac myocytes, neurons, and epithelial cells. Typical output from eNOS and nNOS is in the nM range. iNOS produces a large burst of $^{\bullet}NO$ in response to cytokines and endotoxins across a variety of cell types including neutrophils, epithelial cells, vascular smooth muscle, hepatocytes and chondrocytes (Xie et al. 1992; Lincoln et al. 1997). nNOS and eNOS differ from iNOS in their dependency upon calcium (Ca^{2+}) to produce synthesize $^{\bullet}NO$ (Cho et al. 1992;Garcin et al. 2004; Dudzinski et al. 2007; Venema et al. 1996). The efficiency of calmodulin binding for nNOS and eNOS is mediated by intracellular calcium levels whereas calmodulin is already tightly bound to iNOS.

The presence of so many cofactors suggests that nitric oxide synthases are very highly regulated. Lack of the cofactor BH_4 can cause the uncoupling of the eNOS dimer leading to production of superoxide (Chen et al. 2011). NOSs have also been shown to be regulated by posttranslational modifications. S-Glutathionylation can also uncouple the eNOS dimer serving as an autoregulatory mechanism for $^{\bullet}NO$ production (Chen et al. 2010). S-nitrosylation of iNOS has also been shown to destabilize the dimer (Rosenfeld et al. 2010).

1.2.3 Nitric oxide in health and disease

Nitric oxide has long played an important role in human health and disease, even when it had not yet been identified as the culprit (Butler et al. 2006). As with most great scientific discoveries, it all began with an observation. An English surgeon noticed that when he had a patient suffering from severe chest pain, he could alleviate the symptoms

by removing blood (Butler et al. 2006). This suggested to him that the remedy for angina pectoris was somehow related to lowering blood pressure. The surgeon's friend told him of how inhaling amyl nitrite helped to lower the blood pressure of his animals and so the surgeon commenced in using this therapeutic remedy for those suffering from chest pain (Gamgee et al. 1868; Brunton et al. 1867). Nitroglycerin which contained a nitro group (-NO_2) was also used as a vasodilator over the next century. It would be many years later before a series of experiments conducted by Moncada, Furchgott, Ignarro & Murad revealed the identity of nitric oxide as the true vasodilator. This Nobel Prize winning discovery will be discussed in the following section.

Nitric oxide has been classically identified as having a role in the body's innate immune response and neurotransmission. As was previously described, macrophages were instrumental in revealing the endogenous production of nitric oxide (Hibbs et al. 1987; Stuehr et al. 1989; Marletta et al. 1988; Hibbs, et al. 1989). In response to certain stimuli, iNOS can produce a burst of the $^{\bullet}NO$ which targets invading pathogens and participates in anti-tumor activities through a variety of mechanisms. Mice lacking the gene for iNOS are much more susceptible to parasitic infection and replication of bacteria (Wei et al. 1991; MacMicking et al. 1995). $^{\bullet}NO$ has been shown to impair mitochondrial function by disrupting iron-sulfur centers within oxidoreductases as well as altering mitochondrial membrane potential (Kroncke et al. 1995; Hibbs et al. 1987; Stuehr et al. 1989). $^{\bullet}NO$ can also react with non-heme iron, resulting in Fe release which might also promote lipid peroxidation and serve as an additional mechanism of cellular damage (Reif et al. 1990).

While all three isoforms of NOS are found throughout the brain, nitric oxide produced from neuronal NOS has been the best characterized within the central nervous system. A few of its important roles involve neuroprotection, neurotoxicity, and synaptic plasticity. Glutamate binds to the NMDA-receptor which allows calcium (Ca^{2+}) entry into the neurons thereby activating NOS. Once it is produced, $^{\bullet}NO$ acts as a retrograde messenger to strengthen synaptic activity. It has been postulated that this function of nitric oxide is important during long term potentiation (LTP), an important process underlying learning and memory in the brain.

Nitric oxide can also serve a neuroprotective function by regulating its own production. Disulfide bridge formation in the NMDA-receptor channel has been previously shown to decrease the influx of Ca^{2+} through the channel (Lei et al. 1992). Nitric oxide can modify these same two cysteines and help promote the formation of this disulfide bridge (Lipton, Singel, & Stamler, 1994; Lipton & Stamler, 1994). In addition, $^{\bullet}NO$ can also inhibit the binding of glutamate to the NMDA receptor, preventing the flow of Ca^{2+} through the channel and regulate NO synthesis.

When observing the presence of $^{\bullet}NO$ throughout the central nervous system, peripheral nervous system, and immune system, it is easy to imagine how its dysfunction might lead to disease. Dysregulation of nitric oxide has been implicated in ischemia (Mugge et al. 1991; Harrison et al. 1992; Maseri et al. 1991), atherosclerosis (Rubanyi et al. 1993), septic shock (Thiemermann et al. 1993; Petros et al. 1991), pre-eclampsia (Buhimschi et al. 1998) and many others disorders.

Nitric oxide has also been used as a therapeutic agent as it has been found to play an important role in wound healing (Frank et al. 2002; Shi et al. 2000) and protection after ischemic injury (Lima et al. 2009). In fact, researchers Jonathan Stamler and Joseph Bonaventura hold a United States patent for "Red blood cells loaded with S-nitrosothiol and its uses". As the patent abstract states, "loaded red blood cells can be used in methods of therapy for conditions which are characterized by abnormal O_2 metabolism of tissues, oxygen-related toxicity, abnormal vascular tone, abnormal red blood cell adhesion, or abnormal O_2 delivery by red blood cells." United States Patent #6153186 (http://www.wikipatents.com/US-Patent-6153186/red-blood-cells-loaded-with-s-nitrosothiol-and-uses-therefor). Direct inhalation of nitric oxide has been used to treat preterm infants with bronchopulmonary dysplasia (Kinsella, et al. 2007). As researchers continue to identify the role of nitric oxide in human physiology, it is even more pressing to identify the mechanisms by which nitric oxide may exert its function and how these functions are regulated.

1.2.4 Nitric oxide as a signaling molecule

Although nitrovasodilators such as nitroglycerin were known to alleviate the symptoms of pectoris angina since 1867, their mechanism of action was not fully elucidated until over 120 years later. The discovery of nitric oxide as an endogenous vasodilator came from a series of elegantly designed experiments across multiple laboratories. In 1977 & 1978, the Murad laboratory demonstrated that both gaseous $^{\bullet}NO$ and $^{\bullet}NO$ released from different nitrovasodilators could activate guanylate cyclase, converting GTP to cyclic GMP (Katsuki et al. 1977; Arnold et al. 1977; Schultz &

Schultz, 1977). It was also noted that this effect was inhibited by hemoglobin and myoglobin (Murad, et al. 1978). Shortly thereafter, the Ignarro laboratory reported that activation of guanylate cyclase by •NO resulted in smooth muscle relaxation (Gruetter, et al. 1979); however, it was still unknown that •NO existed endogenously.

The Furchgott Laboratory monitored the response of the aorta to the cholinergic agonist carbachol using a protocol which required the isolation of aortic rings; however, when a new technician prepared helical strips of the aorta instead of rings, he found that he could no longer induce smooth muscle relaxation. This finding highlighted two important discoveries: 1) an intact endothelium was necessary for smooth muscle relaxation and 2) acetylcholine must bind to receptors on the surface of the endothelium to produce the molecule responsible for smooth muscle relaxation (Furchgott et al. 1980). This yet identified molecule was later termed "endothelium-derived relaxation factor" (EDRF).

While both Furchgott and Ignarro independently speculated that EDRF was in fact •NO, it still remained inconclusive (Moncada et al. 1988). Once concurrent research identified the endogenous synthesis of nitrites and nitrates (Ignarro, et al. 1981; Iyengar, et al. 1987), this speculation immediately became more concrete. A series of experiments by Moncada and Ignarro finally revealed that EDRF was nitric oxide (Ignarro, et al. 1987; Ignarro, et al. 1987; Palmer et al. 1987) and it was synthesized from terminal guanidine nitrogen of L-arginine in vascular endothelial cells (Palmer et al. 1988).

In 1998, Furchgott, Ignarro, and Murad were awarded the Nobel Prize in Medicine and Physiology for their combined contributions in elucidating the role of nitric oxide in vasodilation. The press release accompanying the award made mention of nitric

oxide as a “signaling molecule”. This newly identified role for nitric oxide was clinched with the key discovery that eNOS produced •NO within endothelial cells. Previous work had shown that nitric oxide was produced in response to a stimulus, specifically targeted to the heme of soluble guanylate cyclase, and necessary for a specific physiological response, i.e. dephosphorylation of myosin light chain resulting in vasodilation. This new discovery added that nitric oxide was spatially restricted after its production by eNOS. This series of events became the canonically described cGMP-dependent pathway whereby which nitric oxide can act as a second messenger and induce a physiological response.

1.3 S-nitrosylation as an emerging posttranslational modification

Once it was determined that nitric oxide bound to the heme of soluble guanylate cyclase, it still remained unclear how •NO stably diffused from nitric oxide synthase to its target sGC. As was previously described, •NO can react with a variety of intracellular targets. Nitric oxide derived species are known to react with sulfhydryls and form more stable adducts of S-nitrosothiols (Oae, et al. 1983). Stamler et al. hypothesized that •NO could prolong its half-life and deliver •NO to targets such as sGC by reacting with reduced thiols on protein cysteine residues (Stamler, et al. 1992). By using both endogenous and exogenous sources of •NO, they found that several proteins could form S-nitroso adducts, including serum albumin. A series of later experiments by this same group detected S-nitrosylated serum album circulating in human plasma, suggesting that S-nitrosylated proteins could serve as endogenous intermediates for •NO delivery (Stamler et al. 1992).

In 1996, the Stamler group identified an S-nitrosylated cysteine residue on the Beta chain of hemoglobin (Cysβ93) (Jia, et al. 1996). Upon oxygenation of hemoglobin, Cysβ93 was S-nitrosylated (SNO-Hb) in the lung resulting in release of nitric oxide and delivery of O_2 to peripheral tissues through circulation. This suggested that SNO-Hb may be involved in the normal regulation of blood flow and maintenance of blood pressure. The role of $^{\bullet}NO$ in vasodilation was thought to be a very well characterized mechanism. Therefore, the identification of a new role for nitric oxide in vasodilation was a bit shocking, especially since it involved a new role for an enzyme which had also been heavily scrutinized for decades previously.

Even with the discovery of functional consequences of S-nitrosylation, there are still large deficits in our understanding and validation that it is a newly identified means of nitric oxide signaling within the body. The mechanism by which S-nitrosylation occurs has not conclusively been identified. Additionally, how specificity is derived still remains unclear. The following sections discuss how recent advances in the identification of S-nitrosylated proteins have increased our knowledge of this emerging posttranslational modification.

1.3.1 Methods for identification of S-nitrosylated cysteines

The crux to categorizing any emerging posttranslational modification is to identify its targets. With recent advances in technology, the development of techniques for detecting S-nitrosylated proteins has exponentially enhanced our understanding of S-nitrosylation and helped to elucidate its ubiquitous role in nitric oxide signaling. Proof of an S-nitrosylation event initially began using spectroscopic techniques to identify S-

Nitroso bovine serum albumin (Stamler et al. 1992). Stamler et al. utilized UV-Visible spectroscopy and NMR spectroscopy to show that •NO was bound to the protein. To quantify the amount of SNO present, they developed an assay which lysed the S–NO bond resulting in liberated •NO which could be detected via chemiluminescence after its reaction with ozone (Stamler et al. 1992; Stamler & Feelisch, 1996). Utilizing Saville chemistry, mercury (II) chloride ($HgCl_2$) was also used to remove nitric oxide for the purposes of quantification (Saville et al. 1958*;* Xu et al. 1998; Mannick et al. 1999). In the case of hemoglobin, a very well characterized protein, UV-Vis spectroscopy proved extremely informative in proving that nitric oxide was bound to a thiol and not the heme (Jia et al. 1996). However, it required its isolation, thereby mandating previous knowledge of its identity. Therefore, initial identifications of S-nitrosylated proteins did not allow for *a priori* hypotheses regarding their existence or identification.

In 2001, Jaffrey et al. published the first method which globally identified S-nitrosylated proteins contained within complex mixtures such as tissues (Jaffrey et al. 2001). The biotin switch technique (BST) consisted of three main steps: 1) the blocking of reduced thiols with methyl methanethiosulfonate (MMTS), 2) reduction of S-nitrosylated cysteine residues using ascorbate, and 3) biotinylation of previously S-nitrosylated cysteine residues with *N*-[6-(biotinamido)hexyl]-3'-(2'-pyridyldithio)propionamide (biotin–HPDP). Because MMTS is a thiol-specific agent, ascorbate selectively decomposes nitrosothiols, and biotin-HPDP is a sulfhydryl-specific agent, the method allows for the specific labeling of S-nitrosylated cysteine residues. Biotinylated proteins were purified using avidin, then separated and resolved using SDS-PAGE. Known proteins can be probed with the corresponding antibody or individual

bands can be excised and identified by mass spectrometric analysis. While the BST was the first tool of its kind, concerns still exist regarding its efficiency to identify S-nitrosylated proteins. The reduction of S-nitrosothiols by ascorbate has been called into question due to its poor sensitivity and its ability to reduce disulfide bonds (Zhang, et al. 2005; Giustarini et al. 2008). Moreover, a key objective for identifying scores of S-nitrosylated proteins is to reveal the specificity of cysteines endogenously targeted for this modification. However, this is impossible to do when identifying the protein without the specific site of modification. Two papers were published in 2006 which offered proteomic techniques for identifying sites of S-nitrosylation in complex mixtures (Hao et al. 2006; Greco et al. 2006). Briefly, the two comparable methods introduced a trypsinization step before biotinylation which allowed for enrichment of peptides containing modified cysteines.

Since the development of the BST in 2001, there have been many derivatives aimed at improving its deficiencies (Sun et al. 2007; Kettenhofen et al. 2008,; Sinha et al. 2010) and development of other promising techniques which directly label and detect S-nitrosocysteine (Torta et al. 2010; Wang et al. 2008; Faccenda et al. 2010; Zhang et al. 2010). More recently, Benhar et al. developed a quantitative BST method using stable isotope labeling by amino acids in cell culture (SILAC) (Benhar et al. 2010). The authors employed their technique to characterize the denitrosylation of SNO-cysteines by thioredoxin in Jurkat cells. While the above described methods point toward significant advances in the field of S-nitrosylation, detection of S-nitrosylated proteins is often still dependent upon supplementation by exogenous sources of nitric oxide. An optimal

method would be sensitive enough to detect and accurately quantify endogenous S-nitrosylation events.

1.3.2 Alteration of protein activity as a function of S-nitrosylation

With the advent of the Biotin Switch Technique and its derivatives, many more proteins have been identified as S-nitrosylated. For many researchers, S-nitrosylation has provided the missing link between observing a role of nitric oxide in human physiology and pinpointing its specific mechanism of action. A comprehensive discussion of all such proteins would prove to be impossible within the limits of this dissertation; therefore, several key studies are highlighted which demonstrate how S-nitrosylation can alter a wide range of protein functions and further extend the role of nitric oxide in human health and disease.

Nitric oxide has long been known to play an important role in neurophysiology. In 2004, the Lipton group identified a role for S-nitrosylation in sporadic Parkinson's disease (Yao et al. 2004). S-nitrosylation of the E3 ubiquitin ligase parkin in SH-SY5Y cells led to an increase in its activity and ultimately resulted in its own ubiquitination. Inhibition of parkin can result in a decreased clearance of its substrates and ultimately lead to cell death. This fact is made even more apparent by the detection of S-nitrosylated parkin in human brains of those with sporadic Parkinson's disease. Later studies involving the S-nitrosylation of glyceraldehyde-3-phosphate dehydrogenase (GAPDH) led to an additional role of nitric oxide in regulating E3 ubiquitin ligase activity. It has been well established that GAPDH translocates to the nucleus during apoptosis (Sawa, et

al. 1997; Ishitani, et al. 1998; Dastoor, et al. 2001). Because GAPDH lacks a nuclear localization signal, how GAPDH is able to enter the nucleus has remained a mystery. In 2005, Hara et al. showed that nitric oxide S-nitrosylates GAPDH thereby increasing its ability to bind to the E3 ubiquitin ligase Siah1, and induces translocation of the complex into the nucleus (Hara et al. 2005). Once inside, GAPDH promotes the stabilization of Siah1, allowing for it to carry out its role in apoptosis. This discovery propelled a myriad of studies which continue to identify how this mechanism is regulated (Sen, et al. 2008; Sen, et al. 2009; Kornberg, et al. 2010).

In addition to regulating the activity of ubiquitin ligases, S-nitrosylation has also been shown to modulate other posttranslational modifications such as phosphorylation. Previous reports have shown that nitric oxide can negatively regulate the signaling cascade of c-Jun N-terminal kinases also known as JNKs (Park et al. 1996; Lo, et al. 1996; Kim et al. 1997; Wang et al. 1998; Lander et al. 1996; Jun et al. 1999). As a member of the mitogen activated protein (MAP) kinase family, JNKs are important in the cellular response to different stresses. They are activated through phosphorylation by MAP kinases MKK4 and MMK7 and typically inactivated by phosphatases (Ip, et al. 1998). Park et al. demonstrated that endogenous production of $^{\bullet}$NO by activation of iNOS resulted in suppression of JNK activity in microglia and macrophages (Park et al. 2000). Using a series of experiments, the authors showed that JNK activity was attenuated by nitric oxide, more specifically, by a cGMP-independent chemical modification of Cys116 which they identified as S-nitrosylation. Conversely, S-nitrosylation has also been shown to enhance the activity of other kinases. Rahman et al. presented an investigation into

tyrosine kinase c-Src and found that S-nitrosylation of Cys498 resulted in its activation and ultimately its invasion into cancer cells (Rahman, et al. 2010).

S-nitrosylation has also been shown to play a role in the regulation of DNA transcription. NF-κB is a transcription factor thought to regulate over 200 genes which are involved in the inflammatory response (Marshall, et al. 2000; Shishodia, et al. 2004; Xie, et al. 1994). It is activated by its release from inhibitory proteins within the cytoplasm and translocation to the nucleus. IκB kinase (IKK) is one of the proteins responsible for inducing the degradation of these inhibitory proteins thereby activating NF-κB. Reynaert et al. demonstrated that S-nitrosylation of Cys179 in IKK inhibited its activity resulting in prolonged inactivation of NF-κB (Reynaert et al. 2004). By inhibiting endogenous production of •NO in Jurkat cells, the authors were able to again activate IKK. Interestingly, additional evidence has also shown that NF-κB itself is S-nitrosylated, offering an additional mechanism for by which •NO can regulate its transcriptional activity (Matthews, et al. 1996; delaTorre, et al. 1997).

Major classes of proteins have been found to be S-nitrosylated. Coupled with the discovery of S-nitrosylation across different types of cells and tissues (Gow et al., 2002), this underscores the widespread effects that nitric oxide can have across different biological processes. Nevertheless, it is important to acknowledge that identifying a protein as being susceptible to S-nitrosylation does not prove that it is endogenously S-nitrosylated. Lack of sensitive detection technologies often mandate that proteins are frequently supplemented with exogenous sources of nitric oxide to aid in their identification. Exogenous donors can vary greatly in the nitric oxide moiety that is

produced. And as is described in the following sections, the chemistry of a nitric oxide moiety may influence which cysteines are actually targeted.

1.3.3 Proposed mechanisms of *S*-nitrosylation formation

Perusing the literature on S-nitrosylation may leave the reader slightly confused due to the assorted terminology. Several key terms are used to describe this newly emerging protein modification by nitric oxide. The difference in their definitions stems from the proposed mechanism by which $^{\bullet}NO$ modifies cysteine residues to form S-nitrosocysteine (Protein-Cys-NO). The most commonly used term is "*S*-nitrosylation". This historically describes the reaction of a nitric oxide radical with a transition metal ("nitrosylation") to form a product which then reacts with a protein cysteine thiol ("*S*-nitrosylation") (Stamler, et al. 1992). Another term very commonly used is "nitrosation" or "transnitrosation". This term traditionally refers to the addition or transfer of a nitrosonium ion (NO^+) to a thiolate anion (SH^-) whereas "trans-*S*-nitrosation" specifies the transfer to a protein cysteine residue. "S-nitrosylation" is now more routinely used to encompass any reaction resulting in the addition of a nitric oxide moiety to a protein cysteine thiol.

There are several proposed mechanisms which can result in the formation of protein S-nitrosocysteine. The first mechanism describes the direct reaction of an NO radical with a transition metal. $^{\bullet}NO$ can react with a metal at a heme center such as Fe^{3+} to form Fe^{2+} and NO^+ (Pacher et al. 2007). The nitrosonium ion is then capable of reacting with the reduced thiol of nearby cysteine residues (Wade & Castro 1990). An additional metal-catalyzed mechanism hypothesizes that proteins can react with free

pools of iron in the cell to form dinitrosyliron complexes which can S-nitrosylate cysteine residues (Bosworth et al. 2009; Boese et al. 1995).

Additional mechanisms for forming S-nitrosocysteine involve the transfer of a nitrosonium ion to a reduced thiol of a cysteine residue. It has been proposed that S-nitrosoglutathione (GSNO), a major endogenous S-nitrosothiol, is involved in the transnitrosation of protein cysteine. Although it can be synthesized within the laboratory using sodium nitrite and GSH in an acidic environment, the mechanism by which GSNO forms endogenously still remains unclear (Zhang et al. 2004; Keszler et al. 2009; Gow et al. 1997; Tullett et al. 2001). It is also possible for S-nitrocysteine residues within proteins to then react with the reduced thiols of GSH or other protein cysteine residues and transfer a nitrosonium ion. This is what is referred to as a "protein-assisted" transnitrosation. This mechanism was observed with the protein thioredoxin (Mitchell et al. 2005). After its own reaction with GSNO, SNO-thioredoxin (SNO-Trx) can transnitrosate a select cysteine residue in the enzyme caspase-3. Experiments conducted by the Marletta group illustrate that SNO-Trx and not GSNO is the favored mechanism by which this specific cysteine forms S-nitrosocysteine (Mitchell et al. 2007).

The last proposed mechanism of S-nitrosation involves the autoxidation of $^{\bullet}NO$ to form higher oxides that serve as transnitrosating agents. Due to its lipophilic character, $^{\bullet}NO$ is known to favor hydrophobic environments (Moller et al. 2007). Therefore, $^{\bullet}NO$ can congregate in hydrophobic regions of the protein where it can also react with O_2 and nitrogen dioxide to form the transnitrosating agent dinitrogen trioxide N_2O_3 (Nedospasov et al. 2000; Gow et al. 1997; Liu et al. 1998; Moller, et al. 2007).

There is a diversity of mechanisms which ultimately result in the formation of protein-SNO, each of which is dependent upon the chemical structure of nitric oxide. Therefore, being able to identify the chemical species of nitric oxide may help to pinpoint which mechanism is occurring and may contribute to our understanding of the specificity of this posttranslational modification.

1.3.4 Denitrosylation: Reversing the signal

To convincingly describe S-nitrosylation as a signaling mechanism of nitric oxide, it is essential to show the reversibility of the modification. There are two major endogenous systems which have been identified to influence the stability of S-nitrosocysteine: the GSH/S-nitosoglutathione/S-nitrosoglutathione reductase system and the thioredoxin/thioredoxin reductase system. Thioredoxin (Trx) is directly involved in an enzyme-mediated mechanism of denitrosylation whereas the glutathione system indirectly mediates S-nitrosylation through metabolism of GSNO by the enzyme S-nitrosoglutathione reductase (GSNOR).

In addition to its roles as both a reductant and transnitrosating agent (Mitchell et al. 2005; Mitchell et al. 2007), thioredoxin has also been shown to serve as a denitrosylating enzyme. Nikitovic and Holmgren first demonstrated an indirect role for the thioredoxin system through its metabolism of the low molecular weight thiol GSNO (Nikitovic et al. 1996). Stoyanovsky and colleagues further demonstrated that the Trx system was also capable of denitrosating protein-SNO (Sengupta, et al. 2007). The proposed mechanism involves active site cysteines 32 and 35 (Sengupta, et al. 2007). Because of its increased nucleophilicity, Cys32 is thought to be the target of NO. Cys32

and Cys35 then form a disulfide bond allowing NO to then be transferred intramolecularly to the other cysteine residues (Cys62, Cys69, & Cys72) which have previously been shown to be S-nitrosylated. For protein denitrosation, the work of Mitchell & Marletta with caspase-3 may provide insight as to how thioredoxin might interact with target proteins (Mitchell et al. 2007). E70A/K72A mutations in hTrx resulted in some loss of contact, suggesting that these charged residues may help facilitate protein-protein interactions between the denitrosating agent and its targets. Proteomic studies have also been used to identify proteins which might be potential denitrosylation targets of thioredoxin (Benhar et al. 2010). Using a model which overexpressed Trx, recent work done by Fu et al. identified 55 putative protein targets of thioredoxin in the mouse heart (Fu et al. 2009). Interestingly, previous reports have identified several of these proteins as being targets of S-nitrosylation.

The thioredoxin system can be regulated through a variety of mechanisms. Stamler and colleagues first demonstrated that caspase-3 activation was tightly tethered to its denitrosylation upon induction of the Fas apoptotic pathway (Mannick et al. 1999). Nearly 10 years later, they were able to show that denitrosylation of caspase-3 was carried out by mitochondrial thioredoxins (Benhar et al. 2008), suggesting a stimulus-coupled regulatory mechanism. Recently, Forrester and colleagues have identified Thioredoxin-interacting protein (Txnip), a protein which can also regulate the denitrosation activities of thioredoxin (Forrester et al. 2009). And most obviously, thioredoxin requires the presence of NADPH and thioredoxin reductase to control the redox state of its catalytic cysteines.

Glutathione has long been known for its essential antioxidant properties in the cell. Although the specific *in vivo* mechanism remains elusive, GSH can react with a nitric oxide moiety to form the transnitrosating agent GSNO (Zhang et al. 2005; Gow et al. 1997). Once it was determined that GSNO readily forms S-nitrosocysteine endogenously, understanding how this process was regulated became of great importance. In 2001, Liu et al. identified GSNO reductase (GSNOR), an endogenous enzyme which could regulate the intracellular levels of GSNO (Liu et al. 2001). GSNOR is an endogenous alcohol dehydrogenase (Class III) which can oxidize an alcohol to a ketone or aldehyde. Previous investigations showed that it was highly specific for GSNO (Jensen et al. 1998). GSNOR regulates the availability of GSNO by converting it to oxidized glutathione (GSSG) in the presence of NADPH. The Stamler group generated knockouts of this enzyme showing increased levels of SNO-hemoglobin as compared to wildtype (Liu et al. 2004). This suggests that the equilibrium that exists between GSNO and protein-SNO is disrupted upon removal of GSNOR.

Glutathione itself is also capable of denitrosating protein-cysteine residues (Romero et al. 2009; Paige et al. 2008). Denitrosation of proteins by GSH was investigated using a quantitative proteomic method which monitored the stability of S-nitrosylated cysteine residues (Paige et al. 2008). The authors revealed a subset of proteins that were insensitive to denitrosation via GSH and even remained modified after synthesis of $^{\bullet}$NO was inhibited. Additional experiments with the reductant DTT also revealed no decrease in S-nitrosylation. Only after the proteins were denatured were they able to remove SNO. This suggested that conformational changes within the protein may

take place to prevent denitrosation from occurring, thereby increasing the longevity of S-nitrosocysteine.

Investigations continue into identifying additional proteins which might serve as denitrosating agents or aid in the process of regulating denitrosylation events. To date studies have shown that other enzymes including protein disulfide isomerase (Sliskovic et al. 2005), xanthine oxidase (Trujillo et al. 1998), superoxide dismutase (Jourd'heuil et al. 1999; Johnson et al. 2001), and glutathione peroxidase (Hou et al. 1996) may play a role in the metabolism of S-nitrosothiols.

1.4 Specificity of cysteines targeted for S-nitrosylation

A large gap in knowledge exists regarding the specificity of endogenous S-nitrosylation. While it has been well documented that not all proteins are S-nitrosylated and more specifically, not all cysteine residues within an S-nitrosylated protein are modified, it is very important to determine how this specificity is derived. The best example for illustrating this phenomenon is the skeletal muscle Ca^{2+} release channel/ryanodine receptor 1 (RYR1) protein (Sun et al. 2001). With a total of 50 cysteines per subunit, only a single cysteine, Cys3635, has been identified as being S-nitrosylated (Sun et al. 2003).

1.4.1 Cysteine reactivity

Although cysteine residues are not the most frequently occurring amino acids, they are among one of the most conserved (Fomenko et al. 2008). Cysteine residues are most notably known for their role in maintaining protein structure by forming disulfide

bonds. However, with a nucleophilic sulfhydryl side chain and a pKa of 8.3, cysteines are highly reactive under physiological conditions. Not only are they susceptible to oxidation, but they can be coordinated to metals, serve as catalytic sites, or sites of posttranslational modification. Many investigations have been aimed at predicting the propensity of cysteines to undergo different chemical modifications (Fomenko et al. 2007). Marino et al. utilized the structures of oxidoreductases and the biophysical properties of their catalytic cysteines to predict similarly reactive cysteine residues (Marino et al. 2009). They developed an algorithm which took into account the primary and secondary structures, cysteine accessibility, and reactivity. This algorithm was then applied to a test set of proteins as well as the entire *Saccharomyces cerevisiae* proteome. Their results correctly identified all thiol oxidoreductases in the test set and identified 42 proteins in the *S. cerevisiae* proteome, 33 of which were known oxidoreductases. This suggests that the reactivity of cysteines to undergo a specific chemical modification can be deciphered from its surrounding environment. This was also seen in global investigations into disulfide bridge formation (Petersen et al. 1999). In addition, identifying the specificity of cysteines which undergo S-glutathionylation has long been a subject of interest (Thomas et al. 1995; Giustarini et al. 2005; Tao et al. 2004).

1.4.2 S-nitrosylation and the cysteine microenvironment

A study conducted by Marino and Gladyshev was the first comprehensive interrogation into the specificity of S-nitrosylation (Marino & Gladyshev 2010). Using a dataset of S-nitrosylated cysteines (and a randomly chosen set of Cys residues) curated from the literature, the authors investigated their structural and biophysical properties in

an attempt to uncover any attributes specific to S-nitrosylation. As was described previously, a potential mechanism of S-nitrosylation is the autoxidation of $^{\bullet}NO$ which is favored in hydrophobic environments (Liu et al. 1998; Nedaspov et al. 2000; Moller et al. 2007); therefore, cysteines targeted for S-nitrosylation via this mechanism would likely be present in hydrophobic regions of a protein. Hydrophobic SNO-cysteines were observed in several proteins including the ryanodine receptor and argininosuccinate synthetase (Hao et al. 2004; Sun et al. 2001). Using both the flanking amino acid sequence and an 8 Angstrom radius, Kyte-Doolittle hydropathy indices were calculated for each SNO-Cys and random Cys. Both approaches revealed no significant difference between modified and random cysteines, suggesting that hydropathy was not a major determinant.

Based upon an observation of SNO-Cys93β in hemoglobin, Stamler et al. hypothesized that the presence of charged residues flanking a cysteine residue may regulate its nucleophilicity and ultimately target it for S-nitrosylation (Stamler et al. 1997). Using these data, the authors derived a linear consensus motif of (H,K,R)(C)(hydrophobic)X(D, E) where X can be any amino acid (Stamler et al. 1997). Perez-Mato et al. later proposed that pairs of charged residues could also play a role in navigating GSNO-mediated mechanisms of transnitrosation (Perez-Mato et al. 1999). Many individual S-nitrosylated proteins have since been identified as containing either a linear or structural acid/base motif within a 6 Å radius (Choi et al 2000; Kim et al. 2002). Several studies have attempted proteomic investigations into the occurrence of this acid/base motif, but were limited in their findings due to low numbers (Greco et al. 2006; Hao et al. 2006). Marino et al. found that a more distant motif existed with surface

exposed charged residues which were thought to help stabilize GSNO and/or facilitate protein-protein interactions necessary for transnitrosation.

Surface exposure has also been used to evaluate the ability of cysteines to be S-nitrosylated. With several proposed S-nitrosylation mechanisms, the size of the S-nitrosylating or transnitrosating agent would undoubtedly influence its accessibility to different cysteines within the protein. A high-resolution structure of tubulin illustrated this fact when only one of the four cysteines modified endogenously was found to be surface exposed; however, upon supplementation with GSNO, four additional cysteine residues were modified (Nogales et al. 1999; Roychowdhury et al. 2000; Kim et al. 2004). Knipp et al. demonstrated that Cys221 of Zn(II)-free dimethylarginase-1 (DDAH-1) was S-nitrosylated via gaseous $^{\bullet}$NO yet supplementation by S-nitrosohomocysteine only modified solvent-accessible cysteine residues (Knipp et al. 2003). Marino et al. found used a 1.2 Å probe to calculate that 35% of SNO-cysteines were buried and not accessible to a $^{\bullet}$NO molecule.

The investigation by Marino et al. represents a great effort into the global investigation of the specificity of S-nitrosylation. While the diversity of data initially appears to be inconclusive for a specific mechanism, the authors themselves suggest that this may represent that different cysteines are modified by different mechanisms. The better experiment would be to isolate a specific population or subpopulation of S-nitrosylated cysteine and characterize its attributes specific to its precise mechanism. An additional limitation of the Marino et al. study is the use of proteins that are modified ex

vivo and therefore represent putative targets but not necessarily the in vivo sites of S-nitrosylation.

1.5 Structural implications of S-nitrosylation

1.5.1 Insights from the structures of S-nitrosylated proteins

While a host of proteins have been identified as being S-nitrosylated, a current search of the Protein Data Bank yields only 9 structures of S-nitrosylated proteins, four of which are related structures of similar proteins. It has been suggested that this obvious deficit of structures is due not only to the lability of the modification (Derakshan et al. 2008) but also to the sensitivity of the S-NO bond to radiation (Scheiter et al. 2007; Weischel et al. 2007; Rosenfeld et al. 2010). Therefore, our present understanding of the structural consequences of S-nitrosylation is limited to these six unique/individual (non-redundant) proteins.

Not surprisingly, the first published structure of an S-nitrosylated protein was that of human hemoglobin (SNO-HbA: PDBid 1BUW) (Chan et al. 1998). The Arnone Group at the University of Iowa determined the X-ray crystal structure at a resolution of 1.8 Å. Crystals of SNO-HbA were prepared by repeatedly exposing the carbonmonoxy form of the protein to gaseous NO under anaerobic conditions over a time-course of 10 days. This resulted in residue Cysteine-93 of both β chains being converted from cysteine to S-nitrosocysteine (with nitric oxide additionally replacing the four CO ligands bound to the heme of each tetramer). Of the 6 total cysteines contained within hemoglobin, Cys-93 was the single residue modified (Chan et al. 1998; Jia et al. 1996).

Previous studies have shown that Cysteine-93 is more reactive than its unmodified counterparts (Chiancone et al. 1989). Additionally, it has been well characterized that Cys93 is more susceptible to modification (S-nitrosylation) while hemoglobin is in its relaxed state rather than tense state. Therefore, it was originally thought that Cys93 became more surface accessible due to conformational changes resulting from oxygen binding. Surface accessible calculations proved, however, that the residue remained buried and only partially exposed when comparing the oxyHbA R structure, the carbonmonoxyHbA R2 structure, and the deoxyHbA structure (Fermi et al. 1984; Kavanaugh et al. 1992). Hydrogen exchange experiments in conjunction with a comparison of the B-factors of high resolution hemoglobin structures revealed an increase in mobility and local unfolding near of COOH-termini of β-subunits (Englander et al. 1992). Because cysteine-93 is in such close proximity to the COOH-terminus, it was deduced that this increased mobility upon ligand binding allows for transient exposure of the residue, thereby making it susceptible/accessible to S-nitrosylation.

Comparison of the carbonmonoxyHbA and SNO-nitrosylHbA structures revealed an obvious absence of electron density at the COOH-termini of SNO-nitrosylHbA. Residues Tyr145β and His146β (which are present in the carbonmonoxy form of the protein) are highly disordered and no longer visible after S-nitrosylation of Cysteine-93. Examination of carbonmonoxyHbA reveals that Cys93β lies near the end of an α-helix and is adjacent to Tyr145β. Upon S-nitrosylation, Cys93β clashes with the side chain of Tyr145β, disrupting the binding pocket that it also shares with Val98β and Pro100β and causing residues 145-146 to become disordered. While S-nitrosylation of hemoglobin induced no obvious conformational changes in the quaternary structure of the protein,

this study offered the first crystallographic evidence of any structural changes which may occur as a structural consequence of S-nitrosylation.

The second structure of a S-nitrosylated protein is an isoform of N^{ω},N^{ω}-dimethyl-L-arginine dimethylaminohydrolase (DDAH-1) which was published nearly 8 years later (PDBid: 2CI1) (Frey, et al. 2008) [clean up]. A cysteine hydrolase, DDAH is responsible for the *in vivo* metabolism of L-N^{ω}-methylarginine (MMA) and L-N^{ω}, N^{ω}-dimethylarginine (ADMA), two well characterized inhibitors of NOS (Ogawa et al. 1989). There are two isoforms of DDAH in mammals, DDAH-1 and DDAH-2 (Leiper et al. 1999) which share less than 50% sequence homology. DDAH-2 is found primarily in the heart, placenta, lung, liver, skeletal muscle, kidney, and pancreas (Leiper et al. 1999). In addition to the liver, kidney, pancreas, and skeletal muscle at very low levels, DDAH-1 is also detected in the brain (Leiper et al. 1999). Increases in DDAH-1 and neuronal NOS expressions were found in injured neurons, underscoring the important role of DDAH-1 in regulation of neuronal nitric oxide generation (Nakagomi et al. 1999).

It was originally discovered that DDAH-1 is inhibited when Zn(II) is coordinated to the enzyme via two sulfur atoms belonging to cysteine residues (Fundel et al. 1996; Bogumil et al. 1998; Knipp, et al. 2001). More recently, it has been shown that DDAH-1 is susceptible to S-nitrosylation when Zn(II) is not bound resulting in abatement of its activity (Knipp et al. 2003). Therefore, S-nitrosylation serves as an additional regulatory mechanism for inhibiting DDAH-1 activity. Upon incubation with the NO donor DEA NONOate (2-*N*,*N*-diethylamino)-diazenolate-2-oxide)), Knipp et al. identified Cys221 and Cys273 (the active site cysteine) as being S-nitrosylated in bovine DDAH-1 (Knipp

et al. 2003). At the time this study was conducted, there were no available crystal structures of a mammalian DDAH. Therefore, a crystal structure of DDAH from the bacterium *Pseudomonas aeruginosa* (PDBid: 1H70) was used to build a homology model of DDAH-1 (Murray-Rust et al. 2001).

The homology model suggests a conservation of five (5) ββαβ-modules from bacterial DDAH to bovine DDAH-1. However, the two structures diverge significantly when observing the secondary structure near the opening of the active site. An N-terminal loop closes the active site in the bacterial protein whereas a helix-turn-helix motif exists in the homology model. The S-nitrosylated form of bovine DDAH-1 was obtained by incubating the protein with S-nitroso-L-homocysteine before crystallization (Frey et al. 2008). Upon binding of S-nitroso-L-homocysteine, the lid of the protein which opens the active site adopts a closed conformation. Instead of Cys221 and Cys273 which were previously identified as being S-nitrosylated, Cysteine-83 is the only residue found to be modified. This was thought to be an off target effect since cysteine 83 is solvent-exposed and on the opposite end of the pore, away from the active site. Modification of cysteine-83 does not appear to alter the overall structure of the protein. It is thought that the major structural changes observed in the structure are due to substrate binding (SNO-cys) rather than the posttranslational modification.

Human SNO-thioredoxin was first crystallized by Weischel et al. in 2007 and then by Hashemy & Holmgren in 2008 (Weischel et al. 2007*;* Hashemy & Holmgren 2008). Because a comparison of the two resolved structures shows conflicting results, SNO-thioredoxin is one of the most well-studied S-nitrosylated proteins. At a resolution

of 1.65 Å, the structure by Weischel et al. revealed the formation of S-nitrosocysteine at residues Cys62 and Cys69 after exogenous treatment of S-nitrosoglutathione. Comparison of the wildtype and SNO-form revealed a 0.5 Angstrom rotation of a helix after S-nitrosocysteine formation which is hypothesized to move out even farther to accommodate GSNO. This same helix was found to be disordered in the S-nitrosylated form, showing that large [dynamic] motions were taking place as was previously hypothesized (Watson et al. 2003). An additional structure of thioredoxin was determined in 2008 by Hashemy & Holmgren. When thioredoxin was fully reduced, S-nitrosocysteine formed on Cys69 and Cys73 after treatment with S-nitrosoglutathione. When two-disulfide bonds were formed in thioredoxin, only Cys73 was S-nitrosylated. This showed that the redox state of the protein was important in which cysteine residues were susceptible to S-nitrosylation.

The fourth structure of an S-nitrosylated protein was that of blackfin tuna myoglobin (PDBid: 2NRM), (Schreiter et al. 2007). Tuna myoglobins contain a single cysteine within an N-terminal helix. Based upon the reactivity of the single cysteine residue in human myoglobin, it was hypothesized that tuna myoglobins might also be susceptible to S-nitrosylation *in vivo* (Rayner et al 2005; Witting et al. 2001). Crystals of SNO-Mb were obtained by reacting purified blackfin tuna myoglobin with a 10-fold excess of S-nitrosocysteine. This led to a structure of S-nitrosomyoglobin at 1.09 Å resolution using a rotating copper anode x-ray generator [rotating anode source]. The authors attempted to collect structures of SNO-Mb at an even higher resolution using a synchrotron source but found that this resulted in loss of the NO moiety. The presence of a NO moiety near cysteine-10 was confirmed with electron density maps. Two unique

conformations were observed which displayed different rotations around the Cα-Cβ bond (χ1 rotamer). When compared to the reduced cysteine in the unmodified structure of myoglobin, the first conformation (conformer A) was rotated 25° whereas the second conformation (conformer B) displayed a χ1 rotamer of 115°. The χ3 values of both conformers however remained near 0°.

S-nitrosylation of blackfin tuna myoglobin induced significant changes/alterations in the positions of secondary structural elements near the site of modification. Superimposing the unmodified (PDBid: 2NRL) and S-nitrosylated structures resulted in a RMSD value of 1.2 Å for this particular region of the protein. To prevent steric clashes between residues, Leucine-117 (in Loop GH) and Alanine-6 (in Helix A) were wedged apart moved to accommodate the NO moiety. As a result, Helix H and Loop EF (which lie next to Helix A) were also displaced. The authors demonstrated that these structural changes were a direct consequence of S-nitrosylation. With sodium dithionite, they were able to reduce the S-nitrosylated cysteine and observed that the structure of the protein was identical to the unmodified form of myoglobin ("reverts to the same conformation it had prior to S-nitrosylation"). Upon reduction of SNO-cysteine, the authors demonstrate that the NO moiety is removed from cysteine-10 and binds to the heme of myoglobin converting it to its ferrous nitrosyl (FE^{II}-NO) form. When Cys10 is S-nitrosylated, a water molecule is bound to the iron at the heme. After removal of the NO moiety, NO is then free to react with the iron at the heme converting the protein to its ferrous nitrosyl form (Fe^{II} – NO).

The S-nitrosylated structure of protein-tyrosine phosphatase 1B (PTP1B) was resolved in 2008 by Chen et al. (Chen et al. 2008). In the presence of the NO-donor SNAP, PTP1B was crystallized and resolved at a 2.6 Angstrom resolution. S-nitrosocysteine formed at Cys215 which is located in the active site of the protein. Examination of the structure revealed a subtle conformational change in the positions of side chains near Cys215. By comparing the reduced and S-nitrosylated forms of PTP1B, the authors show the emergence of a hydrogen bond network which they hypothesize might play a role in the stabilization of the structure.

The most recently resolved structure of an S-nitrosylated protein is that of hypoxia inducible factor prolyl hydroxylase domain 2 (EGLN). After treatment with NO donors, the structure of EGLN exhibited a positive difference density consistent with S-nitrocysteine formation at Cys302; however, attempts to further refine the structure using stereochemical restraints for an S-nitrosocysteine residue failed since the SNO group could not be fitted within the experimental electron density. The authors concluded that what they were not observing S-nitrosocysteine but instead a reaction intermediate of $^{\bullet}$NO with the thiol.

A comprehensive study conducted by Marino et al. superimposed the structures of these same S-nitrosylated proteins with their corresponding non-nitrosylated structures (Marino et al. 2010). Most strikingly, the authors found that charged residues within the proteins were the most responsive to S-nitrosocysteine formation as they were the major residues which were rearranged. Collectively, these data suggest that the protein does make an attempt to accommodate the presence of S-nitrosocysteine in place of a reduced

thiol. However, the ultimate assessment would be to examine only those structures which are endogenously modified.

1.5.2 Computational tools for extracting structural information from S-nitrosylated proteins

While the aforementioned studies may provide novel insight into the structural consequences of S-nitrosylation, it is presumptive to draw conclusions about hundreds of proteins based upon six different structures. Therefore, it is important to extract as much information as possible from the wildtype structures of proteins found to be S-nitrosylated.

Three-dimensional structures of proteins which have been resolved by NMR or X-ray crystallography are made available in the RCSB Protein Data Bank (www.pdb.org) which presently contains 76,288 structures (as of 10/04/11). In identifying S-nitrosylation as a far-reaching posttranslational modification, SNO-proteins encompass those which have been very well characterized as well as those which are not as well known. Therefore, homology models are often generated for S-nitrosylated proteins without corresponding structures.

Several interesting cases exist where additional information was gleaned by generating homology models of S-nitrosylated proteins. In their investigations into the role of S-nitrosylation in Alzheimer's disease, Cho et al. generated a homology model of dyanamin-related protein 1 (DRP-1) using the structure of bacterial dynamin-like protein (Cho et al. 2009). The three dimensional structure of the protein revealed a spatial consensus motif flanking S-nitrosocysteine and that the modified cysteine was highly

surface accessible. S-nitrosylation results in the dimer formation of DRP-1, contributing to neuronal synaptic damage or cell death. The authors hypothesize that due to the increased presence of copper found in human AD brains, DRP-1 may be S-nitrosylated via a metal-catalyzed mechanism. Therefore, understanding how the protein environment plays a role in such mechanism may assist in developing DRP-1 as a potential drug target.

Molecular dynamics (MD) simulations are another useful tool for understanding the influence of S-nitrosocysteine formation on the remaining structure of the protein. The motions of a protein can be monitored over time to see if there is a global or local response to different stimuli. Han et al. conducted a molecular dynamics simulation of S-nitrosylated thioredoxin in its oxidized and reduced states (Han et al. 2008). Because S-nitrosocysteine is not a commonly occurring amino acid, the author had to first develop force field parameters which could characterize the movements and constraints of SNO-proteins. Comparison of thioredoxin with and without SNO-Cys-69 across MD trajectories showed no large global motions. The RMSD of oxidized thioredoxin was rigid when compared to the RMSD of reduced thioredoxin; however, this difference was also observed independent of S-nitrosocysteine. This suggests that differences in structural constraints are due instead to the redox state of the protein. While MD simulations may not have been fruitful in the case of thioredoxin, when combined with homology modeling, it can serve as a powerful tool for structurally interrogating the influence of S-nitrosocysteine on any protein.

1.6 Rationale and Objectives

S-nitrosylation proves to be an exhaustive body of work which only seems to increase as time goes on. With the advances in technology over the past 10 years, S-nitrosylated proteins modified in vivo are being identified on a much more consistent basis. They have been found to play a role in biological and cellular processes already thought to be very well characterized, sometimes involving proteins which are much less characterized.

However, as more information emerges regarding S-nitrosylation, there are still several large gaps in our knowledge which prevent us from better understanding S-nitrosylation. Firstly, we want to understand why certain cysteines are targeted for S-nitrosylation and not others. Identifying the specificity of S-nitrosylation will help us to better regulate the activity of S-nitrosylation. This mandates that we need to identify S-nitrosylated cysteines and their unmodified counterparts in vivo. **Chapter 2** describes a novel method which allows for the global identification of S-nitrosylated cysteines within the mouse liver. This large dataset also provides a control comparison of SNO-cysteines to their unmodified counterparts allowing for a side-by-side comparison of reactive vs. non-reactive cysteines.

Once $^{\bullet}NO$ is produced, it is important to understand the mechanism by which S-nitrosylated proteins are formed. As was previously described, several hypotheses exist regarding how SNO-proteins are formed. Therefore, being able to identify which mechanism is responsible for modifying which cysteines will provide us with a greater

understanding of how to regulate this process. To this end, **Chapter 3** describes a novel proposed mechanism of GSNO-mediated transnitrosation.

Lastly, I explored the proposition that S-nitrosocysteine formation alters the structure of a protein. While hundreds of proteins have been identified as being modified, very few structures of S-nitrosylated proteins exist which offer a structural explanation of the observed alteration in protein functionality. **Chapter 4** describes a comprehensive study beginning with the identification of an S-nitrosylated protein directly involved in the beta oxidation of fatty acids and attempts to unravel the structural consequences of S-nitrosylation in relation to its observed alterations in protein activity.

This body of work illustrates how the development of a global technique has allowed for the generation of several testable hypotheses. **Chapter 5** concludes with a discussion regarding the implications of the results described in the preceding chapters as well as a comprehensive analysis of future works in the field of S-nitrosylation.

CHAPTER 2

STRUCTURAL PROFILING OF ENDOGENOUS S-NITROSOCYSTEINE RESIDUES REVEALS UNIQUE FEATURES THAT ACCOMMODATE DIVERSE MECHANISMS FOR PROTEIN S-NITROSYLATION

By

Paschalis-Thomas Doulias[a,1], Jennifer L. Greene[a,1], Todd M. Greco[a], Margarita Tenopoulou[a], Steve H. Seeholzer[a], Roland L. Dunbrack, Jr.[b], and Harry Ischiropoulos[a,2]

(published in Proceedings of National Academy of Sciences, September 28th, 2010. Volume 107, Issue 39, pages 16958-16963)

[a]Children's Hospital of Philadelphia Research Institute and Department of Pharmacology, Children's Hospital of Philadelphia and University of Pennsylvania, Philadelphia, PA 19104
[b]Program in Molecular Medicine, Fox Chase Cancer Center, Philadelphia, PA 19111, USA
[1]These authors contributed equally to this work

[2]**Address correspondence to:** Harry Ischiropoulos, Stokes Research Institute, Children's Hospital of Philadelphia, 416D Abramson Research Center, 3517 Civic Center Boulevard, Philadelphia, Pennsylvania, 19104-4318, USA. Phone: (215) 590-5320; Fax: (215) 590-4267; E-mail: ischirop@mail.med.upenn.edu.

2.1 Abstract

S-nitrosylation, the selective posttranslational modification of protein cysteine residues to form S-nitrosocysteine, is one of the molecular mechanisms by which nitric oxide influences diverse biological functions. In this study, unique MS-based proteomic approaches precisely pinpointed the site of S-nitrosylation in 328 peptides in 192 proteins endogenously modified in WT mouse liver. Structural analyses revealed that S-nitrosylated cysteine residues were equally distributed in hydrophobic and hydrophilic areas of proteins with an average predicted pKa of 10.01±2.1. S-nitrosylation sites were over-represented in α-helices and under-represented in coils as compared with unmodified cysteine residues in the same proteins ($\chi 2$ test, $P < 0.02$). A quantile–quantile probability plot indicated that the distribution of S-nitrosocysteine residues was skewed toward larger surface accessible areas compared with the unmodified cysteine residues in the same proteins. Seventy percent of the S-nitrosylated cysteine residues were surrounded by negatively or positively charged amino acids within a 6-Å distance. The location of cysteine residues in α-helices and coils in highly accessible surfaces bordered by charged amino acids implies site directed S-nitrosylation mediated by protein–protein or small molecule interactions. Moreover, 13 modified cysteine residues were coordinated with metals and 15 metalloproteins were endogenously modified supporting metal-catalyzed S-nitrosylation mechanisms. Collectively, the endogenous S-nitrosoproteome in the liver has structural features that accommodate multiple mechanisms for selective site-directed S-nitrosylation.

2.2 Introduction

Cysteine S-nitrosylation is a post-translational modification that results from the formal transfer of nitrosonium from a nitrosating agent to a reduced cysteine (S-nitrosation) and is a mechanism by which nitric oxide can regulate important biological processes within a variety of organs and cellular systems (Hess et al. 2005; Whalen et al. 2007; Hara et al. 2005; Cho et al. 2009; Rizzo et al. 2003; Guo et al. 2008). Data gathered from individual proteins have collectively indicated that this reversible and apparently selective post-translational modification regulates protein activity, localization, and stability (Hara et al. 2005; Cho et al. 2009; Rizzo et al. 2003). Despite the considerable biological importance of this post-translational modification significant gaps exist regarding its *in vivo* specificity and origin. The identification of *in vivo* S-nitrosylated proteins has indicated that not all reduced cysteine residues, and not all proteins with reduced cysteine residues, are modified implying a biased selection. Several biological chemistries have been proposed to account for the S-nitrosylation of proteins *in vivo* (Hess et al. 2005; Bosworth et al. 2009; Zhang et al. 2005). Broadly these include: i) oxidative nitrosation by higher oxides of nitric oxide, ii) trans-nitrosation by either small molecular weight nitric oxide carriers such as S-nitrosoglutathione or dinitrosyliron complexes, iii) catalysis by metalloproteins and iv) protein-assisted transnitrosation as elegantly documented for the S-nitrosylation of caspase-3 by S-nitrosothioredoxin (Mitchell et al. 2005; Benhar et al. 2008). With the exception of the protein-assisted trans-nitrosylation and metalloprotein catalyzed S-nitrosylation, which we presume necessitates protein-protein interaction, the other proposed mechanisms are rather non-discriminatory unless the microenvironment of selective cysteine residues in proteins can specifically accommodate these chemical modifications. Therefore structural interrogation of endogenous S-nitrosylated proteins with site specific

identification of the modified cysteine residues could provide valuable insights to appreciate the biological selectivity of this post-translational modification. Attempts to investigate this very important biological question have not been possible largely because of the deficit of datasets of *in vivo* modified proteins (Marino et al. 2010). Previous structural analyses have been attempted using limited data sets or by including all sites of modification identified after exposing tissues or cells to S-nitrosylating agents (Marino et al. 2010). However, as the authors of these articles have indicated these sites of modification represent putative sites but not necessarily those modified *in vivo* (Marino et al. 2010). We employed organomercury reagents that react directly, efficiently and specifically with S-nitrosocysteine and thus enable the precise identification of S-nitrosocysteine containing peptides and independently S-nitrosylated proteins to assemble the *in vivo* S-nitrosocysteine proteome of the mouse liver. Using bioinformatic tools we then interrogated this enriched endogenous S-nitrosocysteine proteome to define the biochemical, biophysical and structural environment of the cysteine residues modified by S-nitrosylation, elements that might inform on how specificity of S-nitrosylation is achieved.

2.3 Materials and Methods

Chemicals and Reagents. All HPLC solvents were purchased from Burdick and Jackson, and unless stated all other reagents were purchased from Sigma-Aldrich (St. Louis, MO). Mercury/PEG/biotin compound was designed by us and synthesized by SoluLink (San Diego, CA). Mercury resin was synthesized as described in Supplementary Methods. Mouse monoclonal antibodies against Hsp70 and GAPDH were purchased from Stressgen (Ann Arbor, MI) and Abcam (Cambridge, MA) respectively. Rabbit polyclonal antibody against very long chain specific acyl-CoA dehydrogenase (VLCADH) was obtained from Santa Cruz (Santa Cruz, CA).

Isolation and preparation of mouse liver protein homogenates for capture of S-nitrosylated proteins. All mouse studies were reviewed and approved by the Institutional Animal Care and Use Committee of the Children's Hospital of Philadelphia Research Institute. Wild type or *Nos3*^{tm1Unc} (eNOS$^{-/-}$) C57BL/6J adult mice were obtained from Jackson Laboratories (Bar Harbor, ME). Mice were anesthetized by CO_2 and perfused through the left ventricle. Intact livers were collected, immediately frozen in liquid nitrogen and stored at -80 °C until use. Liver tissues were homogenized in preparation for proteomic analysis as described in Supplementary Methods online.

Capture of S-nitrosylated proteins using organomercury resin (MRC). MRC solid-phase capture columns were prepared and activated as described in Supplementary Methods. Protein homogenates were loaded onto activated MRC columns, and incubated under stationary conditions for 1h at RT. Next, the columns were extensively washed followed by elution of the bound proteins under reducing conditions. Samples were concentrated 500-fold and analyzed by GeLC-MS/MS analysis as described below and in the Supplementary Methods.

Labeling and affinity capture of S-nitrosylated proteins using organomercury-polyethyleneglycol-biotin (mPEGb). Livers lysates were prepared and then captured by mPEGb compound as described in the Supplementary Methods. After capture, biotinylated proteins were precipitated with 3 volumes of acetone and protein concentration was determined by the BCA assay. Equal protein amounts were incubated with washed neutravidin-agarose beads for 2h at RT with gentle rocking. The supernatant was discarded and the beads were extensively washed. Bound proteins were then eluted under reducing conditions for 20 min at RT under gentle rocking. Samples were concentrated 25-fold and analyzed by gel electrophoresis liquid chromatography-mass spectrometry analysis as described below and in the Supplementary Methods.

Protein digestion and neutravidin affinity peptide capture. For neutravidin affinity capture of biotinylated peptides, S-nitrosylated proteins were labeled with mPEGb, precipitated and resuspended into ammonium bicarbonate containing 0.1 % SDS. Equal amounts of proteins were transferred to Ultra-free MC 10kDa cut-off filters (rinsed with methanol and washed with water) and incubated with trypsin (1:100 enzyme:protein ratio) in the dark for 16h at 37 ^{o}C. Biotinylated peptides were recovered by centrifugation of the filters and incubated with neutravidin beads for 2 hours at RT with gentle rocking. Beads were then extensively washed and peptides were released by reduction of the mercury-thiol bond with 3 % performic acid. Eluted peptides were reduced in volume by Speedvac to < 5 ul and resuspended in 10 ul of 0.1% formic acid. A volume of 5 ul was analyzed by LC-MS/MS. A detailed protocol is available in the Supplementary Methods.

GeLC-MS/MS analysis. The protein fractions obtained from MRC and mPEGb protein capture methods were analyzed by GeLC-MS/MS as described in the Supplementary Methods online. Peptides obtained from mPEGb peptide capture method were analyzed by LC-MS/MS directly as described in the Supplementary Methods.

Generation and evaluation of SEQUEST peptide assignments. A detailed protocol for the generation and evaluation of SEQUEST peptide assignments is available in Supplementary Methods. See Supplementary Figure 2.2 for an overview of the criteria for SEQUEST peptide assignment evaluation.

Denitrosylation assays. Denitrosylation assay was performed by exposing liver lysates to 150 nM Trx, 150 nM Trx reductase and 100 mM NADPH for 30 min at 37 ^{o}C. Proteins were processed by both MRC and mPEGb protein capture methods, followed by GeLC-MS/MS analysis.

Gene ontology and functional protein analysis. Subcellular localization was determined by either existing UniProt (www.uniprot.org) annotation, while gene ontology classification and analysis was performed by UniProt and FatiGO (www.fatigo.org).

Protein sequence and structural analysis. The unprocessed protein precursors obtained from UniProt (www.uniprot.org) were used for all sequence analyses (see accession numbers in Supplementary Table 2.1). Prediction of consensus S-nitrosylation sequence motifs was examined by motif-x, a linear sequence prediction algorithm). Kyte-Doolittle hydropathy plots were generated for each protein using a window of 13 with hydropathy values greater than zero considered hydrophobic. Three-dimensional protein structures were obtained from the Protein Data Bank (PDB, requiring greater than 50 % homology and conservation of the modified cysteine residue. The predicted pKa's for ionizable cysteine residues were calculated using PROPKA 2.0, while relative residue surface accessibility was calculated by Naccess 2.1.1 (http://www.bioinf.manchester.ac.uk/naccess/).

Statistical analyses. Graphs were constructed and statistical analyses were performed using GraphPad Prism 5 (GraphPad Software, Inc., San Diego, CA). Statistical significance was determined by either paired or unpaired non-parametric two-tailed t-tests using either the Mann-Whitney (unpaired) or Wilcoxon matched pairs test.

2.4 Results and Discussion

Complementary MS-Based Proteomics Identify the Endogenous Liver S-Nitrosocysteine Proteome

The reaction of phenylmercury compounds with S-nitrosocysteine results in the formation of a relatively stable thiol–mercury bond (Saville et al. 1958). Therefore, we used an organomercury resin (MRC) synthesized by conjugation of ρ-amino-

phenylmercuric acetate to N-hydroxysuccinimide–activated Affi-Gel 10 agarose beads and a phenylmercury-polyethyleneglycol-biotin (mPEGb) compound to capture S-nitrosylated proteins and peptides (Fig.S2.1). The method consists of three steps: (i) blocking of reduced cysteine residues with methyl methanethiosulfonate (MMTS), (ii) capture and release of S-nitrosylated proteins or peptides, and (iii) liquid chromatography/tandem MS analysis. β-Mercaptoethanol or performic acid was used to release captured proteins or peptides, respectively. Mild performic acid was used to selectively and quantitatively release the bound peptides and more importantly oxidize cysteine thiols to sulfonic acid, thereby creating a unique MS signature that permits site-specific identification of the modified cysteine residues (Pesavento et al. 2007). Under the workflow used (Fig. S2.1), 100% of cysteine-containing peptides were detected with the sulfonic acid modification.

To further explore this possibility we used the Trx ex vivo denitrosylation assay (Paige et al. 2008) to identify sites of S-nitrosylation that can interact with Trx. Freshly isolated liver homogenates were treated with a Trx system (Trx/Trx-reductase/NADPH). This treatment resulted in a 72% reduction in protein S-nitrosocysteine levels as quantified by chemiluminescence. In comparison with the untreated liver S-nitrosoproteome (Table S2.1), 72 proteins were no longer identified after Trx treatment (Table S2.4). Linear motif analysis revealed two motifs in this subset of S-nitrosylated proteins. The highest-scoring motif had exclusively aspartic acid at position −1, whereas the second motif had exclusively threonine at position +5 (Fig. 2.3E). Notably, both motifs contained charged amino acids at positions before and after the cysteine residue,

consistent with the idea that charged amino acids in S-nitrosocysteine–containing motifs may facilitate interaction with Trx.

To control for the inclusion of false-positive protein S-nitrosocysteine that may result from incomplete blocking of reduced cysteine residues or nonspecific interactions with the resins

during enrichment, pretreatment with UV, DTT, and copper ascorbate (Cu-Asc) reduction or reaction with mercury chloride were used to displace NO before the reaction with the phenylmercury compounds (Fig. 2.1A and Fig. S2.2A). For these experiments, we used mouse liver homogenates with 50 ± 10 pmol protein S-nitrosocysteine per milligram of protein as quantified by reductive chemistries coupled to ozone-based chemiluminescence. Displacement of NO from S-nitrosocysteine residues by pretreatment with UV, DTT, Cu-Asc, or mercury chloride decreased protein S-nitrosocysteine levels by greater than 99% as quantified by chemiluminescence (n = 3) and also eliminated reaction with the phenylmercury compounds (Fig. 2.1A and Fig. S2.2A). On average, only 3% of peptides (Fig. 2.1B) and 5% of proteins (Fig. S2.2B) were identified as false positives (present in untreated and UV-pretreated samples), demonstrating that the method maintains high specificity at each step. This false positive rate compares favorably with the greater than 90% specificity reported for immobilized metal affinity

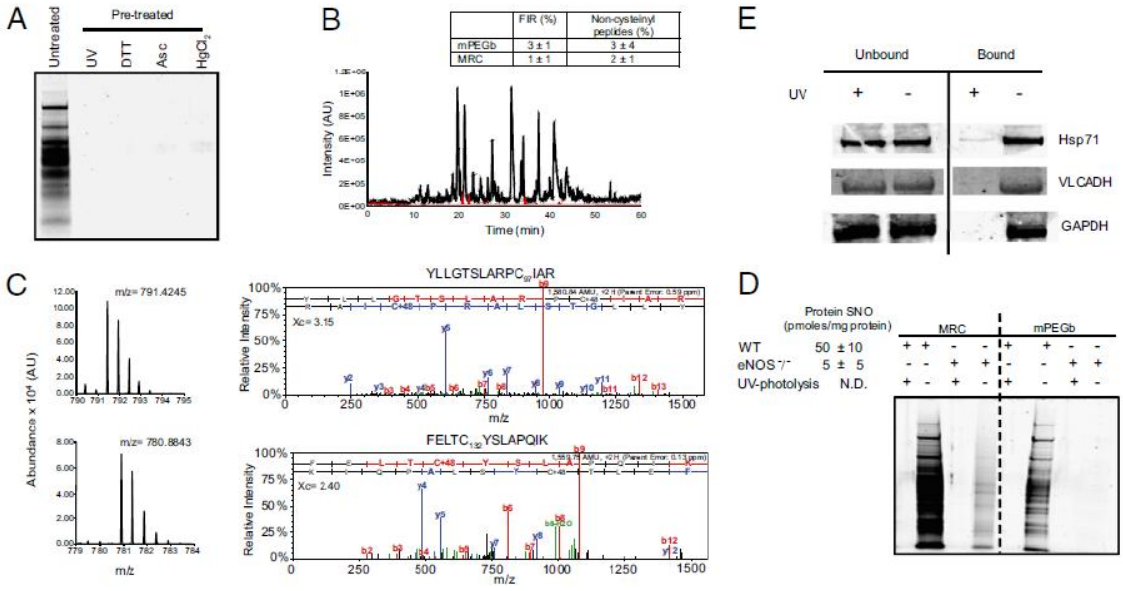

Figure 2.1: Site-specific identification and UV photolysis confirmation of S-nitrosocysteine. (A) Representative short (approximately 2 cm) colloidal blue-stained protein gel of mPEGb protein capture from WT mouse liver that was processed by GeLC-MS/MS analysis. Colloidal blue protein staining of bound fractions from mPEGb protein capture of untreated liver homogenates showed protein enrichment. Pretreatment with UV (for 30 min), DTT (10 mM), Cu-Asc (5 mM Asc/copper 0.1 mM), or HgCl2 (20 mM) prevented this capture, demonstrating specificity for protein S-nitrosocysteine. (B) Representative base peak chromatograms from mPEGb peptide capture demonstrates reduction in ion intensity after UV treatment (red) compared with the untreated sample (black). For clarity, the chromatogram corresponding to UV treatment was plotted with a y-axis offset of 1E4. Inset: Average false-positive identification rate (FIR ± SD) from mPEGb and MRC represented the percentage of peptides that were identified in both the UV-treated and untreated samples across three independent biological replicates. Also reported is the percent of noncysteinyl peptides identified (Supplemental Materials and Methods). (C) Representative MS spectra of doubly charged sulfonic acid-containing tryptic peptides, YLLGTSLARPC97IAR (monoisotopic m/z, 791.4256; Top, Left) and FELTC132YSLAPQIK (monoisotopic m/z, 780.8851; Bottom, Left), from argininosuccinate synthase. MS/MS spectra confirmed the sequence and site of sulfonic acid-containing peptides (C+48) from argininosuccinate synthase identified in mouse liver (Supplemental Materials and Methods). MS/MS spectra passed automatic and manual filter criteria (Fig. S2), and were identified with high SEQUEST cross correlation (Xc) scores at ppm mass error. Cys132 has been previously reported as a target of S-nitrosylation in human argininosuccinate synthase (20), whereas the identification of Cys97 corresponded to a previously unidentified site of S-nitrosocysteine formation. (D) Colloidal blue protein staining of bound fractions from MRC and mPEGb enrichment of S-nitrosylated proteins from WT and eNOS−/− mouse livers. UV photolysis demonstrated specificity of the enrichment. The levels of protein S-nitrosocysteine were quantified by reductive chemistries coupled to chemiluminescent based detection (41).

The amount of S-nitrosylated protein captured by mPEGb from eNOS−/− livers (lane 8) was below the limit of detection by colloidal blue staining. (E) Western blot analysis of bound and unbound fractions from WT mouse liver that were processed by MRC protein capture.

chromatography used for the enrichment of phosphopeptides from mouse liver (Villén et al. 2008). Therefore, pretreatment with UV served as negative control throughout based on previous studies that documented the elimination of S-nitrosocysteine without affecting other cysteine modifications (Forrester et al. 2007; Derakhshan et al. 2007). Collectively, these experiments showed that the reaction of protein S-nitrosocysteine with the phenylmercury compounds is specific and efficient and achieved selective identification of the modified residue, the ultimate qualifier for the unambiguous assignment of S-nitrosylated proteins through the inclusion of negative controls.

The ability of the method to reveal endogenous S-nitrosoproteomes was assessed in WT mouse liver homogenates. Initially, three different mouse livers were analyzed independently for protein and peptide capture by using both the MRC and mPEGb approach with 3 mg of starting material. From the three biological replicates, sulfonic acid-containing peptides identified by SEQUEST database searches were pooled and those also present in the UV-pretreated samples were removed. Similarly, all proteins identified by protein capture were pooled (those also identified in the UV-pretreated samples were removed). The use of solid-phase and in-solution–based enrichment approaches was largely complementary, as the number of shared protein identifications between protein capture methods was approximately 50%, whereas each method individually contributed about the same number of unique protein identifications (Table S2.1). As the MRC capture method allows for higher input, site-specific peptide capture

by this method was also performed with the use of 30 mg of liver extract originating from three different mice. The inclusion of these additional biological replicates reduced biological variance and improved the depth of the analysis while maintaining less than 3% false identification rate. Overall by matching sulfonic acid containing peptides with corresponding protein identifications, we precisely pinpointed 328 S-nitrosocysteine–containing peptides in 192 proteins in untreated livers with a high level of confidence (complete list is provided in Table S2.1 and all of the MS/MS spectra from peptide capture can be viewed at http://www.research.chop.edu/tools/msms/spectra.pdf). The depth of this analysis represents a significant advancement versus present methodologies (Paige et al. 2008). The majority of the proteins identified in the current study, 186, corresponded to previously unidentified endogenous targets of S-nitrosylation in the mouse liver, whereas six proteins (GAPDH, hemoglobin, β-tubulin, argininosuccinate synthase, alcohol dehydrogenase, and catalase) have been previously identified as endogenously S-nitrosylated in hepatocytes and other organ systems (Jaffrey et al. 2001; Hao et al. 2006; Hao et al. 2004; López-Sánchez et al. 2008). Proteins were also distributed across a wide range of molecular weights (13–272 kDa) and cellular localization including membrane-associated proteins, demonstrating the efficacy of the method to identify S-nitrosocysteine independent of protein size and location. We selected very long chain specific acyl-CoA dehydrogenase, heat shock cognate 71 protein, for which endogenous S-nitrosylation was not previously described, and GAPDH, which has been known to be S-nitrosylated and independently confirmed their selective enrichment by Western blot analysis after protein capture (Fig. 2.1E).

To further probe the biological specificity of our method while demonstrating its utility for comparison of endogenous S-nitrosoproteomes, we analyzed livers from mice lacking endothelial NO synthase ($eNOS^{-/-}$). Using chemiluminescence-based quantification, a 10-fold decrease in protein S-nitrosocysteine levels of $eNOS^{-/-}$ livers was measured as compared with WT livers. Concomitantly, a reduced reactivity with phenylmercury compounds was observed (Fig. 2.1D). From the $eNOS^{-/-}$ livers, 36 sulfonic acid-containing peptides in 26 proteins were identified (Supplemental Table 2.2), of which 24 were also identified in the WT liver. The data indicate that the majority of the endogenous liver S-nitrosoproteome is dependent on eNOS-generated NO.

S-Nitrosylation Is Implicated in Multiple Metabolic Pathways

Proteomic experiments generate rich, diverse datasets that benefit from computational analysis to extract biologically relevant and potentially novel information. Consequently, functional and ontological analyses were conducted to assist in identifying cellular, molecular, and biological functions in which S-nitrosylation may play a role in the liver. Sixty-five percent of S-nitrosylated proteins were localized to the cytoplasm and mitochondrion, representing a significant enrichment compared with the mouse genome (P=4.9e−34 and P=7.2e−22, respectively; Figure S2.3A). A subset of S-nitrosylated proteins were found to be present in cell membranes, whereas the remaining proteins were distributed across nearly all cellular compartments (Figure S2.3A). Gene ontology analysis revealed that 99 S-nitrosylated proteins had catalytic activity largely composed of oxidoreductases (39%) and transferases (17%; Fig. S2.3B). These functions were also found to be significantly overrepresented (P=1.28e−20 and 3.2e−3, respectively) in the liver S-nitrosoproteome compared with the mouse genome (Al-

Shahrour et al. 2004). This is not surprising, as the molecular functions of S-nitrosylated proteins were assigned to diverse metabolic processes (i.e., amino acid synthesis, energy synthesis, lipid metabolism) that take place within the liver. Analysis of the data has also confirmed the presence of multiple S-nitrosylated cysteine residues in nearly 45% (86 of 192) of the liver S-nitrosoproteome. Poly-S-nitrosylation is present in all top-ranking molecular functions, suggesting that multiple sites of S-nitrosylation in vivo may regulate protein activity. This is in accordance with other known posttranslational modifications such as phosphorylation and lysine acetylation in which poly-phosphorylation and poly-acetylation are considered regulators of protein function and signaling (Olsen et al. 2006; Choudhary et al. 2009). To place these functional assignments into the context of biochemical and molecular signaling pathways, S-nitrosylated proteins were assembled into biological protein interaction and signaling networks (Ingenuity Systems). The analysis was restricted to investigate liver-related pathways. Sixteen S-nitrosylated proteins were significantly clustered in a network that encompassed liver responses to the hormone leptin (Fig. S2.3C). Leptin is an adipocyte-secreted hormone that primarily acts on the central nervous system to regulate energy homeostasis. Leptin also regulates liver metabolism, evident by the significant accumulation of lipids (fatty liver) in mice deficient in leptin (ob/ob) (Halaas et al. 2005; Pelleymounter et al. 1995) or leptin long-form receptor (db/db) (Mohan et al. 2008). The regulation of liver metabolism is attributed to the leptin-dependent repression of liver stearoyl-CoA desaturase-1, the rate limiting step in monosaturated fat biosynthesis (Cohen et al. 2004). In addition, recent data indicate that leptin also regulates liver mitochondrial respiratory chain protein expression, mitochondrial function and structure (Singh et al. 2009), remarkably similar

to the previously recognized regulation of mitochondrial function by NO (Brown et al. 1994; Nisoli et al. 2004). Interestingly, delivery of S-nitroso-N-acetylcysteine by gavage to ob/ob mice prevented the development of fatty liver (de Oliveira et al. 2008). Mice deficient in eNOS also experience abnormal fat deposition in the liver (Schild et al. 2008), which was attributed in part to regulation of mitochondrial fatty acid synthesis and activation of AMP-activated protein kinase (Schild et al. 2008). Moreover, 14 of the 16 proteins in the leptin network (Fig. S2.3C) were absent in eNOS−/− liver S-nitrosocysteine proteome analysis, suggesting a potential relationship between eNOS-derived S-nitrosylation and leptin regulation of fatty acid metabolism. Although it requires further experimentation, the data indicate that S-nitrosylation may be a molecular link between the actions of leptin and NO in liver fatty acid biosynthesis and mitochondrial metabolism. Overall, cellular localization and functional analyses revealed that the S-nitrosylated proteins identified in the liver were largely cytosolic and mitochondrial enzymes that function as oxidoreductases and transferases, which are critical for regulating amino acid, energy, and lipid biosynthesis, and may coordinate the regulation of metabolic pathways by leptin and NO.

Biochemical, Biophysical, and Structural Properties of the Modified Cysteine Residues

This enriched S-nitrosoproteome was interrogated for the structural properties of the modified cysteine residues by using various bioinformatic tools and available crystal structures of proteins. Table 2.1 provides the basic biochemical and biophysical properties of the modified cysteine residues using reduced unmodified cysteine residues in the same proteins as a comparison group. Kyte-Doolittle hydropathy indices in 13-

residue windows were calculated to determine the influence of primary structure of the protein on modified cysteine residues (Figure 2.2A).The average hydropathy index value was calculated to be −0.03 ± 0.69 (n=309) which did not differ significantly when compared with the mean value of the unmodified cysteines within the same proteins (0.10 ± 0.77, n = 1,382). Using crystal structures (Protein Data Bank) and the Propka 2.0 algorithm (Li et al. 2005), the average predicted pKa of 142 cysteine residues S-nitrosylated in vivo was 10.0, which was not significantly different from the average pKa of reduced unmodified cysteine residues in the same proteins (pKa of 9.88). Only 15 modified cysteine residues had predicted pKa values lower than 7.4 (5.66 ± 1.24), indicating that these particular residues may be deprotonated at physiological pH (Figure 2.2B). Secondary structure analysis revealed that S-nitrosocysteine residues were present in β-sheets (28%), helices (40%), and coils (32%). Unmodified cysteine residues within the same proteins were localized primarily

Table 2.1: Biochemical and biophysical properties of S-nitrosylated and unmodified cysteine residues within the same proteins

Variable	S-nitrosocysteine residues	Unmodified cysteine residues
Hydropathy Index	0.03 ± 0.69 (n=309)	0.1 ± 0.77 (n=382)
Predicted pK_a	10.0 ± 2.10 (n=142)	9.88 ± 2.20 (n=559)
Helices, %	40*	29
β-sheets, %	28	32
Coils, %	32#	39
RSA^	71% buried (n=99)	77% buried (n=561)

	29% exposed (n=40)	23% exposed (n=171)

*P < 0.02, #P < 0.01 using unmodified residues as control group.
^Residue surface accessibility (RSA) for cysteine residues was calculated by the accessible surface area normalized
by the accessible surface area of cysteine in the extended tripeptide Ala-Cys-Ala. A value of ≤10% was used as
cutoff to denote a buried cysteine.

in coils (39%) and equally distributed across helices and β-sheets (Table 2.1). Statistical analysis revealed an overrepresentation and underrepresentation of modified cysteines in helices and coils, respectively ($P < 0.02$). None of the cysteine residues found to be S-nitrosylated participate in disulfide bonding in their known structures and none has been reported to date to be modified by glutathiolation and alkylating agents (www.uniprot.org). Furthermore, by using predictive algorithms and literature searches, it was found that less than 20% of the cysteine residues were predicted to be sites of oxidation (Sanchez et al. 2008). These data and analysis indicate that the majority of the in vivo sites of S-nitrosylation represent a unique population of cysteine residues not chemically modified through other biological processes.

S-Nitrosocysteine Residues Are Equally Distributed in Hydrophobic and Hydrophilic Areas of the Proteins

The overall slightly negative hydropathy index (Table 2.1) is not indicative of a trend for S-nitrosylated cysteine residues to localize in hydrophilic regions of the protein. Further inspection of the hydropathy indices of modified cysteine residues revealed that 139 of the 309 cysteine residues reside nearly in hydrophobic regions, whereas 170 of the 309 are located in hydrophilic regions. This observation led us to further examine

whether S-nitrosylated cysteines belong to two distinct populations regarding their hydrophobicity/hydrophilicity. Kernel density estimation revealed that hydropathy indices exhibited a roughly normal distribution (Figure 2.2A, Left), indicating that they corresponded to a single population of cysteine residues. Unmodified cysteine residues within the same proteins also showed a roughly normal distribution as well (Figure 2.2A, Right), indicating that there is no distinction between S-nitrosylated and unmodified cysteine residues within the same proteins to localize in hydrophobic or hydrophilic areas of proteins. Previous studies have indicated that S-nitrosylation is favored in hydrophobic regions of the proteins (Nedospasov et al. 2000), presumably because of the increased localized concentration of NO-derived oxides, which may provide a suitable microenvironment for the S-nitrosylation of these cysteine residues. The present data imply that, for a subset of proteins, hydrophobicity may serve as a determinant for selective targeting of cysteine residues for S-nitrosylation.

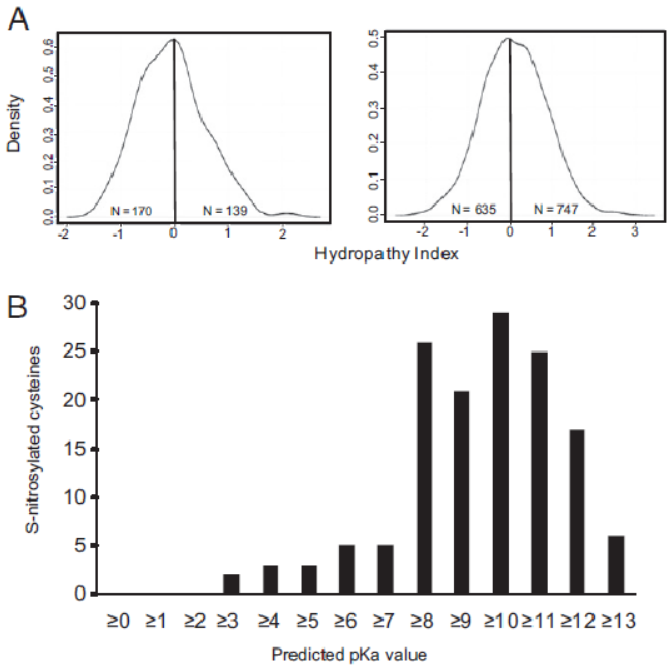

Figure 2.2: Hydropathy index and pKa values of S-nitrosylated residues. (A) Kernel density plot of hydropathy indices for S-nitrosocysteine (Left) and unmodified cysteine residues (Right). Hydropathy index was calculated for all S-nitrosylated (n = 170 hydrophilic, n = 139 hydrophobic) and unmodified (n = 635 hydrophilic, n = 747 hydrophobic) cysteine residues within a 13 amino acid window, with a negative value indicating hydrophilicity. (B) Predicted pKa value for each S-nitrosylated cysteine was calculated from the experimental structures and the distribution was represented as a histogram.

S-Nitrosylation Occurs on Cysteine Residues Adjacent to Flexible Regions Within the Protein

To further explore the location of S-nitrosylated cysteine residues in protein secondary structure, the frequency of secondary structures for flanking residues (positions −10 to +10) was calculated and compared with the respective frequencies of the unmodified cysteine residues using the $\chi 2$ test. A shift in secondary structure mainly from coils to helices was observed over the range of positions from −6 to 0 ($P < 0.05$), consistent with the presence of the majority of S-nitrosocysteine residues in α-helices (Figure 2.3A). Moreover, a 10% increase in the frequency of coils from positions 0 to +3 ($P < 0.001$) concomitant with a reduction in β-sheet frequency ($P < 0.001$) indicative of a change in secondary structure was observed C-terminal from the modified cysteine residues. Unmodified cysteine residues within the same proteins were localized primarily in coils and with lower frequency in β-sheets and helices (Fig. S2.4A). Moreover, the frequency of coils did not change significantly across all flanking residues (−10 to +10), indicating that shifts in secondary structure were only between helices and β-sheets. Collectively, these data demonstrate that modified cysteine residues are predominantly present in secondary structures of proteins which may facilitate site-directed S-nitrosylation by protein-protein interactions.

Surface Accessibility of S-Nitrosocysteine Residues

The relative residue surface accessibility (RSA) for all cysteines (modified and unmodified) within the S-nitrosoproteome was calculated with Naccess 2.1.1 using the radius of a water molecule (1.4 Å2) as a probe (Lee et al. 1971). Ninety-nine S-nitrosylated residues (71%) were calculated with an RSA of 10% or lower, indicating that those residues were not accessible to the solvent, whereas the remaining 40 modified cysteines (29%) had a relative RSA greater than 10%, meaning they were solvent-accessible. Unmodified cysteines within the same proteins exhibited similar distribution between buried (77%) and solvent-accessible residues (23%). A quantile–quantile probability plot was used to determine if there was enrichment for exposed or buried cysteines within the modified versus the un-modified group of cysteine residues (Figure 2.3C). To produce this plot, the RSA values of modified and unmodified cysteine residues were sorted and values of RSA for each percentile were plotted against each other (i.e., RSA of smallest 1% of modified cysteine residues vs. RSA of smallest 1% of unmodified cysteine residues, smallest 2% vs. smallest 2%). The plot demonstrates that

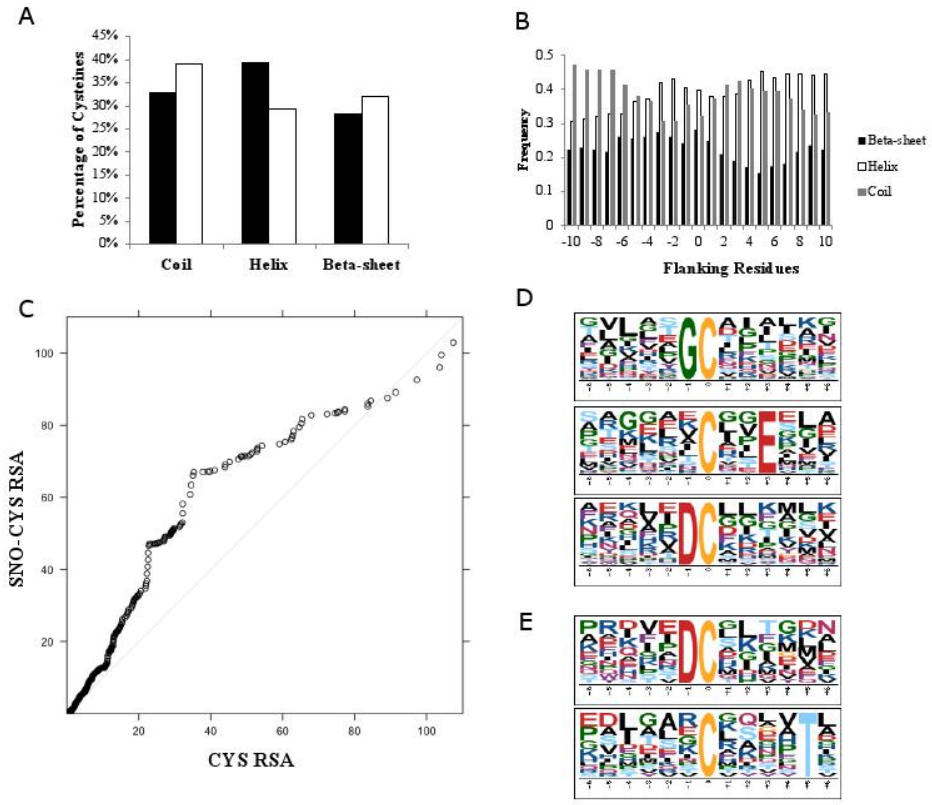

Figure 2.3: Analysis of primary sequence, distribution in secondary structures, and surface accessibility of S-nitrosylated cysteine residues. (A) The frequency of S-nitrosocysteine (n = 142; black bars) and unmodified cysteine residues (n = 473; white bars) within the same proteins in different secondary structures was calculated using the available crystal structures. (B) Distribution of residues flanking S-nitrosylated cysteines in secondary structures. SNO-cysteines are located at position 0 and the frequency for 10 residues upstream (−10) and 10 residues downstream (+10) was calculated as described earlier. (C) Quantile–quantile plot of relative RSA for S-nitrosylated (x axis) versus unmodified (y axis) cysteine residues. RSA values were calculated from the biological assemblies defined by PISA (42) for available crystal structures. (D) Top three scoring sequence motifs for residues flanking S-nitrosylated cysteine residue. Note the presence of charged as well as aliphatic amino acids able to "accommodate" protein and small-molecule binding. (E) Top two sequence motifs assigned to the residues sensitive to Trx system.

S-nitrosocysteine residues have a distribution skewed toward larger surface-accessible areas than unmodified cysteine residues within the same proteins. In addition, 70% of S-nitrosylated cysteine residues within 6 Å were surrounded by negatively or positively

charged amino acids that had their side chains pointed away from cysteine thiol groups. Although the presence of charged residues in the vicinity of the modified residues did not impact their predicted pKa, it may facilitate site specific modification by accommodating protein or S-nitrosoglutathione association. This is in agreement with findings of Mitchell et al., who demonstrated that charged residues near cysteine 73 were required for interaction and transnitrosylation of procaspase-3 (Mitchell et al. 2007). Accordingly, the presence of cysteine residues in highly exposed areas of proteins and in proximity to charged amino acids suggests a protein or small molecule transnitrosation assisted mechanism of S-nitrosylation.

Metal Catalyzed S-Nitrosylation

Studies exploring the S-nitrosylation of proteins in cells indicated that more than 50% of the cellular formation of protein S-nitrosocysteine is derived by dinitrosyliron complexes (Bosworth et al. 2009). Within the liver S-nitrosoproteome, 13 S-nitrosylated cysteine residues, which are directly involved in the chelation of metal ions, were identified (Table S2.3). Metal ligation may provide site-directed modification of these residues. Alternatively, dinitrosyliron complexes could be stabilized near cysteine residues by interactions with neighboring acidic residues. As stated, more than 70% of the modified cysteine residues are in close proximity (<6 Å) to acidic residues, which could serve as interacting sites for dinitrosyliron complexes. Moreover, 15 metalloproteins were identified as endogenously S-nitrosylated, suggesting a self-catalyzed mechanism of S-nitrosylation similar to the proposed mechanism for the selective S-nitrosylation of hemoglobin (Weichsel et al. 2005). The possibility also exists

that these metalloproteins can catalyze S-nitrosylation of interacting proteins, as has been indicated previously (Weichsel et al. 2005). This will require protein–protein association and, as discussed later, the majority of the S-nitrosylated proteins, either in primary sequence or within the tertiary structure, contain charged amino acids that can provide interactive interfaces for specific transfer of a NO equivalent from a metalloprotein to cysteine residues.

Linear Motifs

To further interrogate structural elements that may distinguish modified cysteines from unmodified within the same proteins, flanking amino acids were examined for the presence of linear motifs using the program Motif-X (Schwartz et al. 2005). The top scoring motif for modified cysteines (n = 37, 12%) had glycine exclusively at position −1 ($P \leq 0.001$) and consisted mostly of hydrophobic residues (Figure 2.3D). Remarkably, the second (n = 31, 10%) and third (n=25, 8%) top scoring motifs had negatively charged amino acids exclusively at positions +3 and −1, respectively ($P \leq 0.001$; Figure 2.3D). The same analysis for unmodified cysteines within the same proteins revealed top sequence motifs lacking negatively charged amino acids flanking cysteine residues (Fig. S2.4B), indicating that specific elements of the primary structure are required for a cysteine to be S-nitrosylated in vivo. These motifs could serve as scaffolds for protein and small molecule binding such as thioredoxin (Trx) or S-nitrosoglutathione. To further explore this possibility we used the Trx ex vivo denitrosylation assay (Paige et al. 2008) to identify sites of S-nitrosylation that can interact with Trx. Freshly isolated liver homogenates were treated with a Trx system (Trx/Trx-reductase/NADPH). This

treatment resulted in a 72% reduction in protein S-nitrosocysteine levels as quantified by chemiluminescence. In comparison with the untreated liver S-nitrosoproteome (Table S2.1), 72 proteins were no longer identified after Trx treatment (Table S2.4). Linear motif analysis revealed two motifs in this subset of S-nitrosylated proteins. The highest-scoring motif had exclusively aspartic acid at position −1, whereas the second motif had exclusively threonine at position +5 (Figure 2.3E). Notably, both motifs contained charged amino acids at positions before and after the cysteine residue, consistent with the idea that charged amino acids in S-nitrosocysteine–containing motifs may facilitate interaction with Trx.

In conclusion, by using unique, highly specific MS-based proteomic methods, we identified an expanded endogenous S-nitrosoproteome from WT mouse liver. Despite that S-nitrosylated cysteine residues had, in general, similar hydropathy distribution and predicted pKa values as nonmodified cysteine residues in the same proteins, closer interrogation of the surrounding primary and secondary structures revealed distinctions that direct site-specific S-nitrosylation of certain cysteine residues. The structural analysis of these proteins also uncovered structural features that can accommodate multiple mechanisms for S-nitrosylation in vivo. In addition, the data also revealed a putative link among leptin, eNOS, and protein S-nitrosylation in the regulation of liver fatty acid metabolism. Overall, the use of global proteomic methods enabled structural and functional characterization of the in vivo S-nitrosocysteine proteome and the formulation of testable new hypotheses that can be explored in the future using targeted approaches.

ACKNOWLEDGMENTS

We thank the Protein Core at the Children's Hospital of Philadelphia Research Institute for their assistance with mass spectrometry, Dr. Santosh S. Venkatesh for assistance with the $\chi 2$ test, Dr. David Schwartz (Solulink Biosciences, San Diego, CA) for the synthesis of organomercury-

polyethyleneglycol-biotin, and Dr. Qi Fang for support with structural analysis. This work was supported by National Institutes of Health Grants AG13966 and HL054926, National Institute of Environmental Health Sciences Center of Excellence in Environmental Toxicology Grant ES013508 (to H.I), and National Institute of General Medical Sciences Award F31GM085903 (to J.L.G.). H.I. is the Gisela and Dennis Alter Research Professor of Pediatrics.

2.5 Supplementary Methods

Affi-Gel-10 mercury resin (MRC). An organomercurial derivative of Affi-Gel-10 N-hydroxysuccinimide-activated agarose gel was synthesized according to the protocol on the Biorad web site (Hercules, CA). One hundred ml of settled Affi-Gel 10 was transferred into a Buchner funnel and washed with 300 ml of anhydrous isopropyl alcohol. Two grams of para-amino-mercuric acetate, dissolved in 30 ml of dimethylformamide, was added to 100 ml of washed Affi-Gel 10 and incubated for 4h at RT with gentle rocking. Unreacted succinimide groups are then blocked with 130 mM ethanolamine for 1h at RT with gentle rocking. Next, the gel slurry is transferred into a Buchner funnel and washed sequentially with 250 ml dimethylformamide and 700 ml of anhydrous isopropyl alcohol. Resin was stored as a 1:1 slurry in anhydrous isopropyl alcohol at 4 ^{o}C and was used within 3 months (Mcdonagh et al. 1976).

Synthesis of mPEG-biotin. Biotinyl (3-{2-[2-(3-amino-propoxy)-ethoxy]-ethoxy}-propyl)-amide (Scheme 2.1) **4**: To a solution of 4,7,10-trioxododecane1,13-diamine (**3**; 30 g; 145 mmol; 9 equiv; Fluka, Scheme 2.1) in anhydrous DMF (40 ml) was added drop

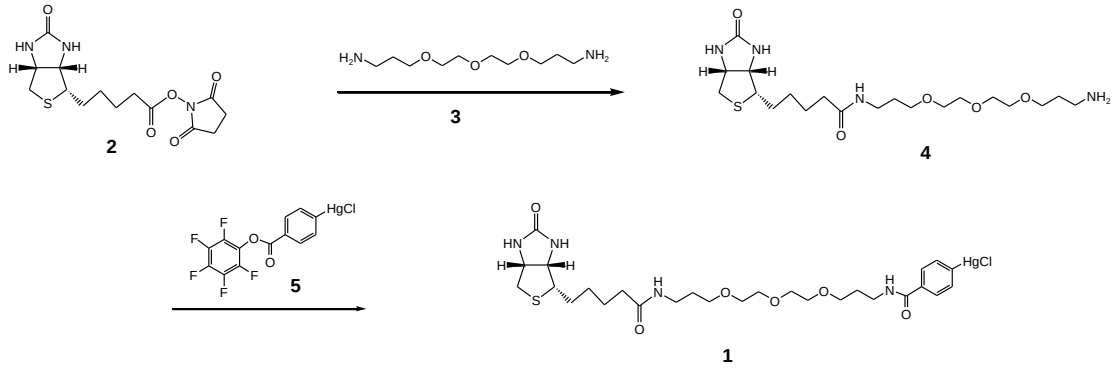

Scheme 2.1: Chemical synthesis of mPEG-biotin compound.

wise a solution of biotin succinimidyl ester (**2**; 5.44 g 16.0 mmol; SigmaAldrich, Scheme 2.1) in 120 ml dry DMF over 30 minutes under argon. The resulting thick white suspension is stirred a further 30 min and the solid that formed was removed by filtration and washed with DMF. The clear filtrate was concentrated and the crude product was precipitated by the addition of diethyl ether. The solids were isolated by filtration and a slurry solution was made and filtered repeatedly with ether (3 times) and ethyl acetate (3 times). The solids were dried under high vacuum overnight to afford the crude 4 (6.05g, 85% yield) as a white sticky solid (Scheme 2.1). The product was purified by flash chromatography using dichloromethane/methanol/ triethylamine (95/5/1).

Biotin/Peg3/(4-chloromercuriobenzamide) (Scheme 2.1, **1)**: To a mixture of 4-chloromercuriobenzoic acid (1.0 g: 2.8 mmol; Spectrum Chemical) in anhydrous DMF (5 ml) was added a solution of pentafluorophenol (0.515 g; 2.8 mmol; SigmaAldrich) and EDC (0.537 g; 2.8 mmol; SigmaAldrich, Scheme 2.1). The reaction mixture was stirred at room temperature for 5 hours until complete as determined by TLC (hexanes/ethyl acetate (1/2)). Triethylamine (0.73 ml ml; 3 equivalents) and a solution of 4 (1.175 g; 1.0 equivalents) in DMF (3 ml) were then added (Scheme 2.1). The reaction was completed after stirring for 1 h as determined by TLC (DCM/MeOH/TEA (90/10/1; UV and dimethylaminocinnaldehyde spray detections). The solvent was removed on the rotavap and the crude product was precipitated by the addition of diethyl ether. The solids were washed repeatedly with ether (3X), ethyl acetate (3X). The desired product 1 (0.57 g:

27.5% yield) was purified by flash chromatography using DCM/MeOH/TEA (90/10/1). Mass spectral analysis revealed a mass of 809 (785.6 + Na); expected mass =785.6.

Quantification of Protein-SNO using reductive chemistries coupled to ozone-based chemiluminescence. Liver lysates were exposed to GSNO for 30 min or left untreated (endogenous levels of protein-SNO), followed by acetone precipitation to remove low molecular weight nitrosothiols. An aliquot of each sample was illuminated under a conventional UV-transilluminator for 7 or 30 min to serve as a negative control. The UV-illuminated, untreated, and GSNO-exposed samples were blocked with MMTS. The reaction efficiency of the phenylmercury reagents was assessed by splitting the GSNO-exposed sample into 3 aliquots. One aliquot was mixed for 1 hr at RT with 2 ml activated mercury resin (MRC), the second was mixed for 1h at RT with 3.5mM mPEG-biotin, and the third was left untreated (GSNO-treated control). The MRC-treated sample was centrifuged at 1000 x g for 5 min and the supernatant was collected. Protein from the mPEG-biotin-treated sample was precipitated with acetone to remove excess mPEG-biotin and resuspended in MES/DTPA/SDS buffer. Total protein was normalized between all samples, and protein S-nitrosocysteine content was quantified by reductive chemistries coupled to ozone-based chemiluminescence as previously described (Fang et al. 1998; Greco et al. 2006).

Isolation and preparation of mouse liver protein homogenates for capture of S-nitrosylated proteins. Isolated livers were homogenized into 3 ml of lysis buffer (250 mM Hepes-NaOH, pH 7.7, containing 1 mM DTPA, 0.1 mM neocuproine, 1 % Triton X-100, and protease inhibitors) on ice using a Teflon pestle and a Jumbo Stirrer (Fisher Scientific). The homogenates were then centrifuged at 13, 000xg for 30 min at 4 ^{o}C. The soluble protein fraction was collected and the protein concentration was determined by the Bradford assay. Each sample consisted of 24 mg of protein in 48 ml of lysis buffer (0.5 mg/ml). Liver protein lysates were supplemented with 100 mM mannitol, 5 mM MMTS and split into equal aliquots (24 ml). One aliquot was illuminated under a conventional UV-transilluminator for 7 min on ice and the other left untreated on ice. As an alternative to UV photolysis, negative controls were generated by treatment with 10

mM DTT for 30 min at 37 ^{o}C unless otherwise mentioned. Next, samples were precipitated by the addition of 3 volumes of acetone for 20 min at -20 ^{o}C followed by centrifugation at 3,000xg for 10min at 4 ^{o}C. Pellets were then washed twice with 1ml of cold acetone, solubilized in 24 ml blocking buffer (250 mM HEPES-NaOH, pH 7.7, containing 1 mM DTPA, 0.1 mM neocuproine, 2.5% SDS, and 20 mM MMTS), and incubated for 30 min at 50 ^{o}C with frequent vortexing. Following blocking, excess MMTS was removed by protein precipitation with 3 volumes of acetone for 20 min at -20 ^{o}C followed by centrifugation at 3000xg for 10min at 4 ^{o}C. Protein pellets were resuspended into 5 ml of blocking buffer (without MMTS) per sample and precipitated as described above. Protein pellets were then resuspended in 1.6 ml of loading buffer (250 mM MES, 1 mM DTPA, pH 6.0, 1% SDS) and aliquoted into 0.8 ml for analysis by organomercury resin and 0.8 ml for analysis by organomercury-polyethyleneglycol-biotin-based enrichment, as described below. Both protein capture methods were performed in parallel and uninterrupted up to the point of Colloidal blue gel staining (see GeLC-MS/MS analysis below).

Capture of nitrosylated proteins using organomercury resin (MRC). MRC solid-phase capture columns were prepared as follows: 4 ml of gel slurry was added to disposable polypropylene columns and washed with 3 bed volumes of isopropanol. Next the resin was washed with 6 bed volumes of H_2O. Then, the resin was activated by washing with 40 ml of 0.1 M $NaHCO_3$, pH 8.8, and then equilibrated by washing with 40 ml of 50 mM MES, pH 6.0, containing 50 mM NaCl, and 1 mM DTPA. Blocked protein lysates (0.4 ml), prepared as described above, were diluted to 1.5 ml with loading buffer, applied to activated MRC columns and incubated under stationary conditions for 1h at RT. Next, the columns were washed with 10 bed volumes of 50 mM Tris-HCl, pH 7.4, containing 300 mM NaCl, 1 % SDS, followed by 10 bed volumes of the same buffer except containing 1 % Triton X-100 instead of SDS. Columns were washed with 5 bed volumes of 50 mM Tris-HCl, pH 7.4, containing 50 mM NaCl, followed by elution of the bound proteins with 10 ml of the same buffer containing 50 mM β-mercaptoethanol. Samples were concentrated 500-fold and analyzed by GeLC-MS/MS analysis.

On-column protein digestion (MRC peptide capture). Blocked protein lysates (0.8 ml) were adjusted to the volume of the resin bed using loading buffer and applied to activated MRC columns (as described above) and incubated under stationary conditions for 1h at RT. Next, the columns were washed with 20 bed volumes of 50 mM Tris-HCl, pH 7.4, containing 300 mM NaCl, 0.5 % SDS, followed by 20 bed volumes of the same buffer, except containing 1 % Triton X-100 instead of SDS and with 1M urea. Columns were then washed with 20 bed volumes of deionized water, followed by 2 bed volumes of 0.1M ammonium bicarbonate. Lysates were incubated with 1 bed volume of 0.1M ammonium bicarbonate containing trypsin (5 μg) in the dark for 16h at RT. The resin was washed with 20 volumes of 1 M ammonium bicarbonate, pH 7.4, containing 300 mM NaCl, followed by 20 volumes of the same buffer without NaCl. Columns were then washed with 20 volumes of 0.1 M ammonium bicarbonate followed by 50 volumes of deionized water. To elute bound peptides, the resin was incubated with 1 bed volume of performic acid in water (produced by reacting 1.0 M formic acid with 0.8 M H_2O_2 for 30 min in the dark) for 30 min at RT. Eluted peptides were recovered by washing the resin with 1 bed volume of deionized water. The volume is then reduced by Speedvac to < 5 μl and adjusted to 10 μL with 0.1% formic acid. Eluted peptides (5 μl) were analyzed by LC-MS/MS as described below.

Labeling and affinity capture of S-nitrosylated proteins using organomercury-polyethyleneglycol-biotin (mPEG-biotin). Blocked protein lysates (0.8 ml) were adjusted to 3.5 mM mPEG-biotin (50 mM mPEG-biotin stock in DMSO) and incubated at RT for 1h with gentle rocking. Biotinylated proteins were split into 2 equal aliquots (one for protein capture, one for peptide capture) and precipitated with 3 volumes of acetone. Protein pellets for mPEG-biotin protein capture were resuspended in 0.2 ml of 25 mM HEPES-NaOH, pH 7.7, containing 0.1 mM DTPA, 0.01 mM neocuproine, and 0.1 % SDS. Protein pellets for mPEG-biotin peptide capture were resuspended in 0.5 ml of 0.1M ammonium bicarbonate containing 0.1 % SDS and immediately processed as described below. Protein concentration of mPEG-biotin protein capture samples were determined by the BCA protein assay and then adjusted to 0.8 ml with 25 mM HEPES-NaOH, pH 7.7, containing 0.1 mM DTPA, 0.01 mM neocuproine. Equal protein amounts

were incubated with washed neutravidin beads (200 μL of slurry per mg of protein washed with 25 mM HEPES-NaOH, pH 7.7, containing 0.1 mM DTPA and 0.01 mM neocuproine) for 2h at RT under gentle rocking. Samples were centrifuged at 800xg for 4 min and then the unbound fraction was removed. Beads were washed with 10 volumes of 50 mM Tris-HCl, pH 7.4, containing 300 mM NaCl and 1 % Triton X-100 followed 10 volumes of 50 mM Tris-HCl, pH 7.4, containing 50 mM NaCl. Bound proteins were eluted with 0.5 ml of 50 mM Tris-HCl, pH 7.4, containing 50 mM NaCl and 100 mM β-mercaptoethanol for 20 min at RT under gentle rocking. Samples were centrifuged at 1000xg for 4 min and the supernatant (eluted peptides) were recovered. This step was repeated to ensure removal of neutravidin-agarose beads. Samples were concentrated 25-fold and analyzed by GeLC-MS/MS analysis.

Protein digestion and mPEG-biotin-neutravidin affinity peptide capture. The protein concentration of mPEG-biotin-labeled proteins (0.5 ml) (prepared above) was determined by the BCA assay and equal amounts of proteins were transferred to Ultra-free MC 10kDa cut-off filters (previously rinsed with methanol and washed with water) and incubated with trypsin (1:100 enzyme:protein ratio) in the dark for 16h at 37 ^{o}C. The following day if densitometric analysis of Colloidal blue-stained gel was satisfactory (see *GeLC-MS/MS analysis* below), samples were then passed through the filters and the filtrate containing the biotinylated peptides was recovered and incubated with neutravidin beads (200 μL slurry per mg of initial protein; washed with 10 volumes of 0.1 M ammonium bicarbonate) for 2 hours at RT under gentle rocking. Samples were centrifuged at 1000xg for 4 min and the unbound fraction was removed. The beads were washed 4 x 2.5 volumes of 1 M ammonium bicarbonate containing 50 mM NaCl, 4 x 2.5 volumes of 1 M ammonium bicarbonate, 2 x 2.5 volumes of 0.1 M ammonium bicarbonate, and finally 2 x 5 volumes of deionized water. Between each wash beads were rocked for 2 min and centrifuged at 1000xg for 1 min. Bound peptides were eluted with 0.5 ml of performic acid in water (produced by reacting 1.0 M formic acid with 0.8 M H_2O_2 for 30 min in the dark) for 30 min at RT with gentle rocking. Samples were centrifuged at 1000xg for 5 min and supernatant (eluted peptides) were recovered. This step was repeated to ensure removal of neutravidin-agarose beads. Samples were reduced

in volume by Speedvac to < 5 μl and adjusted to 10 μl with Millipore water. Eluted peptides (5 μl) were analyzed by LC-MS/MS as described below.

GeLC-MS/MS analysis. The protein fractions obtained from MRC and mPEG-biotin protein capture methods were analyzed by GeLC-MS/MS. For each treatment condition described above, the proteins were mixed with 6X Laemmli sample buffer and equal volumes (20 μl) were loaded on NuPAGE 10% Bis-Tris gels (Invitrogen, Carlsbad, CA). Proteins were electrophoresed in MOPS running buffer for approximately 1 cm and visualized by Colloidal blue (Invitrogen, Carlsbad, CA). Visual inspection and densitometric analysis was performed to verify that the intensity of UV-treated samples were less than 90% of the untreated samples, otherwise samples were not processed. Stained gels can be immediately processed by in-gel trypsin digestion or stored in 2 % acetic acid for up to 1 month. In-gel digestion with trypsin was performed as previously described except each lane was cut into 3 slices and individually digested with trypsin. Tryptic peptide digests were analyzed by either an LTQ linear ion trap (IT) or hybrid LTQ-Orbitrap mass spectrometer (Thermo Electron, San Jose, CA) coupled to an Eksigent 2D LC system (Eksigent Technologies, Livermore, CA) and autosampler. Buffers A and B were 0.1 % formic acid/1 % methanol and 80% acetonitrile/0.1 % formic acid/1 % methanol, respectively. Peptides were loaded isocratically onto a C_{18} trap column (75 um i.d. x 25 mm; New Objective Proteopep 2) at a flow rate of 1 μl per minute in 2% B. Peptides were then eluted onto a C_{18} analytical column (75 um i.d. x 150 mm; New Objective Proteopep 2). A linear gradient was then initiated at a flow rate of 300 nL per minute for 90 min from 3 - 40% B. The mass spectrometer was set to repetitively scan from 375 to 1600 m/z followed by data-dependent MS/MS scans on the five most abundant ions with dynamic exclusion enabled.

Generation and evaluation of SEQUEST peptide assignments. DTA files were generated from MS/MS spectra extracted from the RAW data file (intensity threshold of 2500 for protein capture and 1000 for peptide capture approaches; minimum ion count of 50) and processed by the ZSA and Correction algorithms of the SEQUEST Browser program. DTA files were submitted to Sorcerer-SEQUEST (ver. 4.0.3, rev 11; Sagen Research,

San Jose, CA) using the following parameters: Database searching was performed against a Uniprot database (Release 12.7; 1/2008) containing *Mus musculus* sequences from Swiss-Prot plus common contaminants, which were then reversed and appended to the forward sequences (29, 294 sequences). The database was indexed with the following parameters: mass range of 600 – 3500, tryptic cleavages with a maximum of 1 missed cleavage and static modifications of cysteine by carboxyamidomethylation (+57 amu) for in-gel digestion or by sulfonic acid (+48 amu) and methionine sulfone (+32 amu) for peptide affinity capture. The DTA files were searched with a 2.0 amu or 50 ppm peptide mass tolerance for LTQ or LTQ-Orbitrap, respectively, 1.0 amu fragment ion mass tolerance, and variable modification of methionine (+16 amu) for in-gel digestion, and maximum number of variable modifications of 3.

Potential sequence-to-spectrum peptide assignments generated by Sorcerer-SEQUEST were loaded into Scaffold (version 2.2; Proteome Software, Portland, OR) to validate protein identifications and perform manual inspection of MS/MS spectra as well as to compare protein identifications across experimental conditions. For in-gel digestion experiments, protein identifications were accepted at a threshold of ≥ 99 % protein confidence with ≥ 2 unique peptides at ≥ 90 % confidence. These criteria resulted in an estimated protein false discovery rate (FDR) of ≤ 5 %, as calculated by the number of hits to the reverse protein sequences. For in-solution digestion/peptide affinity capture, empirically defined SEQUEST X_{corr} thresholds were applied to filter peptides IDs with at least one peptide per protein. X_{corr} thresholds were applied to sulfonic acid-containing and non-modified peptides independently so peptide FDR was ≤ 5%. Since one unique peptide per protein was permitted, manual inspection of all MS/MS spectra was performed. The criteria for manual inspection were the following: (i) assignment of the majority of fragment ion abundance, (ii) sulfonic acid (+48 amu) modification supported by either y- or b- ions series (≥ 4 consecutive fragments), and (iii) assigned charge state and diagnostic markers, such as N-terminal proline, C-terminal aliphatic amino acids, and loss of H_2O/ammonia consistent with amino acid sequence (Tabb et al. 2006). Cysteine residues that participated in redox cycling and reflect catalytically active residues, e.g. thioredoxins, peroxiredoxins, and glutaredoxins were included, while eight cysteinyl

peptides that were predicted or experimentally determined to form disulfide bonds were excluded. Although these cysteine residues may represent true S-nitrosylation sites as evidenced by previous studies that have documented endogenous S-nitrosocysteine residues that also participate in disulfide bond formation (Guo et al. 2008; Takahashi et al. 2007), a conservative approach was taken.

Denitrosylation assays. Liver homogenates (6mg of protein per condition) were (1) remained untreated (2) exposed to 150nM Trx, 150nM TrxReductase and 100μmM NADPH for 30 min at 37°C (3) exposed to 1mM GSH for 30min at 37 °C. Unreacted reagents was removed by acetone precipitation (20 min at -20 °C) followed by centrifugation at 3000 x g for 10 min at 4 °C. Then, proteins were processed by MRC and mPEG-biotin protein capture approaches and GeLC/MS/MS analysis.

Gene ontology and functional protein analysis. Subcellular localization was determined by either existing UniProt (www.uniprot.org) annotation, while gene ontology classification was provided by UniProt. Functional Analysis identified the biological functions that were most significant was performed using Uniprot and Fatigo (www.fatigo.org).

2.6 Supplemental Figures

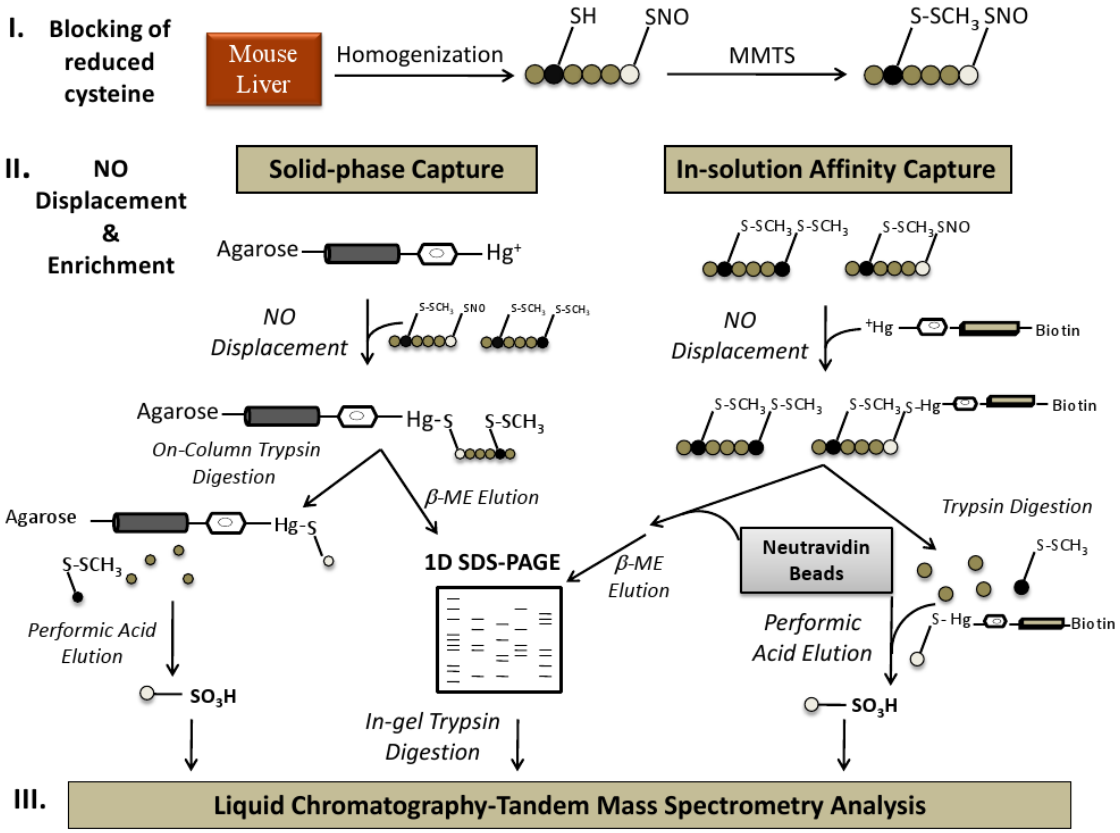

Figure S2.1: Characterization of protein S-nitrosocysteine. (A) The chemical structure of MRC, containing a phenylmercuric acetate functional group tethered to agarose solid-phase resin. (B) The chemical structure of mPEGb, containing a phenylmercury functional group conjugated to biotin by a polyethyleneglycol spacer. (C) The identification and validation of protein S-nitrosocysteine (SNO) was performed by phenylmercury-based capture (PMC). As outlined, SNO-PMC used a complementary solid-phase mercury resin capture (i.e., MRC) and mPEGb. The method is divided into three main steps: (i) homogenization of mouse liver and blocking of reduced protein cysteine, (ii) displacement of cysteine-bound NO by organomercury and/or Neutravidin-based affinity enrichment, and (iii) liquid chromatography-MS/MS analysis. Step I was performed for all analyses. In step II, MMTS-blocked proteins were loaded onto activated solid-phase MRC columns or incubated in-solution with mPEGb. For protein identification, bound proteins from MRC were eluted with b-mercaptoethanol (b-ME), whereas mPEGb-labeled proteins were captured by Neutravidin agarose beads and eluted with b-ME (i). Captured proteins were separated by one-dimensional SDS/PAGE and in-gel trypsin digested. Site-specific identification of S-nitrosocysteine residues was performed by on-column (MRC) and in-solution (mPEGb) peptide capture. From a parallel MRC sample, captured proteins were digested on-column with trypsin, and cysteinyl peptides were eluted by mild performic acid (3%), which cleaved the

phenylmercury mercaptide bond and oxidized the cysteine thiol to sulfonic acid. Also, a parallel mPEGb-labeled protein sample was digested in-solution with trypsin. Then, mPEGb-labeled peptides were enriched by Neutravidin-based capture (ii) and eluted by mild performic acid. Step III (LC-MS/MS peptide analysis) was performed for all approaches, with differences in post-acquisition data analysis between protein and peptide capture approaches (Greco et al. 2006). RAW files generated by LC-MS/MS analysis from protein and peptide capture experiments were processed ExtractMSN to obtain MS2 spectra, searched by Sorcerer-SEQUEST against a concatenated forward-reverse database , and then analyzed by Scaffold (Greco et al. 2006).

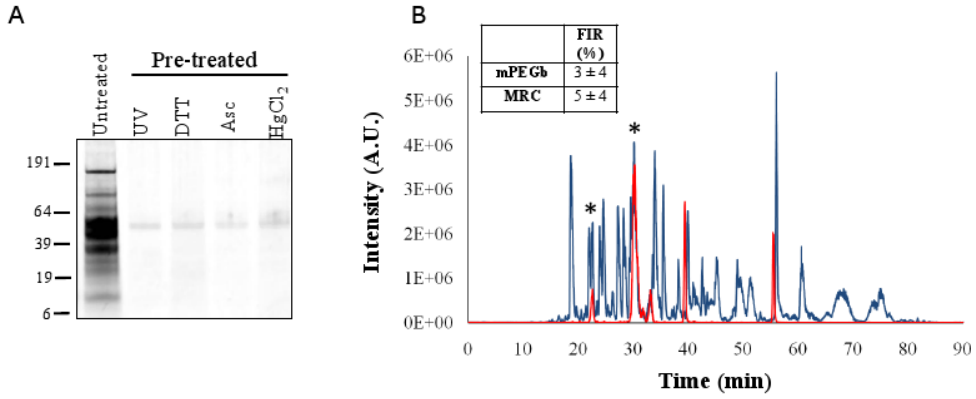

Figure S2.2: GeLC-MS/MS analysis of protein S-nitrosocysteine. (A) Representative short (approximately 2 cm) colloidal blue-stained protein gels of MRC protein capture from WT mouse liver that were processed by GeLC-MS/MS analysis. (B) Representative base peak chromatograms from mPEGb protein capture demonstrate reduction in ion intensity after UV photolysis (red) compared with untreated sample (blue). Chromatograms represent analysis of tryptic peptides derived from a single gel slice. The equivalent gel slice was analyzed from the UV-treated sample. The base peak intensity in the UV-exposed trace (red) corresponded to trypsin autolysis peptides (asterisk). Inset: Average false-positive identification rate (FIR ± SD) represents the percentage of proteins that were identified in both the UV-treated and untreated samples across three independent biological replicates.

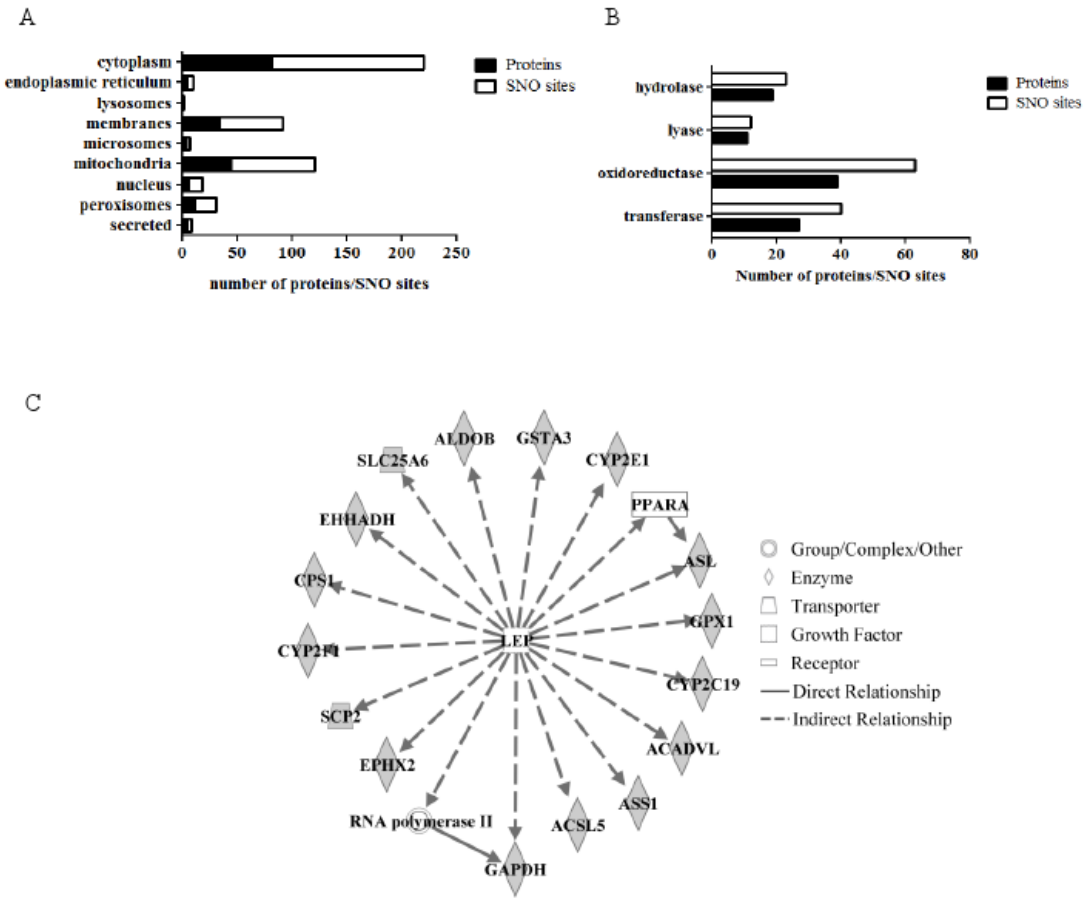

Figure S2.3: Ontological analysis of liver S-nitrosoproteome. (A) Histogram of subcellular localization represented by number of proteins (black bars) and total S-nitrosocysteine (SNO) sites (open bars). The primary cellular localization reported by UniProt was used for proteins with multiple subcellular compartments. (B) Histogram of molecular function gene ontology analysis as a function of number of proteins (black bars) and total S-nitrosocysteine (SNO) sites (open bars). The top four catalytic activities are shown, with oxidoreductase and transferase activities significantly overrepresented in the liver S-nitrosoproteome compared with the entire mouse genome ($P = 1.28e{-}20$ and $3.2e{-}3$, respectively). (C) Sixteen S-nitrosylated proteins from WT liver as determined by Ingenuity Knowledge Base comprised the most significant protein interaction network and clustered around the hormone leptin.

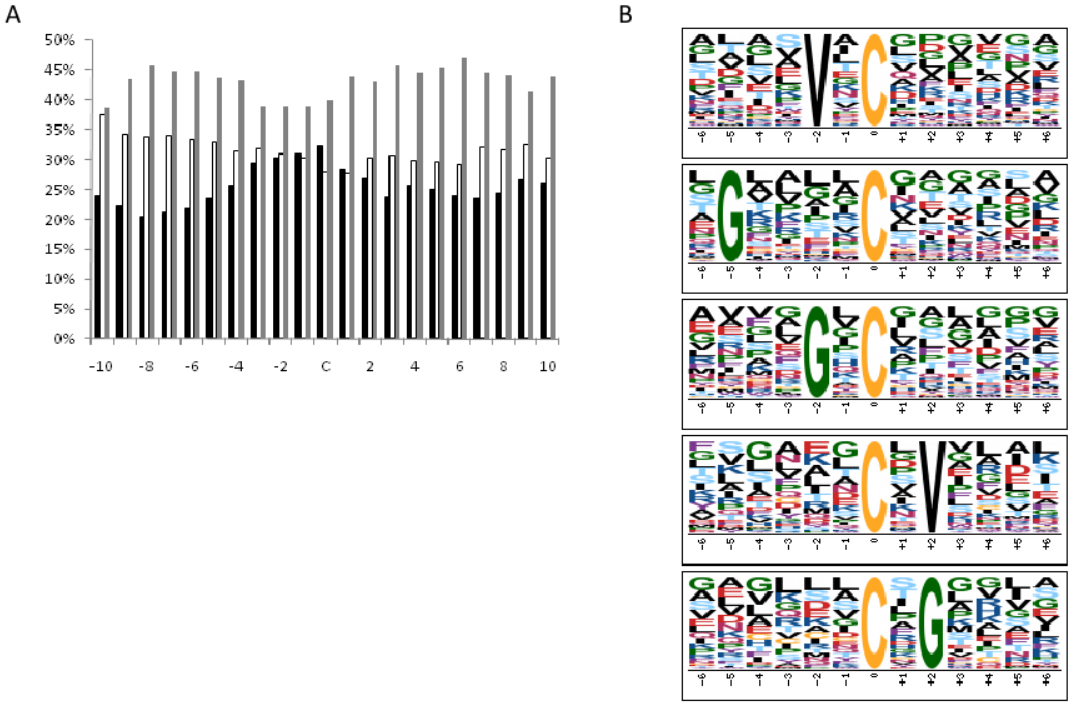

Figure S2.4: Distribution of residues flanking unmodified cysteine residues in secondary structures. (A) Cysteine residues are denoted by Cys (position 0) and the frequency for 10 residues upstream (−10) and 10 residues downstream (+10) was calculated using the available crystal structures. Beta sheets (black bars), helices (white bars), coils (gray bars). (B) Primary sequence motifs for unmodified cysteine residues within S-nitrosylated proteins.

2.7 Supplemental Tables

Supplementary Table 2.1: Endogenously S-nitrososylated proteins in wild type mice liver

Protein name	Uniprot Accession	MW, kDa	Unique Peptides (MRC)[1]	Unique Peptides (mPEGb)[1]	Peptide sequence[2]
1,4-alpha-glucan-branching enzyme	Q9D6Y9	80	3	3	C_{473}VAYAESHDQALVGDK
2-hydroxyacyl-CoA lyase 1	Q9QXE0	64	7	3	GVVPDNNHPNC_{264}VGAAR KLVEQC_{243}SLPFLPTPMGK TMLQNC_{415}LPR
3-hydroxyanthranilate 3,4-dioxygenase	Q78JT3	33	-	5	ASFQPPVC_{23}NKLMHQEQLK
3-ketoacyl-CoA thiolase A, peroxisomal	Q921H8	44	-	5	DC_{177}LTPMGMTSENVAER
3-ketoacyl-CoA thiolase B, peroxisomal precursor	Q8VCH0	44	5	-	DC_{177}LIPMGITSENVAER GC_{218}FHAEIVPVTTTVLNDK VNPLGGAIALGHPLGC_{381}TGAR QC_{123}SSGLQAVANAIAGGIR
10-formyltetrahydrofolate dehydrogenase	Q8R0Y6	99	33	29	MKAVGQSLFGQEVYC_{17}QLRK LRGEDGESEC_{404}VINYVEK SC_{662}ALSNVK TAAC_{587}LAAGNTVVIKPAQVTPLTALK
3-ketoacyl-CoA thiolase, mitochondrial	Q8BWT1	42	17	-	EDC_{179}DRYALQSQQR VVGYFVSGC_{287}DPTIMGIGVPAINGA
40S ribosomal protein S2	P25444	31	-	3	GC_{229}TATLGNFAK
40S ribosomal protein S3	P62908	27	3	5	GLC_{97}AIAQAESLR RAC_{119}YGVLR
40S ribosomal protein S3a	P97351	30	-	3	NC_{96}LTNFHGMDLTR AC_{201}QSIYPLHDVFVR TTDGYLLRLFC_{139}VGFTK
40S ribosomal protein S4, X isoform	P62702	30	-	3	FDTGNLC_{181}MVTGGANLGR LREC_{41}LPLIIFLR
40S ribosomal protein S6	P62754	29	-	3	MKLNISFPATGC_{12}QK
40S ribosomal protein S14	P62264	16	-	2	C_{85}KELGITALHIK

40S ribosomal protein S8	P62242	24	-	3	LLAC$_{174}$IASRPGQC$_{182}$GR
4-hydroxyphenylpyruvate dioxygenase	P49429	45	-	9	HGDGVKDIAFEVEDC$_{103}$DHIVQK
5-oxoprolinase	Q8K010	138	2	-	GHDPSAHVLACFGGAGGQHAC$_{497}$AIAR
60kDa heat shock protein, mitochondrial precursor	P63038	61	11	10	C$_{237}$EFQDAYVLLSEK AAVEEGIVLGGGC$_{442}$ALLR C$_{447}$IPALDSLKPANEDQK
60S ribosomal protein L3	P27659	46	-	4	TVFAEHISDEC$_{114}$K
60S ribosomal protein L12	P35979	18	-	2	C$_{17}$TGGEVGATSALAPK
60S ribosomal protein L17	Q9CPR4	21	-	2	INPYMSSPC$_{144}$HIEMILTEK YSLDPENPTKSC$_{15}$K QC$_{57}$VPFR
60S ribosomal protein L27a	P14115	17	2	-	GVGAC$_{144}$VLVA
60S ribosomal protein L30	P62889	13	2	-	TGVHHYSGNNIELGTAC$_{85}$GK
60S ribosomal protein L7a	P12970	30	-	3	TC$_{199}$TTVAFTQVNSEDKGALAK
Acetyl-CoA acetyltransferase, cytosolic	Q8CAY6	41	3	2	VNIDGGAIALGHPLGASGC$_{360}$R VAPEEVSEVIFGHVLTAGC$_{65}$GQNPTR
Acetyl-CoA carboxylase 1	Q5SWU9	265	3	-	RPGALDPGC$_{812}$VAK
Acetyl-CoA acetyltransferase, mitochondrial precursor	Q8QZT1	45	6	5	IHMGNC$_{193}$AENTAK AIMMASQSLMC$_{138}$GHQDVMVAGGMESMSNVPYVMSR
Acyl-CoA dehydrogenase family member 11	Q80XL6	87	-	2	C$_{546}$KIAIVLGR
Acyl-CoA dehydrogenase family member 9, mitochondrial	Q8JZN5	69	-	3	AYIC$_{617}$AHPLDR FSMGSAVAGMLKKLIELTAEYAC$_{331}$TR
Aconitate hydratase, mitochondrial	Q99KI0	85	11	9	VAVPSTIHC$_{126}$DHLIEAQVGGEK C$_{410}$KSQFTITPGSEQIR VGLIGSC$_{385}$TNSSYEDMGR
Actin, cytoplasmic 1	P60710	42	11	-	C$_{257}$PEALFQPSFLGMESC$_{272}$GLHETTFNSMK
Acyl-coenzyme A synthetase ACSM5, mitochondrial precursor	Q8BGA8	64	2	-	HC$_{342}$LTGGEALNPDVR
Adenosine kinase	P55264	40	3	4	AATFFGC$_{105}$IGIDK TGC$_{352}$TFPEKPDFH

Adenosylhomocysteinase	P50247	48	-	13	SKFDNLYGC$_{195}$R VAVVAGYGDVGKGC$_{228}$AQALR
ADP/ATP translocase 2	P51881	33	-	3	GLGDC$_{160}$LVK
Alanine--glyoxylate aminotransferase 2, mitochondrial precursor	Q3UEG6	57	6	-	TEVNQIHEDC$_{463}$K GAYHGC$_{199}$SPYTLGLTNVGIYK
Alcohol dehydrogenase [NADP+]	Q9JII6	36	4	3	HIDC$_{46}$ASVYGNETEIGEALKESVGSGK KVIC$_{260}$IPK
Alcohol dehydrogenase 1	P00329	40	7	8	VIPLFSPQC$_{98}$GEC$_{101}$R IC$_{104}$KHPESNFC$_{112}$SR VTPGSTC$_{196}$AFGLGGVGLSVILGC$_{212}$K IDGASPLDKVC$_{171}$LIGC$_{175}$GFSTGYGSAVK
Aldehyde dehydrogenase family 8 member A1	Q8BH00	54	5	4	ILC$_{354}$GEGVDQLSLPLR ITQLSAPHC$_{347}$K
Aldehyde dehydrogenase X, mitochondrial	Q9CZS1	58	5	-	TIPMDGEHFC$_{171}$FTR
Aldehyde dehydrogenase, cytosolic 1	O35945	55	-	2	KFPVLNPATEEVIC$_{50}$HVEEGDKADVDK
Aldehyde dehydrogenase, mitochondrial precursor	P47738	56	14	14	LLC$_{388}$GGGAAADR
Alpha-aminoadipic semialdehyde dehydrogenase	Q9DBF1	56	3	3	C$_{633}$GGLPAPEHSDNPLR SSVVPVEGC$_{342}$PELPHK GSDC$_{450}$GIVNVNIPTSGAEIGGAFGGEKHTGGGR
Amine oxidase [flavin-containing] B	Q8BW75	58	3	2	LLHDC$_{26}$GLSVVVLEAR
Apoptosis-inducing factor 1, mitochondrial precursor	Q9Z0X1	67	-	5	C$_{255}$LIATGGTPR
Argininosuccinate lyase	Q91YI0	52	7	-	VFGRC$_{307}$AGLLMTLK QTC$_{129}$SKLSALLRVLIGTMVDR
Argininosuccinate synthase	P16460	46	-	19	FELTC$_{132}$YSLAPQIK YLLGTSLARPC$_{97}$IAR
Arginyl-tRNA synthetase, cytoplasmic	Q9D0I9	76	4	3	MLLC$_{638}$EAVAAVMAKGFDILGIKPVQR
Aspartate aminotransferase, mitochondrial precursor	P05202	47	12	9	TC$_{187}$GFDFSGALEDISK VGAFTVVC$_{295}$K NLDKEYLPIGGLAEFC$_{106}$K
ATP synthase subunit alpha,	Q03265	60	16	18	LYC$_{244}$IYVAIGQKR

mitochondrial					
ATP synthase subunit gamma, mitochondrial precursor	Q91VR2	33	3	2	GLC$_{103}$GAIHSSVAK
ATP-binding cassette sub-family D member 3	P55096	75	5	3	NTSLAGAAFLLLC$_{24}$LLHKR
ATP-citrate synthase	Q91V92	120	5	5	GVTIIGPATVGGIKPGC$_{623}$FK KPASFMTSIC$_{835}$DER YIC$_{20}$TTSAIQNR
Betaine--homocysteine S-methyltransferase 1	O35490	45	14	-	QVADEGDALVAGGVSQTPSYLSC$_{131}$K AGASIVGVNC$_{267}$HFDPSVSLQTVK YIGGC$_{299}$C$_{300}$GFEPYHIR AYLMSQPLAYHTPDC$_{256}$GK
Bifunctional aminoacyl-tRNA synthetase	Q8CGC7	170	-	3	VTEAVEC$_{856}$LLSLK
Calcium-binding mitochondrial carrier protein Aralar 2	Q9QXX4	101	14	14	AGQTTYNGVTDC$_{566}$FRK
Carbamoyl-phosphate synthase [ammonia], mitochondrial precursor	Q8C196	165	-	64	VVAVDC$_{225}$GIK C$_{920}$LGLTEAQTR TSAC$_{761}$FEPSLDYMVTK SAYALGGLGSGIC$_{600}$PNKETLIDLGTKA
Carbonic anhydrase 3	P16015	29	-	8	EAPFTHFDPSC$_{182}$LFPAC$_{187}$R TC$_{68}$RVVFDDTYDRSMLR
Calreticulin	P14211	48	7	6	C$_{163}$KDDEFTHLY
Catalase	P24270	60	-	17	SALEHSVQC$_{425}$AVDVKR LC$_{460}$ENIAGHLK
Catechol O-methyltransferase	O88587	29	2	2	GSSSFEC$_{234}$THYSSYLEYMK
Cathepsin B	P10605	37	2	3	GENHC$_{319}$GIESEIVAGIPR
Complement C3	P01027	186	6	3	VELLHNPAFC$_{873}$SMATAK
Corticosteroid 11-beta-dehydrogenase isozyme 1	P50172	32	4	2	C$_{78}$LELGAASAHY EEC$_{241}$ALEIIK
Cystathionine gamma-lyase	Q8VCN5	44	2	-	ISFVDC$_{136}$SK LADIGAC$_{171}$AQIVHK

Cytochrome b-c1 complex subunit 1	Q9CZ13	53	4	-	NALVSHLDGTTPVC$_{410}$EDIGR LC$_{380}$TSATESEVTR
Cytochrome c, somatic	P62897	12	3	-	IFVQKC$_{15}$AQC$_{18}$HTVEK
Cytochrome P450 27, mitochondrial	Q9DBG1	61	-	3	IGC$_{230}$LKPSIPEDTAAFIR
Cytochrome P450 3A11	Q64459	58	5	4	FALMNMKLALTKIMQNFSFQPC$_{469}$K
Cytochrome P450 3A41	Q9JMA7	56	2	-	VMQNFSFQPC$_{469}$QETQPLK
Cytochrome P450 2C50	Q91X77	56	3	4	FIDLVPNSLPHEVTC$_{372}$DIK RIC$_{435}$AGEGLAR DIC$_{51}$QSFTNLSK VQEEARC$_{151}$LVEELRK
Cytochrome P450 2C54	Q6XVG2	56	9	-	FIDLVPNNLPHEVTC$_{372}$DIK
Cytochrome P450 2D10	P24456	57	5	4	RSC$_{446}$LGEPLAR
Cytochrome P450 2E1	Q05421	57	3	-	DVTDC$_{268}$LLIEMEKEK SLDINC$_{261}$PR RVC$_{437}$VGEGLAR EFKLC$_{488}$VIPR
Cytochrome P450 2F2	P33267	56	7	4	DFIDC$_{267}$FLTK PFQLC$_{487}$MHIR RLC$_{436}$LGEPLAR
Cytosol aminopeptidase	Q9CPY7	56	8	3	QVIDC$_{445}$QLADVNNLGK
D-beta-hydroxybutyrate dehydrogenase, mitochondrial	Q80XN0	38	-	5	AILITGC$_{63}$DSGFGFSLAK GFLVFAGC$_{86}$LMK TIQLNVC$_{115}$NSEEVEK
D-dopachrome decarboxylase	O35215	13	-	6	LC$_{24}$AATATILDKPEDR STEPC$_{57}$AHLLVSSIGVVGTAEQNR
Delta-1-pyrroline-5-carboxylate dehydrogenase, mitochondrial	Q8CHT0	62	8	4	FC$_{94}$YADKALLNR LAGEC$_{314}$GGKNFHFVHSSADVDSVVSGTLR
Dimethylaniline monooxygenase [N-oxide-forming] 3	P97501	61	5	-	GTC$_{397}$TLPSVMDMMDDIDEK VLVGLGNSGC$_{197}$DIAAELSHVAQK
Dihydrolipoyl dehydrogenase, mitochondrial precursor	O08749	54	3	2	VC$_{484}$HAHPTLSEAFR
Dihydropteridine reductase	Q8BVI4	26	2	4	GAVHQLC$_{158}$QSLAGK

Dihydropyrimidinase	Q9EQF5	57	7	-	KMLALGITGPEGHELC$_{220}$RPEAVEAEATLR AITIASAVNC$_{242}$PLYVVHVMSK DQTC$_{484}$TPVPVKR
Dihydroxyacetone kinase	Q8VC30	60	7	7	IC$_{382}$TTLIGLEEHLNALDR
Dolichyl-diphosphooligosaccharide--protein glycosyltransferase subunit 1	Q91YQ5	68	6	4	LKTEGSDLC$_{546}$DR VAC$_{478}$ITEQVLTLVNKR
Electron transfer flavoprotein subunit alpha, mitochondrial	Q99LC5	35	4	6	QFSYTHIC$_{109}$AGASAFGK
Electron transfer flavoprotein subunit beta	Q9DCW4	28	5	5	HSMNPFC$_{42}$EIAVEEAVR
Electron transfer flavoprotein-ubiquinone oxidoreductase, mitochondrial	Q921G7	68	7	7	AAQIGAHTLSGAC$_{118}$LDPAAFK VTVFAEGC$_{248}$HGHLAK LQINAQNC$_{585}$VHC$_{588}$K
Elongation factor 2	P58252	95	5	9	STLTDSLVC$_{41}$K DLEEDHAC$_{567}$IPIKK TFC$_{290}$QLILDPIFK C$_{369}$ELLYEGPPDDEAAMGIK
Enoyl-CoA hydratase, mitochondrial	Q8BH95	31	6	5	LVEEAIQC$_{225}$AEK
Epoxide hydrolase 2	P34914	63	13	11	VTGTQFPEAPLPVPC$_{230}$NPNDVSHGYVTVKPGIR
Ester hydrolase C11orf54 homolog	Q91V76	35	2	-	AHIMPAEFSSC$_{226}$PLNSDEAVNK RTGELNFVSC$_{187}$MR
Estradiol 17 beta-dehydrogenase 5	P70694	37	-	14	VC$_{98}$LEQSLK YKPVC$_{188}$NQVEC$_{193}$HPYLNQGK LLDFC$_{206}$R
Fatty acid synthase	P19096	272	-	12	FVFTPHMEAEC$_{1128}$LSESTALQK DC$_{1590}$MLGMEFSGR C$_{1464}$ILLSNLSNTSHAPK
Fatty acid-binding protein, liver	P12710	14	-	9	NEFTLGEEC$_{69}$ELETMTGEK
Formimidoyltransferase-cyclodeaminase	Q91XD4	60	4	2	TVYTFVGQPEC$_{60}$VVEGALHAAR AC$_{438}$ALQEGLR
Fructose-1,6-bisphosphatase 1	Q9QXD6	37	13	10	AQGTGELTQLLNSLC$_{39}$TAIKAISSAVR
Fructose-bisphosphate aldolase B	Q91Y97	39	14	-	C$_{135}$AQYKKDGVDFGK IADQC$_{158}$PSSLAIQENANALAR RAMANC$_{336}$QAAQGQYVHTGSSGAAATQSLFTASYTY

Glutamate dehydrogenase 1, mitochondrial	P26443	61	-	20	IIKPC$_{112}$NHVLSLSFPIR C$_{172}$AVVDVPFGGAKAGVK AC$_{254}$VTGKPISQGGIHGR
Glutathione peroxidase 1	P11352	22	-	8	GLVVLGFPC$_{76}$NQFGHQENGK
Glutathione S-transferase A3	P30115	25	-	3	KPFDDAKC$_{212}$VESAK
Glutathione S-transferase Mu 1	P10649	26	8	7	C$_{174}$LDAFPN
Fumarylacetoacetase	P35505	40	7	-	VGFGQC$_{408}$AGK GEGMSQAATIC$_{315}$R TFLLDGDEVIITGHC$_{396}$QGDGYR
Glutamine synthetase	P15105	42	4	3	RPSANC$_{346}$DPYAVTEAIVR C$_{269}$IEEAIDK LVLC$_{99}$EVFK AC$_{183}$LYAGVK
Glyceraldehyde-3-phosphate dehydrogenase	P16858	36	7	-	VPTPNVSVVDLTC$_{245}$R IVSNASC$_{150}$TTNC$_{154}$LAPLAK
Glycerol-3-phosphate dehydrogenase, mitochondrial	Q64521	81	3	2	C$_{270}$KDVLTGQEFDVR
Glycerol-3-phosphate dehydrogenase [NAD+], cytoplasmic	P13707	38	4	5	C$_{341}$LQNHPEHM
Glycerol kinase	Q64516	61	2	-	C$_{299}$VFSEHGLLTTVAYK
Glycine dehydrogenase [decarboxylating], mitochondrial	Q91W43	113	3	-	C$_{230}$HPQTIAVVQTR TFC$_{763}$IPHGGGGPGMGPIGVK
Glycine N-methyltransferase	Q9QXF8	33	-	5	SFAHLPDC$_{147}$K LSYYPHC$_{247}$LASFTELVR NYDYILSTGC$_{186}$APPGK
Glycogen phosphorylase, liver form	Q9ET01	97	10	14	INMAHLC$_{446}$IVGC$_{450}$HAVNGVAK
Heat shock cognate 71 kDa protein	P63017	71	18	15	GPAVGIDLGTTYSC$_{17}$VGVFQHGK
Heat shock protein 75 kDa, mitochondrial	Q9CQN1	80			IIIHLKSDC$_{263}$KDFASESR
Hemoglobin subunit beta	P02088/ P02089	16	2	4	GTFASLSELHC$_{94}$DK
Homogentisate 1,2-dioxygenase	O09173	50	3	-	YISGFGNEC$_{14}$ASEDPRC$_{21}$PGSLPK SNNGLAVHIFLC$_{138}$NSSMENR QGGFLPGGSLHSAMTPHGPDADC$_{377}$FEK

Hydroxymethylglutaryl-CoA lyase, mitochondrial	P38060	34	2	2	KNANC$_{141}$SIEESFQR LLEAGDFIC$_{307}$QALNR
Hydroxymethylglutaryl-CoA synthase, mitochondrial	P54869	57	-	15	MGFC$_{96}$SVQEDINSLC$_{106}$LTVVQR ALDRC$_{269}$YAAYR MIFHTPFC$_{305}$K
Isocitrate dehydrogenase [NADP], mitochondrial	P54071	51	3	3	C$_{113}$ATITPDEARVEEFKLK DLAGC$_{418}$IHGLSNVK
Kynurenine 3-monooxygenase	Q91WN4	54	2	2	SHC$_{299}$VLMGDAAHAIVPF C$_{139}$IPEEGVLTVLGPDKVPR
L-gulonolactone oxidase	P58710	50	5	3	TYGC$_{19}$SPEMYYQPTSVGEVR DSC$_{360}$YMNIIMYRPYGK
L-lactate dehydrogenase A chain	P06151	36	2	8	DYC$_{84}$VTANSK ITVVGVGAVGMAC$_{35}$AISILMK VIGSGC$_{163}$NLDSAR
Liver carboxylesterase 31	Q63880	63	14	10	DASINPPMC$_{100}$LQDVER
Liver carboxylesterase 31-like precursor	Q8VCU1	63	3	-	DASINPPMC$_{97}$LQDVEK
Long-chain specific acyl-CoA dehydrogenase, mitochondrial	P51174	48	2	3	C$_{166}$IGAIAMTEPGAGADLQGVR LAELKTHIC$_{342}$VTR
Long-chain-fatty-acid--CoA ligase 1	P41216	78	20	18	ALKPPC$_{55}$DLSMQSVEIAGTTDGIRR GIQVSNNGPC$_{109}$LGSR C$_{242}$GVEIISLK GAMITHQNIINDC$_{298}$SGFIK
Long-chain-fatty-acid--CoA ligase 5	Q8JZR0	76	6	3	C$_{226}$GVEMLSLHDAENIGK KPVPPKPEDLSVIC$_{259}$FTSGTTGDPK TAGHVGTPVAC$_{471}$NFVK
Malate dehydrogenase, mitochondrial precursor	P08249	36	6	6	GYLGPEQLPDC$_{89}$LK
Membrane-associated progesterone receptor component 1	O55022	22	4	3	GLATFC$_{129}$LDK
Methylcrotonoyl-CoA carboxylase beta chain, mitochondrial	Q3ULD5	61	3	3	AATGEEVSAEDLGGADLHC$_{267}$R
Methionyl-tRNA synthatase, cytoplasmic	Q68FL6	101	-	2	ILATSFIC$_{789}$TLPAGHR
Microsomal glutathione S-transferase 1	Q91VS7	18	4	3	VFANPEDC$_{50}$AGFGKGENAK

NADPH--cytochrome P450 reductase	P37040	77	5	3	EQGKEVGETLLYYGC$_{566}$R LIHEGGAHIYVC$_{630}$GDAR VHPNSVHIC$_{472}$AVAVEYEAK
Nicotinate-nucleotide pyrophosphorylase [carboxylating]	Q91X91	32	2	3	C$_{111}$SGIASAAATAVEVAR YGLQVGGAAC$_{159}$HR
Non-specific lipid-transfer protein	P32020	59	12	12	ADC$_{495}$TITMADSDLLALMTGK
Ornithine aminotransferase, mitochondrial	P29758	48	-	3	VLPMNTGVEAGETAC$_{150}$K
Peptidyl-prolyl cis-trans isomerase A	P17742	18	7	3	IIPGFMC$_{62}$QGGDFTR
Peroxisomal bifunctional enzyme	Q9DBM2	78	10	13	LC$_{17}$NPPVNAISPTVITEVR
Peroxiredoxin-4	O08807	31	-	4	TRENEC$_{54}$HFYAGGQVYPGEASR
Peroxiredoxin-6	O08709	25	3	4	DFTPVC$_{47}$TTELGR
Peroxisomal carnitine O-octanoyltransferase	Q9DC50	70	3	-	AFVFDVLHEGC$_{210}$LITPPELLR
Peroxisomal coenzyme A diphosphatase NUDT7	Q99P30	27	-	5	IDFDLHDLIPSC$_{223}$ER
Peroxisomal multifunctional enzyme type 2	P51660	79	7	12	NNIHC$_{189}$NTIAPNAGSR IC$_{277}$DFSNASKPQTIQESTGGIVEVLHK
Peroxisomal sarcosine oxidase	Q9D826	44	2	-	TFSDIQDVQILC$_{299}$HFVR C$_{319}$MYTNTPDEHFILDC$_{333}$HPK
Peroxisomal trans-2-enoyl-CoA reductase	Q99MZ7	32	2	-	ELLHLGC$_{43}$NVVIASR
Phenylalanine-4-hydroxylase	P16331	52	5	4	VFHC$_{265}$TQYIR NLADSINSEVGILC$_{445}$HALQK
Phosphate carrier protein, mitochondrial	Q8VEM8	40	4	-	AVEEYSC$_{52}$EFGSMK C$_{272}$AIVSHPADSVVSVLNK
Phosphoglycerate kinase 1	P09411	44	5	3	AAVPSIKFC$_{50}$LDNGAK
Phosphoglucomutase-1	Q9D0F9	62	5	11	LSLC$_{374}$GEESFGTGSDHIR
Plastin-3	Q99K51	70	8	3	VDLNSNGFIC$_{34}$DYELHELFK
Probable D-lactate dehydrogenase, mitochondrial precursor	Q7TNG8	52	5	-	ALALGGTC$_{439}$TGEHGIGLGK
Probable 2-oxoglutarate dehydrogenase	A2ATU0	103	-	2	LVGC$_{393}$AIIHVNGDSPEEVVR

E1 component DHKTD1, mitochondrial					
Probable imidazolonepropionase	Q9DBA8	46	2	-	ELHLSLSATYC$_{189}$GAHSVPK
Probable urocanate hydratase	Q8VC12	74	10	9	AAAIVGC$_{265}$IGVIAEVDKAALVK
Profilin-1	P62962	15	-	4	C$_{128}$YEMASHLR
Propionyl-CoA carboxylase beta chain, mitochondrial	Q8VC12	58	2	-	C$_{92}$ADFGMAADKNKFPGDSVVTGR
Protein disulfide-isomerase A3	P27773	57	-	16	FIQDSIFGLC$_{244}$PHMTEDNKDLIQGK
Protein transport protein Sec23A	Q01405	86			MVQVHELGC$_{180}$EGISK
Protein transport protein Sec61 subunit alpha isoform 1	P61620	52	3	-	FLEVIKPFC$_{13}$VILPEIQKPER
Pyruvate carboxylase, mitochondrial precursor	Q05920	130	24	14	ADFAQAC$_{131}$QDAGVR FC$_{663}$EVAKENGMDVFR DMAGLLKPAAC$_{752}$TMLVSSLR
Regucalcin	Q64374	33	10	10	MEKDEQIPDGMC$_{207}$IDAEGK DYSEMYVTC$_{262}$AR
Retinal dehydrogenase 1	P24549	54	17	18	IGPALSC$_{186}$GNTVVVKPAEQTPLTALHLASLIK
Retinol dehydrogenase 7	O88451	36	2	-	VLAAC$_{60}$LTEK
Ribosome-binding protein 1	Q99PL5	173	10	22	LKELESQVSC$_{1198}$LEK C$_{1136}$EELSSLHGQLK
S-adenosylmethionine synthetase isoform type-1	Q91X83	43	-	4	IC$_{35}$DQISDAVLDAHLK VALEQQSPDIAQC$_{121}$VHLDR TAC$_{377}$YGHFGR
Sarcoplasmic/endoplasmic reticulum calcium ATPase 2	O55143	115	6	6	C$_{560}$LALATHDNPLK NYLEQPGKEC$_{998}$VQPATK
Sarcosine dehydrogenase mitochondrial precursor	Q99LB7	102	-	13	STVC$_{382}$GPESFTPDHKPLMGEAPELR DPLHEELLGQGC$_{498}$VFQER C$_{672}$QLMDSSEDLGMLSIQGPASR
SEC14-like protein 4	Q8R0F9	46	-	2	VC$_{128}$EMLLHEC$_{135}$ELQSQK YNAHMVPEDGSLNC$_{355}$LK
Selenium-binding protein 1	P17563	52	-	10	GPREEIVYLPC$_{31}$IYR C$_{8}$GPGYSTPLEAMK GGSVQVLEDQELTC$_{371}$QPEPLVVK
Selenium-binding protein 2	Q63836	52	-	15	C$_{8}$GPGYPTPLEAMK

					C_{131}NVSNTHTSHC_{141}LASGEVMVNTLGDLQGNGK FLHDPSATQGFVGC_{268}ALSSNIQR GGSVQVLEDQELTC_{371}QPEPLVVK
Sodium/potassium-transporting ATPase subunit alpha-1	Q8VDN2	113	6	7	AC_{663}VVHGSDLK LIIVEGC_{705}QR
Sorbitol dehydrogenase	Q64442	38	6	-	VMIKC_{350}DPNDQNP VLVC_{179}GAGPVGMVTLLVAK
Src substrate cortactin	Q60598	61	2	-	HC_{112}SQVDSVR
Staphylococcal nuclease domain-containing protein 1	Q78PY7	102			EVC_{96}FTIENKTPQGR GIVKMVLSGC_{31}AIIVRGQPR
Succinate dehydrogenase [ubiquinone] flavoprotein subunit, mitochondrial	Q8K2B3	72	10	6	GVIALC_{238}IEDGSIHR TYFSC_{266}TSAHTSTGDGTAMVTR
Sulfite oxidase, mitochondrial	Q8R086	61	6	-	HEVTVTLQC_{265}AGNR LC_{300}DVLAQAGHR
Sulfotransferase 1A1	P52840	34	2	-	LMTGC_{283}DFTFR IPFLEFSC_{82}PGVPPGLETLK
Synaptic glycoprotein SC2	Q9CY27	36	2	-	LC_{18}FLDKVEPQATISEIK
Thioredoxin domain- containing protein-4	Q9D1Q6	47	3	-	VDC_{92}DQHSDIAQR
Thiosulfate sulfurtransferase	P52196	33	7	-	KVDLSQPLIATC_{248}R
Threonyl-tRNA synthetase, cytoplasmic	Q9D0R2	83	5	-	FMADTDLDPGC_{655}TLNKK
Triosephosphate isomerase	P17751	27	-	3	IIYGGSVTGATC_{218}K VSHALAEGLGVIAC_{127}IGEK
Tryptophan 2,3-dioxygenase	P48776	48	9	-	EVLLC_{266}LFDEK
Tubulin beta chain	P68372 (+5)	50	9	2	EIVHIQAGQC_{12}GNQIGAK
Ubiquitin-like modifier-activating enzyme 1	Q02053	118	7	-	YSRPAQLHIGFQALHQFC_{340}ALHNQPPRPR
UPF0465 protein C5orf33 homolog	Q8C5H8	51	3	-	SEGHLC_{181}LPVR
UDP-glucuronosyltransferase 1-1	Q63886	60	-	7	VKNVLLAVSENFMC_{225}R MVFIGGINC_{282}LQK

UDP-glucuronosyltransferase 2B5	P17717	61	-	8	FLSLC$_{128}$KDVVSNK
Uricase	P25688	35	3	6	NGIKHVHAFIHTPTGTHFC$_{141}$EVEQMR NIETFAMNIC$_{95}$EHFLSSFNHVTR
Valyl-tRNA synthetase	Q9Z1Q9	140	8	3	C$_{681}$GEMAQAASAAVTR
Very long-chain acyl-CoA synthetase	O35488	70	11	9	GEVGLLVC$_{427}$KITQLTPFIGYAGGK
Very long-chain specific acyl-CoA dehydrogenase, mitochondrial precursor	P50544	71	11	9	SSAIPSPC$_{238}$GK
Vigilin	Q8VDJ3	142	7	4	RC$_{948}$DIIIISGR
Xanthine dehydrogenase/oxidase	Q00519	146	4	-	C$_{828}$MLDRDEDMLITGGR

Sequence-to-spectrum assignments from three biological replicates were combined in Scaffold. The proteins listed above satisfied three criteria: (1) identified by at least one protein capture method (≥2 unique peptides), (2) confirmed by a sulfonic acid-containing peptide sequence and (3) not identified in the respective UV-exposed samples. Uniprot accession numbers correspond to the full-length unprocessed precursor when available (www.uniprot.org). Additional accessions were listed if the observed peptides could not distinguish between protein isoforms. All the MS/MS spectra from peptide capture can be viewed at http://www.research.chop.edu/tools/msms/spectra.pdf;.

[1]Number of unique peptides identified in protein capture experiment from 3 biological replicates (does not include sulfonic acid-containing peptides). A null value indicates the protein did not meet the threshold criteria and was considered not identified.

[2]Cysteinyl-containing tryptic peptide sequences identified by peptide capture. The indicated cysteine residue(s) was identified as sulfonic acid and corresponds to the unprocessed mouse precursor protein.

Supplementary Table 2.2. Endogenously S-nitrosylated proteins in eNOS$^{-/-}$ mouse liver

Protein name	Uniprot Accession	MW, kDa	Unique Peptides (MRC)[1]	Unique Peptides (mPEGb)[1]	Peptide sequence[2]
40S ribosomal protein S3	P62908	27	4	-	GLC$_{97}$AIAQAESLR[3]
60S ribosomal protein L12	P35979	18	2	4	C$_{17}$TGGEVGATSALAPK[3]
60S ribosomal protein L17	Q9CPR4	21	2	6	QC$_{57}$VPFR[3] INPYMSSPC$_{144}$HIEMILTEK[3]
60S ribosomal protein L24	Q8BP67	18	4	-	C$_{36}$ESAFLSK
Alcohol dehydrogenase 1	P00329	40	4	3	VIPLFSPQC$_{98}$GEC$_{101}$R[3]
Argininosuccinate synthase	P16460	46	2	2	YLLGTSLARPC$_{97}$IAR[3] FELTC$_{132}$YSLAPQIK[3]
ATP synthase subunit gamma, mitochondrial precursor	Q91VR2	33	2	2	GLC$_{103}$GAIHSSVAK[3]
Betaine--homocysteine S-methyltransferase 1	O35490	45	4	-	AYLMSQPLAYHTPDC$_{256}$GK[3] AGASIVGVNC$_{267}$HFDPSVSLQTVK[3] YIGGC$_{299}$C$_{300}$GFEPYHIR[3]
Carbamoyl-phosphate synthase [ammonia], mitochondrial precursor	Q8C196	165	9	7	VVAVDC$_{225}$GIK[3] TSAC$_{761}$FEPSLDYMVTK[3] C$_{920}$LGLTEAQTR[3] GNDVLVIEC$_{1256}$NLR
Catalase	P24270	60	3	4	SALEHSVQC$_{425}$AVDVKR[3] LC$_{460}$ENIAGHLK[3]
Cytochrome P450 2C29	Q64458	56	5	3	VQEEAQC$_{151}$LVEELR FIDLLPTSLPHAVTC$_{372}$DIK IC$_{435}$AGEGLAR
Cytochrome P450 2E1	Q05421	57	3	-	SLDINC$_{261}$PR[3]
Dehydrogenase/reductase SDR family member 1	Q99L04	34	2	-	LAADC$_{177}$AHELR
Dihydroxyacetone kinase	Q8VC30	60	3	-	GLC$_{155}$GTVLIHK
Electron transfer flavoprotein-ubiquinone oxidoreductase, mitochondrial precursor	Q921G7	68	4	-	LQINAQNC$_{585}$VHC$_{588}$K[3]
Elongation factor 2	P58252	95	3	3	C$_{728}$LYASVLTAQPR
Formimidoyltransferase-cyclodeaminase	Q91XD4	60	2	-	AC$_{438}$ALQEGLR[3]

Glyceraldehyde-3-phosphate dehydrogenase	P16858	36	2	-	VPTPNVSVVDLTC$_{245}$R[3]
Iron-sulfur cluster assembly enzyme ISCU, mitochondrial precursor	Q9D7P6	18	3	-	LHC$_{139}$SMLAEDAIK
Isocitrate dehydrogenase [NADP] cytoplasmic	O88844	47	-	2	DLAAC$_{379}$IK
L-lactate dehydrogenase C chain	P00342	36	3	-	VIGSGC$_{163}$NLDSAR
Long-chain-fatty-acid--CoA ligase 1	P41216	78	3	2	C$_{242}$GVEIISLK[3]
Nicotinate-nucleotide pyrophosphorylase [carboxylating]	Q91X91	32	4	3	C$_{111}$SGIASAAATAVEVAR[3]
Peptidyl-prolyl cis-trans isomerase A	P17742	18	-	3	IIPGFMC$_{62}$QGGDFTR[3]
Selenium-binding protein 1	P17563	52	2	4	C$_{8}$GPGYSTPLEAMK[3]
S-formylglutathione hydrolase	Q9R0P3	31	-	3	C$_{11}$FGGLQK

Three eNOS$^{-/-}$ mouse livers were analyzed by MRC and mPEG-biotin protein capture methods and the mPEG-biotin peptide capture method (see Fig. 1C). Sequence-to-spectrum assignments from three biological replicates were combined in Scaffold. The proteins listed above satisfied three criteria: (1) identified by at least one protein capture method (≥2 unique peptides), (2) confirmed by a sulfonic acid-containing peptide sequence, and (3) not identified in the respective UV-exposed samples. Uniprot accession numbers correspond to the full-length unprocessed precursor when available (www.uniprot.org). Additional accessions were listed if the observed peptides could not distinguish between protein isoforms.

[1]Number of unique peptides identified in protein capture experiment from 3 biological replicates (does not include sulfonic acid-containing peptides). A null value indicates the protein did not meet the threshold criteria and was considered not identified.

[2]Cysteinyl-containing tryptic peptide sequences identified by peptide capture. The indicated cysteine residue(s) was identified as sulfonic acid and corresponds to the unprocessed mouse precursor protein.

[3]Cysteinyl-containing peptide sequences that were also identified in the wild type mouse liver (Supplementary Table 1).

Protein name	Accession number	PDB file	Coordinated cysteines
Alcohol dehydrogenase 1	P00329	1u3w	98, 101, 104, 112, 175
Betaine--homocysteine S-methyltransferase 1	O35490	1umy	299, 300
Cytochrome c,	P62897	2b4z	15, 18
Cytochrome P450 2D10	P24456	2f9q	443
Cytochrome P450 2E1	Q05421	3e6i	437
Cytochrome P450 2F2	P33267	2nnj	436
Sulfite oxidase, mitochondrial	Q8R086	2a9d	265

Supplementary Table 2.3: Cysteine residues coordinated with metals

Supplementary Table 2.4: Endogenously S-nitrosylated proteins sensitive to Trx/TrxR-mediated denitrosylation.

Trx-sensitive proteins	**Accession number**	**Molecular weight (kDa)**
1,4-alpha-glucan-branching enzyme	Q9D6Y9	80
10-formyltetrahydrofolate dehydrogenase	Q8R0Y6	99
2-hydroxyacyl-CoA lyase	Q9QXE0	64
40S ribosomal protein S3	P62908	27
40S ribosomal protein S4, X isoform	P62702	30
4-hydroxyphenylpyruvate dioxygenase	P49429	45
5-oxoprolinase	Q8K010	138
60S ribosomal protein L17	Q9CPR4	21
Acetyl-CoA acetyltransferase, cytosolic	Q8CAY6	41
Acetyl-CoA acetyltransferase, mitochondrial precursor	Q8QZT1	45
Aconitate hydratase, mitochondrial	Q99KI0	85
Adenosine kinase	P55264	40
Alanine--glyoxylate aminotransferase 2, mitochondrial precursor	Q3UEG6	57
Aldehyde dehydrogenase family 8 member A1	Q8BH00	54
Aldehyde dehydrogenase X, mitochondrial precursor	Q9CZS1	58
Aldehyde dehydrogenase, mitochondrial precursor	P47738	57
Alpha-aminoadipic semialdehyde dehydrogenase	Q9DBF1	56
Argininosuccinate lyase	Q91YI0	52
Aspartate aminotransferase, mitochondrial precursor	P05202	47

ATP-citrate synthase	Q91V92	120
Betaine--homocysteine S-methyltransferase 1	O35490	45
Bifunctional aminoacyl-tRNA synthetase	Q8CGC7	170
Catalase	P24270	60
Cystathionine gamma-lyase	Q8VCN5	44
Cytochrome b-c1 complex subunit 1	Q9CZ13	53
Cytochrome c, somatic	P62897	12
Cytochrome P450 27, mitochondrial	Q9DBG1	61
Cytochrome P450 2C54	Q6XVG2	56
Cytochrome P450 2E1	Q05421	57
Cytochrome P450 2F2	P33267	56
Cytosol aminopeptidase	Q9CPY7	56
Dihydrolipoyl dehydrogenase, mitochondrial precursor	O08749	54
Dihydroxyacetone kinase	Q8VC30	60
Dimethylaniline monooxygenase [N-oxide-forming] 3	P97501	61
Elongation factor 2	P58252	95
Enoyl-CoA hydratase, mitochondrial precursor	Q8BH95	31
Epoxide hydrolase 2	P34914	63
Ester hydrolase C11orf54 homolog	Q91V76	35
Fatty acid synthase	P19096	272
Fructose-1,6-bisphosphatase 1	Q9QXD6	37
Glycerol-3-phosphate dehydrogenase [NAD+], cytoplasmic	P13707	38

Glycine dehydrogenase [decarboxylating], mitochondrial	Q91W43	113
Glycogen phosphorylase, liver form	Q9ET01	97
Heat shock cognate 71 kDa protein	P63017	71
Hemoglobin subunit beta-1	P02088	16
Hydroxymethylglutaryl-CoA lyase, mitochondrial	P38060	34
Isocitrate dehydrogenase [NAD] subunit alpha, mitochondrial precursor	Q9D6R2	40
Liver carboxylesterase 31 precursor	Q63880	63
Liver carboxylesterase 31-like precursor	Q8VCU1	63
L-lactate dehydrogenase A chain	P06151	36
Long-chain specific acyl-CoA dehydrogenase, mitochondrial	P51174	48
Long-chain-fatty-acid--CoA ligase 1	P41216	78
Long-chain-fatty-acid--CoA ligase 5	Q8JZR0	76
Malate dehydrogenase, mitochondrial precursor	P08249	36
Membrane-associated progesterone receptor component 1	O55022	22
Microsomal glutathione S-transferase 1	Q91VS7	18
Non-specific lipid-transfer protein	P41216	78
Peroxisomal carnitine O-octanoyltransferase	Q9DC50	70
Peroxisomal sarcosine oxidase	Q9D826	44
Phenylalanine-4-hydroxylase	P16331	52
Phosphoglucomutase-1	Q9D0F9	62
Probable urocanate hydratase	Q8VC12	75
Profilin-1	P62962	15

Pyruvate carboxylase, mitochondrial precursor	Q05920	130
Regucalcin	Q64374	33
Sarcoplasmic/endoplasmic reticulum calcium ATPase 2	O55143	115
Sodium/potassium-transporting ATPase subunit alpha-1	Q8VDN2	113
Sorbitol dehydrogenase	Q64442	38
Staphylococcal nuclease domain-containing protein 1	Q78PY7	102
Succinate dehydrogenase [ubiquinone] flavoprotein subunit, mitochondrial	P32020	59
Sulfotransferase 1A1	P52840	34
Thiosulfate sulfurtransferase	P52196	33
Ubiquitin-like modifier-activating enzyme 1 X	Q02053	118
UDP-glucuronosyltransferase 2B5	P17717	61
Uricase	P25688	35
Very long-chain acyl-CoA synthetase	O35488	70
Very long-chain specific acyl-CoA dehydrogenase, mitochondrial precursor	P50544	71

Liver lysates remained untreated or exposed to 150nM Trx, 150nM TrxR, 100uM NADPH, for 30 min at 37 ^{o}C. Following this, protein lysates were processed by the MCR and mPEGb protein capture approaches. Comparisons were made between the protein identifications from Trx sample and the untreated sample. Proteins confirmed as endogenously S-nitrosylated by complementary proteomic approaches (see Supplementary Table 1, main text), which were subsequently identified in the untreated sample but not in the Trx-treated sample were considered as sensitive to reduction and are putative targets for denitrosylation by these species.

CHAPTER 3

ELECTROSTATIC PROPERTIES NAVIGATE GSNO-MEDIATED PROTEIN TRANSNITROSATION

By

Jennifer L. Greene[a,b], Marat Talipov[c], Dmitry Khomyakov[c], Paschalis-Thomas Doulias[d], Margarita Tenopoulou[d], Wei Wei[e], Limin Liu[e], Harry Ischiropoulos[d,f], Qadir Timerghazin[c]

[a]Department of Biochemistry and Biophysics, The Raymond and Ruth Perelman School of Medicine, University of Pennsylvania, Philadelphia, PA 19104, USA
[b]Graduate Group in Biochemistry and Molecular Biophysics, University of Pennsylvania, Philadelphia, PA 19104, USA
[c]Department of Chemistry, Marquette University, Milwaukee, Wisconsin, 53201
[d]Department of Pediatrics, Children's Hospital of Philadelphia Research Institute, Philadelphia, PA, 19104, USA
[e]Department of Microbiology and Immunology, University of California San Francisco, San Francisco, CA 94143
[f]Department of Pharmacology, The Raymond and Ruth Perelman School of Medicine, University of Pennsylvania, Philadelphia, PA 19104, USA

3.1 Abstract

S-nitrosylation is defined as the covalent addition of nitric oxide to selective protein cysteine residues that can regulate protein activity across a variety of organs and cellular systems. Nevertheless, fundamental questions regarding S-nitrosylation still remain unanswered, including the mechanism by which •NO selectively modifies protein cysteine residues to form S-nitrosocysteine. One proposed mechanism mandates the transfer of a nitrosonium ion to a reduced thiol of a cysteine residue. S-nitrosoglutathione (GSNO), a major endogenous S-nitrosothiol, has been proposed as a mediator of these *in vivo* trans-S-nitrosation reactions. Herein, we precisely mapped the site of modification in a population of cysteine residues targeted for transnitrosation by GSNO and reveal specific electrostatic properties within the protein environment for S-nitrosocysteine formation. Using a transnitrosation intermediate, we describe a mechanism for GSNO catalysis that requires a single basic residue rather than the acid-base pair which has previously been described (Perez-Mato et al. 1999). Using this novel mechanism for transnitrosation via GSNO, our GSNOR$^{-/-}$ dataset was then revisited to identify cysteines which may also be targeted via this mechanism. By extracting the structural elements that mediate GSNO transnitrosation, we explore the influence of protein structure on cysteine selectivity.

3.2 Introduction

S-nitrosothiols (RSNOs) are thioesters of nitrite thought to be a major store of nitric oxide (•NO) within the body. RSNOs have been identified across a variety of cell

types and found in many different tissues signifying their role in transport of nitric oxide throughout the body. They have also been shown to play an important role in health and disease (Butler et al. 2006) and have been used in many studies as exogenous sources of nitric oxide. While it is possible to synthesize and utilize these compounds for *in vitro* studies, the *in vivo* mechanisms of S-nitrosothiol formation and stability are not very well understood.

Because of the proposed role of S-nitrosothiols in nitric oxide signaling, many *in vitro* studies have been aimed at investigating those factors that can influence the stability of S-nitrosothiols *in vivo* (Al-Sa'doni et al. 2000). S-nitrosothiols can modify thiols by transfer of a nitrosonium equivalent through a process known as transnitrosation. When this process occurs on reduced cysteine residues within proteins, it can result in alteration of protein function. These S-nitrosylated proteins have been implicated in a variety of cellular processes including apoptosis (Hara et al. 2001), chromatin remodeling (Nott et al. 2008), and cell permeability (Thibeault et al. 2010). Data have shown that it is a discriminating modification that only targets select cysteine residues on specific proteins. However, what remains unclear is how the selectivity of this modification is derived. It has been proposed that multiple chemistries occur *in vivo* resulting in different sites of S-nitrosylation. While it is known that S-nitrosothiols can transnitrosate protein cysteine residues, the mechanism of this exact process (or processes) is unknown.

It has been proposed that S-nitrosoglutathione is a major endogenous trans-S-nitrosating agent. As a tripeptide, GSNO is a much larger molecule than the diatomic species nitric oxide. While its size may appear to be an impediment when compared to $^{\bullet}NO$, the presence of its two additional residues (glutamic acid and glycine) may allow

for more controlled delivery of nitrosonium ion to the targeted cysteine. The literature provides several examples of GSNO-binding proteins that may offer insight into this mechanism during transnitrosation. Crystal structures of human glutathione transferase P1-1 (hGSTP1-1) show that GSNO binds to the enzyme in a manner similar to its substrate GSH by forming hydrogen bonding interactions with glutamic acid and glycine (Oakley et al., Tellez-Sanz et al.). Molecular modeling studies of the transcription factor OxyR also showed that GSNO docks to the protein via hydrogen bonding interactions between the γ-glutamyl amine of GSNO and the γ-carboxylate of Asp202 (Kim et al. 2002). Docking simulations by Staab et al. similarly showed that residues in alcohol dehydrogenase 3 (most recently also identified as GSNO reductase) are capable of forming hydrogen bonds with the tripeptide (Staab et al. 2009).

In addition to hydrogen bonding, electrostatic interactions have also been proposed to influence transnitrosation reactions involving GSNO. Stamler et al. posited that charged residues within hemoglobin were capable of influencing the S-nitrosylation of Cys93β (Stamler et al. 1997). Depending on the conformational state of the protein, the proximity of basic or acidic residues to Cys93β would either promote the S-nitrosylation or denitrosylation of the cysteine, respectively. The role of flanking acidic/basic residues in S-nitrosylation has since been extended to incorporate the reactivity of GSNO within the three dimensional microenvironment of the targeted cysteine. Perez-Mato et al. proposed that γ-COOH of Asp355 in methionine adenosyltransferase (MAT) protonated GSNO resulting in the donation of a nitrosonium ion from GSNO to form SNO-Cys121 (Perez-Mato et al. 1999). Mutation of this Asp355 to serine significantly reduced the ability of GSNO to transnitrosate Cys121 thereby

inactivating MAT. Acidic residues were now thought to play a more direct role in catalysis of GSNO.

Several studies have been aimed at understanding the chemical reactivity of S-nitrosothiols such as GSNO (Aruslamy et al 1999; Wang et al. 2002, Baciu et al. 2003). More recently, work within our own group utilized theoretical studies to better explain which resonance forms of RSNOs were favored under varying conditions (Timerghazin et al. 2007). Density-functional theory coupled with natural resonance theory analysis showed that S-coordination of the SNO group with various Lewis acids can promote the formation of an ionic species, i.e. a nitrosonium ion. While Lewis acids were used as models of basic protein residues, the best assessment of RSNO reactivity would be to investigate its stability within its endogenous protein environment.

To further explore mechanisms necessary for GSNO-mediated transnitrosation to occur *in vivo*, the S-nitrosoproteomes of mouse S-nitrosoglutathione reductase null ($GSNOR^{-/-}$) liver and thymus were resolved. GSNOR is an enzyme previously shown to endogenously metabolize S-nitrosoglutathione (Liu et al. 2004). By comparing these data to their wildtype SNO-proteomes, a $GSNOR^{-/-}$ unique population was derived and further analyzed structurally for insight regarding the underlying molecular mechanism of GSNO-mediated transnitrosation.

Herein, we present a novel approach for investigating the reactivity of GSNO as a function of its protein environment. Using a transnitrosation intermediate, we show that coordination of atoms in the surrounding cysteine environment controls the formation of specific reaction products. Surprisingly, our model suggests that a lone basic residue rather than an acid-base pair is sufficient for GSNO catalysis *in vivo*. Using this novel

mechanism for transnitrosation via GSNO, our GSNOR$^{-/-}$ dataset was then revisited to identify cysteines which may also be targeted via this mechanism.

3.3 Materials and Methods

Chemicals and Reagents. Unless otherwise stated, all chemicals and reagents were purchased from Sigma-Aldrich.

Generation of GSNOR null mice. All mouse studies were reviewed and approved by the Institutional Animal Care and Use Committee of the Children's Hospital of Philadelphia Research Institute. Generation of GSNOR$^{-/-}$ mice has been previously described and characterized (Liu et al. 2004). WT C57BL/6 mice were obtained from Jackson Laboratories and intact organs were recovered as previously described (Doulias et al. 2010). Intact livers and thymus were then immediately frozen in liquid nitrogen and stored at -80 °C until needed.

Sample preparation for identification of S-nitrosylated proteins. Each organ was homogenized in 3 mL of lysis buffer (250 mM Hepes-NaOH, pH 7.7, containing 1 mM DTPA, 0.1 mM neocuproine, 1% Triton X-100, and protease inhibitors) on ice using a Teflon pestle and a Jumbo Stirrer (Fisher Scientific). The homogenates were then centrifuged at 13,000 × g for 30 min at 4 °C. The soluble protein fraction was collected and the protein concentration was determined by the Bradford assay. Each sample consisted of 21 mg of protein in 42 mL of lysis buffer (0.5 mg/mL). Liver protein lysates were supplemented with 100 mM mannitol and 5 mM MMTS and split into 1- 28 mL aliquot (untreated protein and peptide capture) and 1 – 14 mL aliquot (UV-illuminated). The 14 mL aliquot was illuminated under a conventional UV transilluminator for 7 min

on ice and the other aliquot was left untreated on ice. Liver and thymus lysates were then further prepared for capture as previously described (Doulias et al. 2010).

Capture of S-nitrosylated proteins and peptides via organomercury resin capture (MRC). Wildtype and GSNOR$^{-/-}$ SNO-proteomes of mouse thymus and liver were resolved using a previously described mercury-based mass spectrometric approach known as organomercury resin capture (MRC) (Doulias et al. 2010). An organomercurial derivative of Affi-Gel-10 N-hydroxysuccinimide-activated agarose gel for capture of S-nitrosylated cysteines was synthesized as first described (McDonagh et al. 1976) and utilized/prepared as previously described. Protein samples were prepared as described above and loaded onto their respective MRC columns either for protein capture or on-column digestion thereby yielding peptides.

Detection of S-nitrosylated cysteines by mass spectrometric analysis. The protein fractions obtained from the MRC capture method were analyzed by gel electrophoresis liquid chromatography/tandem MS analysis (GeLC-MS/MS) as previously described (Doulias et al. 2010). Protein samples were mixed with 6× Laemmli sample buffer and equal volumes (20 μL) were loaded on NuPAGE 10% Bis-Tris gels (Invitrogen). Proteins were electrophoresed in Mops running buffer for approximately 1 cm and visualized by colloidal blue stain (Invitrogen). Stained gels were immediately processed by in gel trypsin digestion after each lane was cut into three slices and individually. Tryptic peptide digests were analyzed by a hybrid LTQ-Orbitrap mass spectrometer (Thermo Electron) coupled to a 2D LC system (Eksigent) and autosampler. ***Generation and Evaluation of SEQUEST Peptide Assignments.*** Peptide assignments were generated, evaluated, and analyzed as was previously described (Doulias et al. 2010). Briefly, DTA files were

generated from MS/MS spectra extracted from the RAW data file with previously described threshold criteria (Doulias et al. 2010) and submitted to Sorcerer-SEQUEST (version 4.0.3, revision 11; Sagen Research). Database searching was performed against a Uniprot database containing Mus musculus sequences from Swiss-Prot plus common contaminants, which were then reversed and appended to the forward sequences. The database was indexed with previously described parameters including static modifications of cysteine by carboxyamidomethylation (+57 amu) for in-gel digestion or by sulfonic acid (+48 amu) and methionine sulfone (+32 amu) for peptide affinity capture. After generation of potential sequence-to-spectrum peptide assignments by Sorcerer-SEQUEST, Scaffold (version 2.2; Proteome Software) was used to validate protein identifications and perform manual inspection of MS/MS spectra as well as to compare protein identifications across experimental conditions. Threshold criteria for acceptance of protein identification were applied as previously described (Doulias et al. 2010). In-gel digestion experiments required a threshold of at least 99% protein confidence with at least two unique peptides and at least 90% confidence with an estimated protein false discovery rate of no greater than 5%. Xcorr thresholds were applied to sulfonic acid-containing and non-modified peptides independently, so peptide false discovery rate was no greater than 5%. Because one unique peptide per protein was permitted, manual inspection of all MS/MS spectra was performed as previously described.

Generation of GSNOR$^{-/-}$ unique SNO-proteome. Sulfonic acid-containing peptides identified for each biological condition (wildtype or GSNOR null) for both organs (thymus and liver) were pooled into 2-separate lists according to their experimental

condition (untreated or UV-illuminated) (n=2 thymus, n=3 liver). Any peptides found present in both the untreated and UV-illuminated lists were removed from the untreated list. The remaining sulfonic acid-containing peptides were then matched to proteins identified via the MRC protein capture method. The GSNOR$^{-/-}$ unique population was derived by removing any sites of S-nitrosylation which were shared between the wildtype and GSNOR$^{-/-}$ SNO-proteomes.

Gene ontology analysis. Subcellular localization was determined using UniProt Knowledgebase protein database (www.uniprot.org) and statistics were calculated using Babelomics 4.2 (http://babelomics.bioinfo.cipf.es). Ingenuity Pathway Analysis was used to categorize molecular and cellular functions of proteins and calculate statistical significance as compared to the entire mouse proteome.

Calculation of Hydropathy Indices. Kyte-Doolittle hydropathy indices for S-nitrosylated cysteines were calculated in a 13 amino acid window using the ExPASy ProtScale tool.

Linear motif. Linear motifs surrounding all S-nitrosylated cysteines were calculated using the Motif-X program (Schwartz et al. 2005). Sequences of identified SNO-peptides are used as input and compared to the entire mouse proteome to determine if any amino acids are overrepresented. Motifs were also calculated within a 13 amino acid window.

Distribution of secondary structure. Proteins identified as S-nitrosylated were coordinated with their respective three dimensional structures in the RCSB Protein Data Bank (PDB). Matched structures required the conservation of the cysteine residue identified as S-nitrosylated and ≥ 50% sequence homology to target protein. Secondary structure of SNO-cysteine and surrounding residues was obtained when structures were viewed in the PyMOL molecular visualization software.

Predicted pK_a values. The program Propka 2.0 (Li et al. 2005) was used to calculate the predicted pK_a values of S-nitrosylated cysteines using their corresponding three dimensional protein structures.

Calculated surface exposure. The relative residue surface accessibility (RSA) for all cysteines within the S-nitrosoproteome was calculated with Naccess 2.1.1 using the radius of a water molecule (1.4 Å2) as a probe (Lee & Richards et al. 1971). Cysteines with a relative RSA less than 10% were designated as buried whereas a relative RSA greater than 10% meant that the cysteine residue was solvent accessible.

Molecular dynamics simulations. The structure of 2DGV was obtained as previously described above. Molecular dynamics simulations were performed using Amber package with Amber99SB force field. Explicit solvent model was used with a TIP3P water in truncated octahedron periodic box with a spacing distance of 9.0 Å around the molecule.

For modeling of the trans-*S*-nitrosation intermediate, an artificial residue named CYG was defined in place of target cysteine (Figure 3.1). CYG contains two fragments (γ-glutamic acid and nitroxyl disulfide) which are undefined in the standard force field. Therefore, previously defined parameters were used to describe γ-glutamic acid (Rigsby et al. 2007) and parameters for nitroxyl disulfide were calculated using generalized Amber force field (GAFF) combined with B3LYP/6-31G(d) charges fitted by Restrained Electrostatic Potential (RESP) ESP charge Derive (R.E.D.) software (Dupradeau et al. 2010).

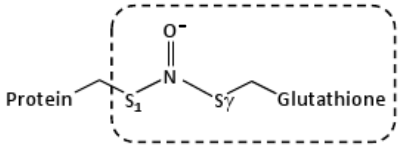

Figure 3.1: CYG intermediate used in molecular dynamics simulations. Dotted line indicates intermediate which replaces cysteine residue and is attached to the protein.

The protocol for MD simulations includes the following steps: waters were minimized, while the protein remains static using an initial 500 steps of the steepest descent (SD) algorithm with an additional 500 conjugate gradient (CG) algorithm steps to ensure complete minimization. The entire system was then minimized with 1000 steps of the SD algorithm and an additional 2500 steps of CG minimization. With the complex again held static, the solvent was then equilibrated to 300 K over the course of 20 picoseconds. For the simulation, time steps of 2 ps were used, periodic boundary conditions were employed, the SHAKE algorithm was applied, and a non-bonded cutoff of 10.0 Å was employed.

For simulated annealing calculations, the same preliminary calculations were used to obtain an equilibrated system at 300 K. A series of MD simulations were run with the protein initially restrained (heating to 600 K for 60 ps, equilibrating at 600 K for 10 ps, cooling back to 300 K in 60 ps) and then unrestrained (heating to 600 K for 60 ps, constant temperature for 10, 30 or 50 ps followed by cooling down to 300 K). Instead of 2ps, the time step was chosen to be 1 ps. Each simulation time was a total of 8 ns resulting in a total sampling time for each modified cysteine of 24 ns (trajectories with different annealing setup were merged). Dynamical Cross-Correlation Matrix (DCCM)

plots were generated with a function available in the Amber toolkit using MD trajectories as inputs. Plots were generated only for arrays of distances over simulation time for charged groups pairs corresponding to DCCM elements greater than 0.75.

Quantum mechanics/molecular mechanics (QM/MM) calculations. ONIOM-PCM/X(ε=4.24)(PBE0/def2-SV(P)+d:Amber95) was used for QM/MM calculations to further investigate the interaction of close-lying arginine and -SN(O)S- group of Cyg675.

3.4 Results

Identification of the GSNOR$^{-/-}$ Unique SNO-proteome

By employing the MRC method, a total of 170 sites belonging to 150 proteins were identified as being unique to the GSNOR null liver and thymus (Table 3.1). This final SNO-proteome was derived by removing 69 sites which were shared between wildtype and GSNOR null organs. With the previous identification of 2 proteins from GSNOR null organs (Wei et al, Lima et al.), this corresponds to the discovery of 99% novel targets of S-nitrosylation in GSNOR null SNO-proteome. Gene ontology analysis using Babelomics 4.2 (Medina et al. 2010) revealed that the top four primary subcellular locations of GSNOR$^{-/-}$ unique proteins were cytoplasm (n=25), mitochondria (n=24), membrane (n=15), and ribosome (n=16) (Figure 3.2A). Those proteins located in membrane, mitochondria, and ribosome were calculated to be statistically significant as compared to the entire mouse proteome (p-values=3.80E-04, 1.13E-10, and 6.12E-07, respectively). The molecular and cellular functions of these proteins were then identified using Ingenuity Pathway Analysis which calculates enrichment as compared to the entire mouse proteome. The majority of proteins were determined to be involved in small

molecule biochemistry (n=52, p-value=1.10E-06) followed by nucleic acid metabolism (Figure 3.2B). Thirty (30) proteins were found to also have additional sites of S-nitrosylation in the wildtype unique population while sixteen (16) proteins were found to be poly-S-nitrosylated (i.e. having more than one cysteine residue modified).

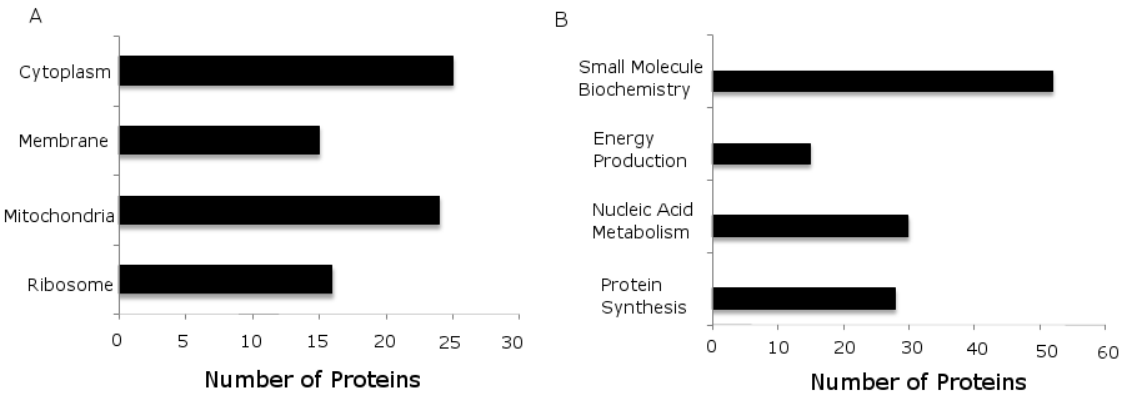

Figure 3.2: Gene ontology analysis of GSNOR null unique proteome. (A) Top four cellular localization of GSNOR$^{-/-}$ unique S-nitrosylated cysteines. (B) Top four statistically significant cellular functions of GSNOR$^{-/-}$ unique S-nitrosylated cysteines.

GSNOR$^{-/-}$ cysteines display large distribution of hydropathy indices

To characterize our GSNOR$^{-/-}$ unique S-nitrosated cysteines further, biochemical and bioinformatic tools were used to interrogate their individual microenvironments. It has been previously suggested that cysteines endogenously targeted for S-nitrosylation lie in areas of increased hydrophobicity (Nedaspov et al. 2000). To further investigate this hypothesis, Kyte-Doolittle hydropathy indices were calculated for GSNOR$^{-/-}$ unique population of cysteine residues within a 13-residue window using the primary amino acid sequence. With an average hydropathy index of -0.158±0.616 (n=154), GSNOR$^{-/-}$ unique cysteines were determined to be slightly hydrophilic. Kernel density approximation was

used to investigate the existence of subpopulations of hydropathy indices. The density of indices peaked near the average value with nearly 60% (n=91) corresponding to cysteines within hydrophilic regions of the protein with the remaining values corresponding to cysteines in hydrophobic regions of the protein (Figure 3.3). GSNOR$^{-/-}$ unique cysteines did not show a predisposition to lie in hydrophobic regions of the protein. This does not differ significantly from what has been previously observed when examining the wildtype liver SNO-proteome (Doulias et al. 2010) and the NO-Cys data set curated by Marino and coworkers (Marino et al. 2010). With such a large amount of variation between hydropathy values, it is difficult to conclude that hydropathy is an indicator of endogenous S-nitrosation via S-nitrosoglutathione.

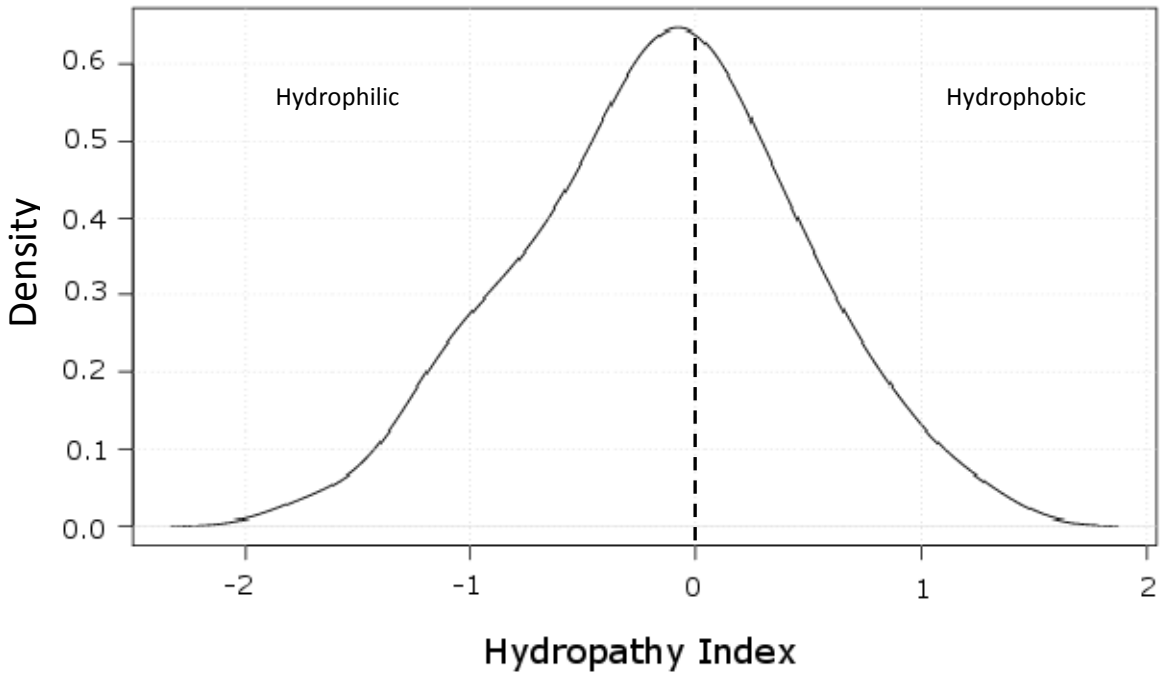

Figure 3.3: **Kernel density plot of S-nitrosylated cysteines from GSNOR$^{-/-}$ unique SNO-proteome**. Hydrophilic cysteines correspond to hydropathy indices values <0 (n=91) whereas hydrophobic values correspond to values ≥0 (n=63).

Accessibility of S-nitrosoglutathione to targeted cysteines

To learn more about the influence of structure on GSNO-mediated mechanisms of transnitrosation, a total of 111 $GSNOR^{-/-}$ unique S-nitrosated cysteines were coordinated with their corresponding three dimensional structures as previously described (Table 3.2). Biological assemblies were downloaded from the Protein Data Bank (PDB) in place of the asymmetric unit to ensure that the protein was in its most physiologically relevant state. To first investigate the accessibility of modified cysteines to small molecules such as the tripeptide S-nitrosoglutathione, the surrounding secondary structures within a 21 amino acid window were characterized. The flanking secondary structure was examined 10 residues upstream and 10 residues downstream of the S-nitrosated cysteine which was denoted by position 0. $GSNOR^{-/-}$ unique S-nitrosated cysteines were present most frequently in coils (38%) closely followed by β-sheets (36%) and found least frequently in α-helices (25%) (Figure 3.4). Modified cysteines were positioned near the end of a short β-strand region (positions -3 to -1) and at the beginning of an extended stretch of coils (position 1 to 10). With the exception of positions -3 to -1, coils were surprisingly the predominant secondary structure surrounding S-nitrosated cysteines (positions -10 to -4). The presence of these cysteines in more flexible regions of the proteins suggests that these proteins may be more adept at accommodating molecules like the tripeptide GSNO.

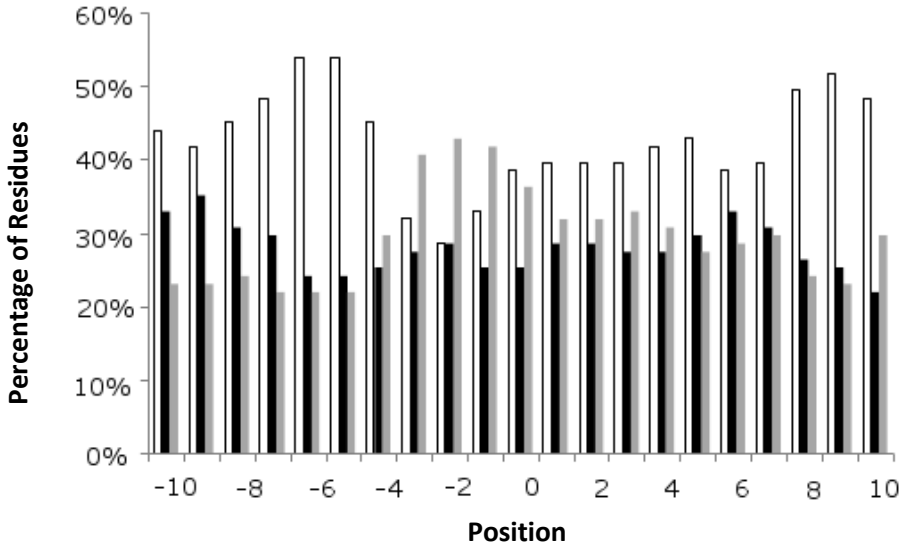

Figure 3.4: Distribution of secondary structure flanking S-nitrosylated GSNOR$^{-/-}$ unique cysteine residue. Position 0 denotes S-nitrosylated cysteine of interest whereas positions -10 to -1 denote residues upstream of cysteine and 1 to 10 denote residues downstream of cysteine (n=91).

To further investigate the mechanism by which GSNO can transnitrosate cysteine residues, the relative residue surface accessibility (RSA) of each GSNOR$^{-/-}$ unique cysteine was calculated. Using the program NAccess, a 1.4Å probe representing the radius of a water molecule was used to calculate RSA values for 65 GSNOR$^{-/-}$ unique cysteines. With a value > 10% indicating solvent exposure, seventy-four percent of cysteines were found to be buried (N = 48) while the remaining 17 were solvent exposed (Figure 3.5). With an average relative RSA

value of 1.38±2.3, buried cysteines remained tightly distributed while solvent accessible cysteines were much more broadly distributed (27.4±22.7). While these data are comparable to what was previously found regarding the wildtype liver (Doulias et al.

2010), it is a surprising result regarding potential mechanisms of GSNO-mediated S-nitrosation. With > 50% of cysteines calculated as not being on the surface of the protein, this alludes to a mechanism which must allow the tripeptide GSNO access to these cysteines. This latter hypothesis is additionally supported by the above described data showing that coils exist as the predominant secondary structure surrounding S-nitrosylated cysteines.

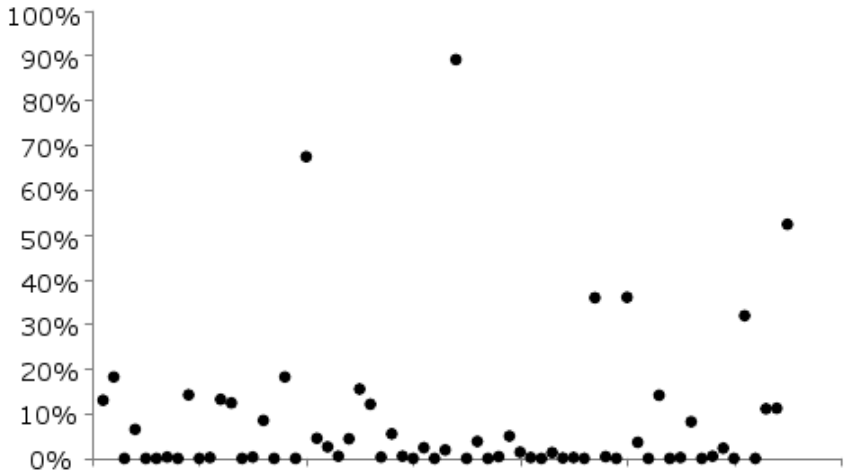

Figure 3.5: Relative residue surface accessibility of GSNOR$^{-/-}$ unique S-nitrosated cysteines (n=48 buried, n=17 exposed)

Predicted reactivity of GSNOR null cysteines

Using the program Propka 2.0, predicted pK_a values were calculated for cysteines within the GSNOR$^{-/-}$ unique SNO-proteome using their corresponding three dimensional structures. Ninety-two (92) cysteines had an average predicted pKa = 9.12±2.45 (Figure 3.6). This is lower than the previously reported average pKa value of 10.0±2.10 (n=142) predicted for the wildtype liver SNO-proteome (Doulias et al. 2010). These data suggest

that the GSNOR$^{-/-}$ unique SNO-proteome may be enriched for a subpopulation of more reactive cysteines.

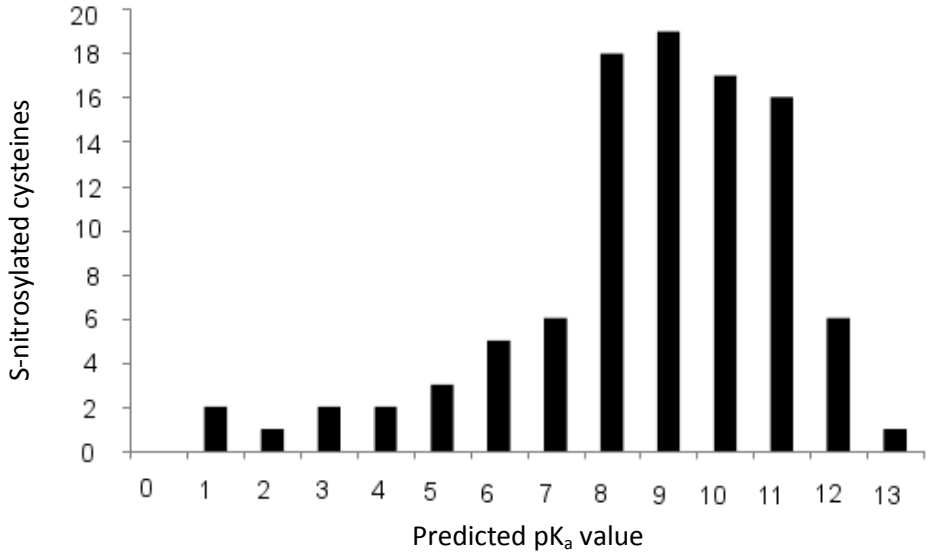

Figure 3.6: **Predicted pKa values for each S-nitrosylated GSNOR$^{-/-}$ unique cysteine calculated using the program Propka 2.0 (n=92)**

Role of three-dimensional environment on transnitrosation via GSNO

Molecular dynamics simulations were performed using the CYG intermediate in place of the cysteine residue (see Materials and Methods) to investigate the mechanism by which GSNO may transnitrosate cysteines endogenously (Houk et al. 2003). With the intermediate weakly bound between the protein and glutathione, it can effectively represent the influence of the protein environment on the formation of a specific reaction

product (i.e. GSNO or SNO-cysteine). The RNA binding domain of heterogeneous nuclear ribonucleoprotein M (PDB code 2DGV) was selected as the model protein. 2DGV has a small size (92 amino acids) which proves to be fairly stable during molecular dynamic simulations (RMSD 1.14 Å after 2 ns simulation). Although C675 is the only cysteine identified as being S-nitrosylated, 2DGV contains a total of 4 cysteines (C652, C675, C693, & C708). All four cysteines contain charged residues in their respective proximal environments making 2DGV a challenging system for identifying true sites of transnitrosation via GSNO.

To analyze the influence of the protein environment on the intermediate CYG, correlated motions between CYG and other residues were investigated across MD simulations. Interactions of charged and polar groups of His, Arg, Lys, Asp, Glu, Gln, and Asn with S, N, and O atoms of the CYG intermediate were specifically scrutinized. Dynamical Cross-Correlation Matrices (DCCM) were used to visualize these interactions. A single pixel corresponds to the correlation between two specific atoms. Atoms displaying any correlated motions are given a positive cross-correlation coefficient with a value of 1 (white) being the most correlated. Blue pixels correspond to atoms which are the least correlated and therefore completely independent of onanother. DCCM plots were generated for all four cysteines in 2DGV. When compared to unmodified cysteines within the same protein, Cys675 displayed the largest region of atoms responsive to the CYG intermediate (cross-correlation coefficient > 0.75) (Figure 3.7, top right).

Probability plots depicting the distances between highly correlated motions were generated for Cyg675 (Figure 3.8) using trajectories of the MD simulations. Statistically significant interactions between both sulfurs of nitroxyl disulfide and a close-lying

arginine, Arg706, were observed. Both S_γ (sulfur belonging to GSNO) and S_1 (sulfur belonging to protein-cysteine residue) displayed maximum probability distances of slightly less than 4 Angstroms. However, S_1 was equally likely to be either 6 or 8 Å (cumulative probability ~ 0.5) from Arg706 (Figure 3.8a) whereas S_γ showed a much greater likelihood to be 4 Å from Arg706 (Figure 3.8b). Observed distances between S_γ and Arg706 were calculated to be as large as 10 Å, but these states were far less populated and pronounced than the 4 Å distance. The remaining 3 cysteines were also examined to ascertain the influence of each microenvironment on the stabilization of the CYG intermediate (data not shown). Probability plots for Cys693 point to an interaction between S_γ and Lys684 but show that it occurs at a distance of nearly 7 Å. In fact, this same lysine residue was more closely coordinated to the OE atom of CYG. A similar finding of O-coordination was also observed between Cys708 and Arg709.

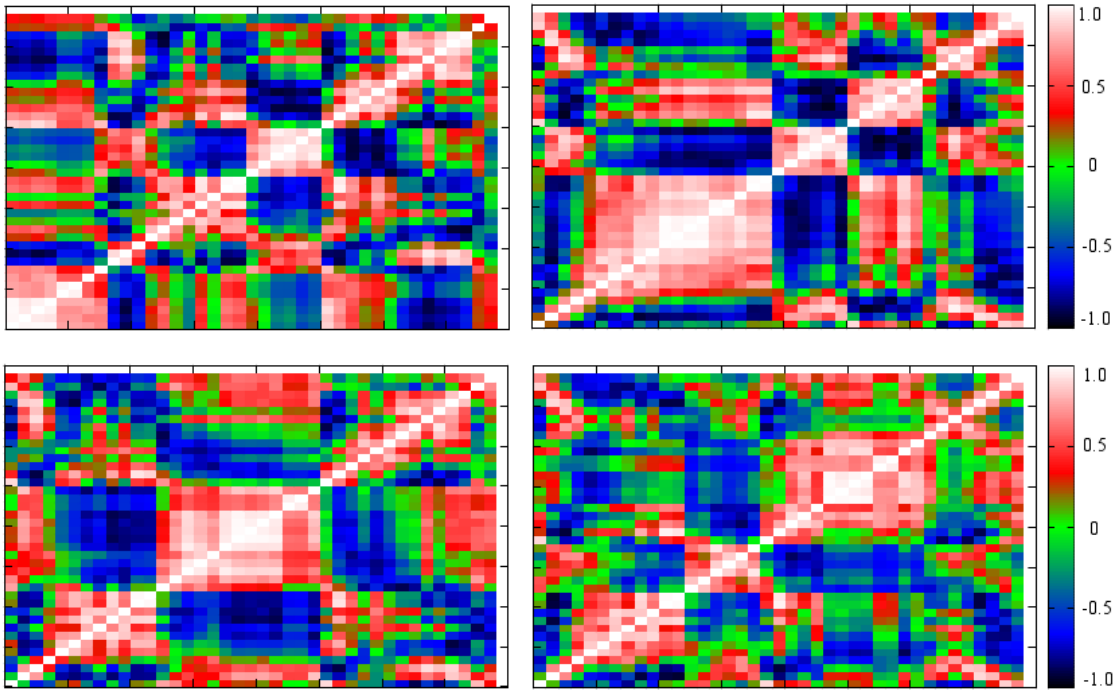

Figure 3.7: DCCM plots of all four cysteines in 2DGV. Cyg652 (top left), Cys675 (top right), Cyg693 (bottom left), & Cyg708 (bottom right). Cyg675 displays the largest region of correlation as evidenced by large rectangular near bottom left of Cyg675 map.

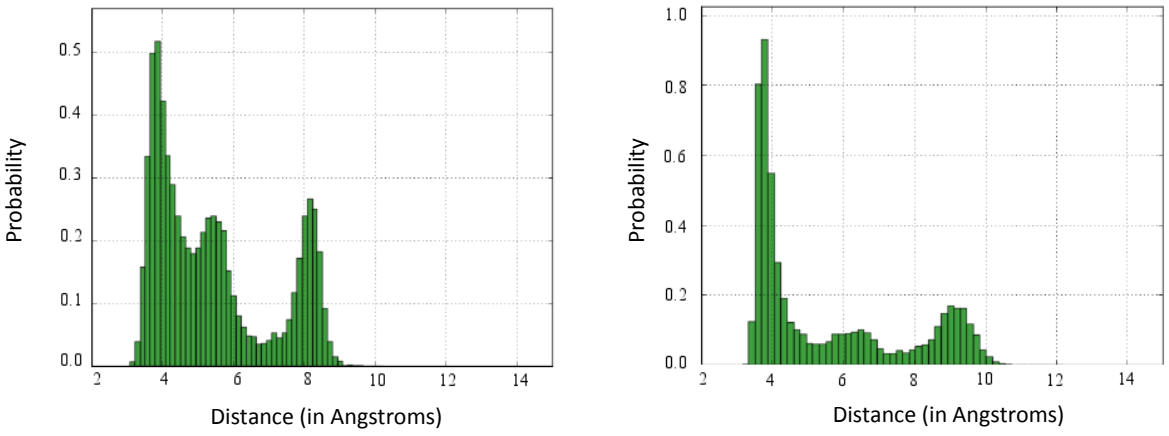

Figure 3.8: Distance probability plots of CYG675 intermediate interaction with neighboring basic residue. (A) Analysis of molecular dynamics trajectories shows interaction between S_1 of CYG675 intermediate and Arg706 occurs most frequently at a 4 Angstrom distance but also exists across a broad range of distances. (B) S_γ of CYG675

also interacts with Arg706 but displays a higher probability of being within a 4 Å distance.

A novel mechanism of S-nitrosation catalysis

A series of hybrid Quantum Mechanics/Molecular Mechanics (QM/MM) calculations were performed to interrogate the interaction between Arg706 and the -SN(O)S- group of Cyg675 and to also determine the final products of the transnitrosation reaction. Coordination of Arg706 at S_γ led to the elongation of the corresponding S_γ-N bond of GSNO (*r*(S-N) = 1.931 Å)), whereas the S_1-N bond became shorter, suggesting an increase in double bond character (Figure 3.9). Coordination to S_γ promotes the formation of protein S-nitrosocysteine whereas coordination to S_1 would lead back to the reactants (GSNO and Protein-SH). These data are additionally supported by our previously published data regarding the chemical reactivity of RSNOs based upon their interactions with Lewis acids (Timerghazin et al. 2007).

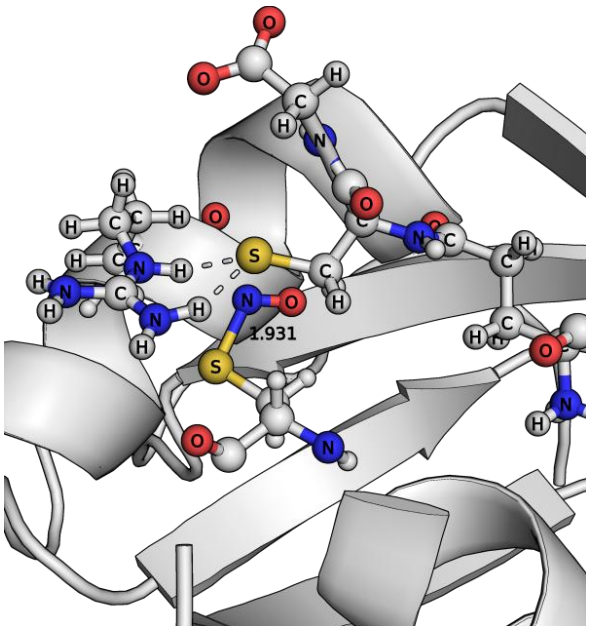

Figure 3.9: **QM/MM calculations demonstrating *S*-coordination of Arg706 to CYG675 in 2DGV**

With a total of 111 S-nitrosocysteines coordinated to three dimensional structures, QM/MM and molecular dynamics calculations for the entire GSNOR$^{-/-}$ unique proteome would prove to be computationally expensive. Therefore, after the identification of this novel GSNO-mediated mechanism in the model system 2DGV, the GSNOR$^{-/-}$ unique proteome was then investigated to determine if any other cysteines might be subject to this particular mechanism. Of the 111 cysteines coordinated to structures, 109 had at least one charged residue within 6 Angstroms. Four cysteines had only acidic residues nearby while twenty-two had only basic residues nearby. A total of 83 cysteines had both a basic and acidic residue within 6 Angstroms.

3.5 Discussion

To date, global investigations into the specificity of S-nitrosylation have revealed a diversity of data, suggestive of multiple mechanisms taking place in vivo (Marino et al. 2009; Doulias et al. 2010). Therefore, the best approach for investigating a specific mechanism would be to isolate those cysteines specifically targeted by that mechanism. By perturbing the endogenous metabolism of GSNO, the $GSNOR^{-/-}$ mouse was used to characterize those cysteines endogenously targeted for transnitrosation via GSNO. By removing any S-nitrosocysteine residues also identified in the wildtype proteomes, a novel $GSNOR^{-/-}$ unique proteome was derived. The biochemical and biophysical properties of these cysteines did not differ significantly from those previously reported for the wildtype proteome (Doulias et al. 2010). This suggests that there must be another mechanism by which these cysteines are targeted for transnitrosation.

The chemical reactivity and stability of S-nitrosothiols has long been of interest to the scientific community (Aruslamy et al. 1999; Wang et al. 2002, Baciu et al. 2003, Timerghazin et al. 2007). As more recent data reveal the importance of RSNOs in health and disease, it becomes even more critical to understand their reactivity in the intracellular environment. GSNO is frequently used as an exogenous source of nitric oxide for S-nitrosylation studies yet the mechanism by which it transnitrosates proteins *in vivo* is not very well understood. Many studies have suggested a role of charged residues in S-nitrosylation. Initially, charged residues were investigated to determine their influence on cysteine nucleophilicity. Perez-Mato et al. further extended the role of charged residues in the reactivity of GSNO during transnitrosation reactions. They proposed a “push-pull” mechanism in the protein methionine adenosyltransferase

whereby which a basic residue would deprotonate cysteine residue ("pull") and an acidic residue would promote donation of a NO^+ from GSNO ("push"). Mutational analysis of the acidic residue resulted in decreased nitrosation, suggesting its role in transnitrosation.

Herein, we describe a novel mechanism of transnitrosation which requires the coordination of a basic residue to S-nitrosoglutathione to promote S-nitrosocysteine formation. Utilizing the CYG intermediate allowed for a novel approach to monitoring reaction intermediates as a function of the surrounding protein environment. Our investigations demonstrate that positively charged residues coordinated to the sulfur atom promote the formation of a nitrosonium ion. In the case of S-Coordination, the bond length between the coordinated sulfur and nitrogen atom may increase, thereby promoting transnitrosation to the alternate sulfur atom. Coordination of arginine to other atoms in CYG such as oxygen CYG may alternatively help to stabilize the intermediate and decrease the likelihood of a transnitrosation reaction taking place. These data suggest that the surrounding protein environment can play both the dual role of catalyzing the formation of protein S-nitrosocysteine as well as stabilizing the S-nitrosocysteine residue once it is formed.

While the overwhelming presence of charged residues suggests that a mechanism similar to 2DGV may occur in vivo for other $GSNOR^{-/-}$ unique proteins, further experiments are needed to test this hypothesis. Although the majority of $GSNOR^{-/-}$ unique cysteines were buried, the presence of charged residues on the surface of the protein may also help to stabilize GSNO such that transnitrosation events can occur. This is what Marino et al. characterized as an extended acid base motif. Understanding the relationship between GSNO docking and base catalyzed-transnitrosation might help to

further distinguish populations of SNO-cysteines modified by GSNO. Those cysteines which have both favorable GSNO docking and base-catalyzed mechanisms of transnitrosation may refer to a population of cysteines which are most readily modified by GSNO. Alternatively, GSNO docking may be favorable near the site of transnitrosation yet no basic residues may be involved in catalysis. Transnitrosation via GSNO is one of several proposed mechanisms for forming SNO-proteins; still, GSNO-mediated transnitrosation may itself contain multiple mechanisms involving protein electrostatics. Therefore, it is becoming increasingly important to design experiments that distinguish the contributions of differing protein electrostatics. Present studies are underway to investigate the influence of favorable GSNO docking on base catalyzed transnitrosation reactions.

Table 3.1: Endogenously S-nitrosylated GSNOR$^{-/-}$ unique proteins in liver and thymus

Organ	Protein name	Uniprot Accession	Protein molecular weight (kDa)	Peptide sequence
Liver	**10-formyltetrahydrofolate dehydrogenase**	Q8R0Y6	99	AVQMGMSSVFFNKGENC$_{707}$IAAGR
Thymus	**26S proteasome non-ATPase regulatory subunit 1**	Q3TXS7	106	C$_{437}$VAYAESHDQALVGDK
Liver	**2-oxo-4-hydroxy-4-carboxy-5-ureidoimidazoline decarboxylase**	Q283N4	20	RLQC$_{141}$QPESELR
Liver	**2-oxoisovalerate dehydrogenase subunit alpha, mitochondrial**	P50136	50	QMPVHYGC$_{194}$K
Liver	**3-hydroxyisobutyryl-CoA hydrolase, mitochondrial**	Q8QZS1	43	RGC$_{44}$GGVITLNRPK
Thymus	**40S ribosomal protein S11**	P62281	18	DVQIGDIVTVGEC$_{131}$RPLSK KC$_{60}$PFTGNVSIR NMSVHLSPC$_{116}$FR
Thymus	**40S ribosomal protein S17**	P63276	16	VC$_{35}$EEIAIIPSKK
Liver	**40S ribosomal protein S2**	P25444	31	KLLMMAGIDDC$_{222}$YTSAR
Thymus	**40S ribosomal protein S26**	P62855	13	LHYC$_{74}$VSCAIHSK
Liver	**40S ribosomal protein S27**	Q6ZWU9	9	ARLTEGC$_{77}$SFR
Liver	**4-aminobutyrate aminotransferase, mitochondrial**	P61922	56	TMGC$_{224}$LATTHSK NKGVVLGGC$_{467}$GDKSIR
Liver	**4-trimethylaminobutyraldehyde dehydrogenase**	Q9JLJ2	56	AGAPPGLFNVVQGGAATGQFLC$_{220}$HHREVAK
Thymus	**60S ribosomal protein L10a**	P53026	25	VLC$_{164}$LAVAVGHVK
Liver	**60S ribosomal protein L10-like**	P86048	25	SRFC$_{23}$RGVPDAK IC$_{71}$ANKYMVK INKMLSC$_{105}$AGADRLQTGMR RLIPDGC$_{195}$GVK

Thymus	**60S ribosomal protein L13a**	P19253	23	C_{38}EGINISGNFYR
Liver	**60S ribosomal protein L14**	Q9CR57	24	C_{54}MQLTDFILKFPHSAR
Liver	**60S ribosomal protein L23**	P62830	15	ISLGLPVGAVINC$_{28}$ADNTGAK
Liver	**60S ribosomal protein L24**	Q8BP67	18	MKVELC$_{6}$SFSGYK
Liver	**60S ribosomal protein L36a**	P83882	12	C_{88}KHFELGGDKK
Liver	**60S ribosomal protein L4**	Q9D8E6	47	SGQGAFGNMC$_{96}$RGGR
Liver	**60S ribosomal protein L6**	P47911	33	AKPHC$_{51}$SRNPVLVR
Thymus	**60S ribosomal protein L7**	P14148	31	FGIIC$_{208}$MEDLIHEIYTVGKR
Thymus	**60S ribosomal protein L8**	P62918	28	TELFIAAEGIHTGQFVYC$_{90}$GKK
Liver	**7-dehydrocholesterol reductase**	O88455	54	AIEC$_{376}$SYTSADGLKHHSK
Thymus	**Actin, cytoplasmic 1**	P60710	42	C_{285}DVDIRKDLYANTVLSGGTTMYPGIADR
Thymus	**Actin-related protein 2**	P61161	45	LC$_{221}$YVGYNIEQEQK
Liver	**Adenylate kinase 2, mitochondrial**	Q9WTP6	26	LAENFC$_{40}$VC$_{42}$HLATGDMLR
Thymus	**Adenylyl cyclase-associated protein 1**	P40124	52	C_{355}VNTTLQIK
Liver	**Aldehyde dehydrogenase X, mitochondrial**	Q9CZS1	58	LGQKEGAKLLC$_{388}$GGER
Liver	**Alpha-aminoadipic semialdehyde synthase, mitochondrial**	Q99K67	103	SSPC$_{776}$EKLKEVVFTK
Liver	**Aspartoacylase-2**	Q91XE4	35	VAVTGGTHGNEMC$_{26}$GVYLAR
Liver	**Aspartyl-tRNA synthetase, cytoplasmic**	Q922B2	57	LQSGIC$_{203}$HLFR
Thymus	**ATP-dependent RNA helicase A**	O70133	149	VRPGFCFHLC$_{779}$SR
Thymus	**ATP-dependent RNA helicase DDX39**	Q8VDW0	49	NC$_{164}$PHVVVGTPGR
Liver	**Bifunctional aminoacyl-tRNA synthetase**	Q8CGC7	170	SC$_{1377}$QFVAVRR
Liver	**C-1-tetrahydrofolate synthase, cytoplasmic**	Q922D8	101	SC$_{326}$KPKLIGNLAR
Liver	**Carnitine O-palmitoyltransferase 1, liver isoform**	P97742	88	C_{394}RQTYFAR
Thymus	**Caspase-6**	O08738	32	IFIIQAC$_{146}$R KLHFC$_{271}$PKPSK
Liver	**Catalase**	P24270	60	LVNADGEAVYC$_{232}$KFHYKTDQGIK
Liver	**Choline dehydrogenase, mitochondrial**	Q8BJ64	66	AKADSAYHPSC$_{516}$TC$_{518}$K

				WSTAC$_{244}$AYLHPVLSRPNLR
Liver	**Citrate synthase, mitochondrial**	Q9CZU6	52	FRGYSIPEC$_{101}$QK YSC$_{359}$QREFALK
Thymus	**Cofilin-1**	P18760	19	LTGIKHELQANC$_{139}$YEEVKDR
Thymus	**Coronin-1A**	O89053	51	DGALICTSC$_{195}$R
Thymus	**Cullin-associated NEDD8-dissociated protein 1**	Q6ZQ38	136	C$_{356}$LDAVVSTRHEMLPEFYK
Thymus	**Cysteine and glycine-rich protein 1**	P97315	21	NLDSTTVAVHGEEIYC$_{58}$K
Liver	**Cysteine-rich protein 2**	Q9DCT8	23	C$_{129}$NKRVYFAEK
Both	**Cysteine-rich protein 2**	Q9DCT8	23	C$_{8}$DKTVYFAEK
Liver	**Cytochrome P450 2D10**	P24456	57	NLGVFPFPVAPYPYQLC$_{496}$AVMREQGH
Liver	**Cytochrome P450 3A11**	Q64459	58	VC$_{378}$KKDVELNGVYIPK
Thymus	**Cytoplasmic FMR1-interacting protein 2**	Q5SQX6	146	C$_{98}$NEQPNRVEIYEK
Thymus	**Cytosolic non-specific dipeptidase**	Q9D1A2	53	DVGAETLLHSC$_{300}$K
Thymus	**D-3-phosphoglycerate dehydrogenase**	Q61753	57	VLISDSLDPC$_{18}$C$_{19}$RK NAGTC$_{369}$LSPAVIVGLLR
Liver	**D-beta-hydroxybutyrate dehydrogenase, mitochondrial**	Q80XN0	38	SPYC$_{209}$ITK
Liver	**Delta-1-pyrroline-5-carboxylate dehydrogenase, mitochondrial**	Q8CHT0	62	SAFEYGGQKC$_{347}$SAC$_{350}$SR
Thymus	**Destrin**	Q9R0P5	19	AVIFC$_{39}$LSADKK
Thymus	**Dihydropyrimidinase-related protein 2**	O08553	62	THNSALEYNIFEGMEC$_{439}$R
Liver	**Dihydropyrimidine dehydrogenase [NADP+]**	Q8CHR6	112	RGLPLAVKPVC$_{1025}$
Liver	**Dimethylaniline monooxygenase [N-oxide-forming] 3**	P97501	60	VVSKVQKSC$_{509}$SHFYSR ILC$_{294}$GMVTIKPNVK
Liver	**Dimethylaniline monooxygenase [N-oxide-forming] 5**	P97872	60	LLLGPC$_{468}$TPVQYR
Thymus	**DNA replication licensing factor MCM7**	Q61881	81	GNIHIC$_{378}$LMGDPGVAK

Thymus	**DNA-directed RNA polymerase II subunit RPB9**	P60898	15	C_{89}GHKEAVFFQSHSAR
Thymus	**ES1 protein homolog, mitochondrial precursor**	Q9D172	28	ALGAKHC_{219}VKGVTEAHVDQK
Liver	**Fatty acid synthase**	P19096	272	VGDPQELNGITRSLC_{313}AFRQAPLLIGSTK
Liver	**Fructose-bisphosphate aldolase B**	Q91Y97	40	ALNDHHVYLEGTLLKPNMVTAGHAC_{240}TK
Thymus	**Galectin-9**	O08573	40	C_{258}GGDIAFHLNPR FEEGGYVVC_{73}NTK GMPFELC_{101}FLVQR
Liver	**GDH/6PGL endoplasmic bifunctional protein**	Q8CFX1	89	C_{390}LPQQIIFYIGHGELGHPAILVSR
Liver	**Gephyrin**	Q8BUV3	83	C_{326}SSKENILR
Thymus	**Glucosamine-fructose-6-phosphateaminotransferase [isomerizing] 1**	Q9Z2Z9	33	C_2GIFAYLNYHVPR ETDC_{461}GVHINAGPEIGVASTK
Liver	**Glutamine synthetase**	P15105	42	KPAETNLRHIC_{117}K
Thymus	**Glutaredoxin-3**	Q9CQM9	38	LTHAAPC_{148}MLFMK
Thymus	**Glutathione reductase, mitochondrial precursor**	P47791	54	GVYAVGDVC_{355}GK
Liver	**Glycerol-3-phosphate dehydrogenase [NAD+], cytoplasmic**	P13707	38	IC_{102}DQLKGHLK
Thymus	**Guanine nucleotide-binding protein G(I)/G(S)/G(T) subunit beta-1**	P62874	37	ELAGHTGYLS$C_{148}C_{149}$R
Thymus	**Guanine nucleotide-binding protein subunit beta-2-like 1**	P68040	35	TNHIGHTGYLNTVTVSPDGSLC_{207}ASGGK
Thymus	**H-2 class II histocompatibility antigen, A beta chain precursor**	P14483	30	TRAELDTVC_{106}RHNYEGPETHTSLR
Thymus	**Heat shock protein HSP 90-beta**	P11499	83	C_{412}LELFSELAEDKENYKK
Thymus	**Heterogeneous nuclear ribonucleoprotein F**	Q9Z2X1	46	DLSYC_{267}LSGMYDHR
Thymus	**Heterogeneous nuclear ribonucleoprotein M**	Q9D0E1	78	DKFNEC_{675}GHVLYADIK

Thymus	**Heterogeneous nuclear ribonucleoproteins C1/C2**	Q9Z204	34	IVGC$_{46}$SVHKGFAFVQYVNER
Thymus	**Histidine triad nucleotide-binding protein 1**	P70349	14	IIFEDDRC$_{38}$LAFHDISPQAPTHFLVIPK
Thymus	**Histone-binding protein RBBP7**	Q60973	48	TPSSDVLVFDYTKHPAKPDPSGEC$_{166}$NPDLR VHIPNDDAQFDASHC$_{97}$DSDKGEFGGFGSVTGK
Liver	**Hydroxymethylglutaryl-CoA lyase, mitochondrial**	P38060	34	TSSKVAQATC$_{323}$KL
Thymus	**Hypoxanthine-guanine phosphoribosyltransferase**	P00493	25	DLNHVC$_{206}$VISETGK
Liver	**Importin-5**	Q8BKC5	124	TKENVNATENC$_{972}$ISAVGK
Liver	**Indolethylamine N-methyltransferase**	P40936	29	VLRC$_{142}$DVTK
Thymus	**Inositol monophosphatase**	O55023	30	EKYPC$_{64}$HSFIGEESVAAGEK
Thymus	**Isocitrate dehydrogenase [NAD] subunit alpha, mitochondrial precursor**	Q9D6R2	40	C$_{351}$SDFTEEIC$_{359}$R
Liver	**Kynureninase**	Q9CXF0	52	GVVC$_{425}$DKREPDGIR NC$_{45}$FYIPK
Liver	**Kynurenine 3-monooxygenase**	Q91WN4	55	VAVIGGGLVGALNAC$_{25}$FLAK
Thymus	**Lamin B1**	P14733	67	C$_{199}$QSLTEDLEFRK
Liver	**L-gulonolactone oxidase**	P58710	50	FTRGDDILLSPC$_{354}$FQR
Thymus	**Lymphocyte antigen 75 precursor**	Q60767	197	C$_{83}$LGLDITK
Thymus	**Macrophage migration inhibitory factor**	P34884	13	LLC$_{81}$GLLSDRLHISPDR
Thymus	**Malate dehydrogenase, cytoplasmic**	P14152	37	SAPSIPKENFSC$_{154}$LTR
Thymus	**Malate dehydrogenase, mitochondrial precursor**	P08249	36	EGVVEC$_{275}$SFVQSK
Liver	**Methylcrotonoyl-CoA carboxylase subunit alpha, mitochondrial**	Q99MR8	79	YC$_{450}$LHQYNIVGLR
Thymus	**Myosin light polypeptide 6**	Q60605	17	ILYSQC$_{32}$GDVMR
Thymus	**NADH dehydrogenase [ubiquinone] 1 alpha subcomplex subunit 10, mitochondrial precursor**	Q99LC3	41	VITVDGNIC$_{67}$SGK

Liver	**NADH dehydrogenase [ubiquinone] iron-sulfur protein 6, mitochondrial**	P52503	13	TGTC$_{104}$GYC$_{107}$GLQFKQHHH
Thymus	**NADH-ubiquinone oxidoreductase 75 kDa subunit, mitochondrial precursor**	Q91VD9	80	FC$_{64}$YHERLSVAGNC$_{75}$R
Thymus	**NADPH--cytochrome P450 reductase**	P37040	77	LIHEGGAHIYVC$_{630}$GDAR VHPNSVHIC$_{472}$AVAVEYEAK
Liver	**Nitrilase homolog 1**	Q8VDK1	36	THLC$_{161}$DVEIPGQGPMR
Thymus	**Non-POU domain-containing octamer-binding protein**	Q99K48	55	FAC$_{147}$HSASLTVR
Thymus	**PDZ and LIM domain protein 1**	O70400	36	GHFFVEDQIYC$_{305}$EKHAR
Thymus	**Peptidyl-prolyl cis-trans isomerase A**	P17742	18	HTGPGILSMANAGPNTNGSQFFIC$_{115}$TAK
Liver	**Peroxisomal 2,4-dienoyl-CoA reductase**	Q9WV68	31	HGC$_{53}$HTVIVGR
Liver	**Peroxisomal acyl-coenzyme A oxidase 1**	Q9R0H0	75	NLC$_{559}$LLYSLYGISQK ASEAHC$_{531}$HYVTVK
Liver	**Peroxisomal carnitine O-octanoyltransferase**	Q9DC50	70	LHGRPGC$_{437}$C$_{438}$YETAMTR
Liver	**Phenylalanine-4-hydroxylase**	P16331	52	VFHC$_{265}$TQYIR
Liver	**Probable cation-transporting ATPase 13A1**	Q9EPE9	132	AVVGNAVPC$_{10}$GARPGGAR
Liver	**Probable urocanate hydratase**	Q8VC12	75	AYPIDQYPC$_{95}$R
Thymus	**Profilin-1**	P62962	15	C$_{71}$SVIRDSLLQDGEFTMDLR
Thymus	**Proliferating cell nuclear antigen**	P17918	29	C$_{62}$DRNLAMGVNLTSMSK
Thymus	**Proliferation-associated protein 2G4**	P50580	44	KADVIKAAHLC$_{149}$AEAALR
Thymus	**Proteasome subunit beta type-10 precursor**	O35955	29	ATNDSVVADKSC$_{70}$EKIHFIAPK
Thymus	**Protein FAM115C**	Q921K8	102	VVLAAHEAMLC$_{279}$APK
Liver	**Protein transport protein Sec31A**	Q3UPL0	134	C$_{1140}$LSSATDPQTKR
Liver	**Pyruvate carboxylase, mitochondrial**	Q05920	130	INGCAIQC$_{376}$R
Thymus	**Pyruvate dehydrogenase E1 component subunit beta, mitochondrial precursor**	Q9D051	39	PVGHC$_{249}$LEAAAVLSK
Liver	**Quinone oxidoreductase**	P47199	35	VHAC$_{45}$GVNPVETYIR
Thymus	**Ras-related protein Rab-14**	Q91V41	24	FMADC$_{40}$PHTIGVEFGTR

Liver	**Regucalcin**	Q64374	33	VEC$_{8}$VLRENYR
Thymus	**RNA-binding protein Raly**	Q64012	33	VAGC$_{51}$SVHKGYAFVQYANER
Liver	**Sarcoplasmic/endoplasmic reticulum calcium ATPase 2**	O55143	115	SMSVYC$_{498}$TPNKPSR
Liver	**Sepiapterin reductase**	Q64105	28	LKSDGALVDC$_{235}$GTSAQK
Thymus	**Serine protease inhibitor A3K**	P07759	47	HFRDEELSC$_{259}$SVLELK
Thymus	**Serine/threonine-protein phosphatase 2A 56 kDa regulatory subunit gamma isoform**	Q60996	55	C$_{334}$VSSPHFQVAER
Thymus	**Serine/threonine-protein phosphatase 6 regulatory ankyrin repeat subunit B**	B2RXR6	107	TC$_{408}$LHAAAAGGNVEC$_{420}$IK
Liver	**S-formylglutathione hydrolase**	Q9R0P3	31	AYDATC$_{206}$LVK
Liver	**Splicing factor 1**	Q64213	70	C$_{282}$GGAGHIASDC$_{292}$KFQRPGDPQSAQDK SITNTTVC$_{279}$TK
Thymus	**Succinate dehydrogenase [ubiquinone] flavoprotein subunit, mitochondrial precursor**	Q8K2B3	73	GC$_{357}$GPEKDHVYLQLHHLPPEQLATR
Liver	**Succinyl-CoA ligase [GDP-forming] subunit alpha, mitochondrial**	Q9WUM5	36	IIC$_{60}$QGFTGK
Thymus	**SUMO-activating enzyme subunit 1**	Q9R1T2	39	DVIIKVDQIC$_{150}$HR
Liver	**T-complex protein 1 subunit theta**	P42932	60	NIQAC$_{36}$KELAQTTR
Liver	**Tetratricopeptide repeat protein 36**	Q8VBW8	20	RQLVLLNPYAALC$_{168}$NR
Thymus	**Thyroid hormone-inducible hepatic protein**	Q62264	17	SIC$_{67}$VEVDHGLLPR
Thymus	**Transcription elongation factor SPT5**	O55201	121	VELHSTC$_{734}$QTISVDR
Thymus	**Transitional endoplasmic reticulum ATPase**	Q01853	89	LADDVDLEQVANETHGHVGADLAALC$_{415}$SEAALQAIR
Thymus	**Transketolase**	P40142	68	TVPFC$_{386}$STFAAFFTR
Thymus	**Trifunctional enzyme subunit beta, mitochondrial precursor**	Q99JY0	51	KDGGQYALVAAC$_{459}$AAGGQGHAMIVEAYPK
Thymus	**Tubulin beta-5 chain**	P99024	50	REIVHIQAGQC$_{12}$GNQIGAK
Both	**Ubiquitin-like modifier-activating enzyme 1**	Q02053	118	C$_{588}$VYYRKPLLESGTLGTK
Liver	**UDP-glucose 6-dehydrogenase**	O70475	55	AADLKYIEAC$_{112}$ARR

Liver	**Uncharacterized protein KIAA0564 homolog**	Q8CC88	213	HNNC$_{1415}$VTLTHTNQVVR
Liver	**UPF0317 protein C14orf159 homolog, mitochondrial**	Q8BH86	66	AFLC$_{419}$KDGDPKSPR
Liver	**Uricase**	P25688	35	C$_{188}$FATQVYC$_{195}$K
Thymus	**Valyl-tRNA synthetase**	Q9Z1Q9	140	C$_{1184}$SIHLQLQGLVDPAR
Thymus	**Voltage-dependent anion-selective channel protein 1**	Q60932	32	EHINLGC$_{140}$DVDFDIAGPSIR YQVDPDAC$_{245}$FSAK
Thymus	**Voltage-dependent anion-selective channel protein 3**	Q60931	31	YKVC$_{65}$NYGLTFTQK
Thymus	**WD repeat-containing protein 1**	O88342	66	C$_{438}$FSIDNPGYEPEVVAVHPGGDTVAVGGTDGNVR

Table 3.2: GSNOR$^{-/-}$ unique proteins coordinated to PDB structures

Protein name	UNIPROT Accession	Peptide sequence	Structure
10-formyltetrahydrofolate dehydrogenase	Q8R0Y6	AVQMGMSSVFFNKGENC$_{707}$IAAGR	2o2p (98%) 405-902
2-oxoisovalerate dehydrogenase subunit alpha, mitochondrial	P50136	QMPVHYGC$_{194/152}$K	2bff (93%) 48-442
3-hydroxyisobutyryl-CoA hydrolase, mitochondrial	Q8QZS1	RGC$_{44/45}$GGVITLNRPK	3bpt (83%) 34-385
40S ribosomal protein S11	P62281	KC$_{60/59}$PFTGNVSIR	3iz6 (68%) 41-126/chain P
40S ribosomal protein S11	P62281	NMSVHLSPC$_{116/115}$FR	3iz6 (68%) 41-126/chain P
40S ribosomal protein S11	P62281	DVQIGDIVTVGEC$_{131/128}$RPLSK	3jyv (74%)69-149/chain Q
40S ribosomal protein S14	P62264	C$_{85}$KELGITALHIK	2zkq (100%) 23-147/chain k
40S ribosomal protein S2	P25444	KLLMMAGIDDC$_{222/130}$YTSAR	2zkq (96%) 101-249/chain e
40S ribosomal protein S27	Q6ZWU9	ARLTEGC$_{77/79}$SFR	3iz6 (84%) 31-80
4-aminobutyrate aminotransferase, mitochondrial	P61922	TMGC$_{224/196}$LATTHSK	1ohv (93%) 39-499
4-aminobutyrate aminotransferase, mitochondrial	P61922	NKGVVLGGC$_{467/439}$GDKSIR	1ohv (93%) 39-499
4-trimethylaminobutyraldehyde dehydrogenase	Q9JLJ2	AGAPPGLFNVVQGGAATGQFLC$_{220/229}$HHREVAK	1a4s (69%) 2-494
60S ribosomal protein L10a	P53026	VLC$_{164/163}$LAVAVGHVK	3izr (63%)3-217
60S ribosomal protein L10-like	P86048	SRFC$_{23/22}$RGVPDAK	2zkr (99%) 4-169 (chain h)
60S ribosomal protein L10-like	P86048	INKMLSC$_{105/104}$AGADRLQTGMR	2zkr (99%) 4-169 (chain h)
60S ribosomal protein L10-like	P86048	IC$_{71/70}$ANKYMVK	2zkr (99%) 4-169 (chain h)
60S ribosomal protein L13a	P19253	C$_{38/37}$EGINISGNFYR	2zkr (97%)7-142 (chain j)
60S ribosomal protein L23	P62830	ISLGLPVGAVINC$_{28}$ADNTGAK	2zkr (100%) 16-139/chain k
60S ribosomal protein L24	Q8BP67	MKVELC$_{6}$SFSGYK	2zkr(100%)4-56/chain u
60S ribosomal protein L36a	P83882	C$_{88}$KHFELGGDKK	2zkr(100%)2-93/chain 4
60S ribosomal protein L4	Q9D8E6	SGQGAFGNMC$_{96/95}$RGGR	2zkr (97%) 7-263/chain c

60S ribosomal protein L7	P14148	FGIIC$_{208}$MEDLIHEIYTVGKR	2zkr (98%)111-270/chain w
60S ribosomal protein L8	P62918	TELFIAAEGIHTGQFVYC$_{90}$GKK	2zkr (99%)2-246/chain a
Actin, cytoplasmic 1	P60710	C$_{285}$DVDIRKDLYANTVLSGGTTMYPGIADR	2btf(100%)2-375
Actin-related protein 2	P61161	C$_{20}$GYAGSNFPEHIFPALVGRPIIR	2p9i (76%)9-362
Actin-related protein 2	P61161	LC$_{221}$YVGYNIEQEQK	1tyq(100%)143-350/chain B
Adenylyl cyclase-associated protein 1	P40124	C$_{355/356}$VNTTLQIK	1k8f (98%)318-474
Aldehyde dehydrogenase X, mitochondrial	Q9CZS1	LGQKEGAKLLC$_{388/369}$GGER	3inj (75%) 26-519
Aspartoacylase-2	Q91XE4	VAVTGGTHGNEMC$_{26}$GVYLAR	3nh4
Aspartyl-tRNA synthetase, cytoplasmic	Q922B2	LQSGIC$_{203/255}$HLFR	1asy (56%) 22-501
ATP-dependent RNA helicase A	O70133	VRPGFCFHLC$_{779/440}$SR	3kx2(25%)374-1115
ATP-dependent RNA helicase DDX39	Q8VDW0	NC$_{164/165}$PHVVVGTPGR	1xti(93%)45-425
ATP-dependent RNA helicase DDX3X	Q62167	VRPC$_{298}$VVYGGAEIGQQIR	2i4i(97%)168-5880
Carbonyl reductase [NADPH] 1	P48758	ALKNC$_{150/149}$RLELQQK	1wma(88%)7-277
Caspase-6	O08738	IFIIQAC$_{146/163}$R	3od5 (86%)14-273
Catalase	P24270	LVNADGEAVYC$_{232/231}$KFHYKTDQGIK	4blc (92%)4-501
Citrate synthase, mitochondrial	Q9CZU6	FRGYSIPEC$_{101/74}$QK	3enj (96%) 28-464
Citrate synthase, mitochondrial	Q9CZU6	YSC$_{359/332}$QREFALK	3enj (96%) 28-464
Cofilin-1	P18760	LTGIKHELQANC$_{139}$YEEVKDR	1q8g (98%)1-166
Coronin-1A	O89053	DGALICTSC$_{195}$R	2aq5
Cysteine and glycine-rich protein 1	P97315	NLDSTTVAVHGEEIYC$_{58}$K	1b8t(89%)1-193
Cysteine-rich protein 2	Q9DCT8	C$_{129/15}$NKRVYFAEK	2cu8 (81%) 126-184
Cysteine-rich protein 2	Q9DCT8	C$_{8/15}$DKTVYFAEK	2cu8 (98%) 1-63
Cytochrome P450 2D10	P24456	NLGVFPFPVAPYPYQLC$_{496/493}$AVMREQGH	2f9q (69%) 37-500
Cytochrome P450 3A11	Q64459	VC$_{378/377}$KKDVELNGVYIPK	1tqn (73%) 30-499
Cytosolic non-specific dipeptidase	Q9D1A2	DVGAETLLHSC$_{300}$K	2zog

Destrin	Q9R0P5	AVIFC$_{39}$LSADKK	1ak6 (95%)2-165
Dihydrolipoyl dehydrogenase, mitochondrial	O08749	VC$_{484/449}$HAHPTLSEAFR	1zmd(95%)37-509
Dihydropyrimidinase-related protein 2	O08553	THNSALEYNIFEGMEC$_{439}$R	2vm8 (98%)14-490
DNA-directed RNA polymerase II subunit RPB9	P60898	C$_{89/78}$GHKEAVFFQSHSAR	3h0g (48%)14-125/chain I
Electron transfer flavoprotein-ubiquinone oxidoreductase, mitochondrial	Q921G7	VTVFAEGC$_{247/215}$HGHLAK	2gmh(93%)38-616
Fatty acid synthase	P19096	VGDPQELNGITRSLC$_{313}$AFRQAPLLIGSTK	3hhd (87%) 2-853
Fructose-bisphosphate aldolase B	Q91Y97	ALNDHHVYLEGTLLKPNMVTAGHAC$_{240/239}$TK	1qo5 (96%) 2-349
Galectin-9	O08573	FEEGGYVVC$_{73}$NTK	2d6n
Galectin-9	O08573	GMPFELC$_{101}$FLVQR	2d6n
Glucosamine-fructose-6-phosphateaminotransferase [isomerizing] 1	Q9Z2Z9	C$_{2/1}$GIFAYLNYHVPR	2bpl (37%)2-682
Glucosamine-fructose-6-phosphateaminotransferase [isomerizing] 1	Q9Z2Z9	ETDC$_{461/459}$GVHINAGPEIGVASTK	2zj3 (83%) 316-682
Glutamine synthetase	P15105	KPAETNLRHIC$_{117}$K	2qc8 (94%) 10-365
Glutathione reductase, mitochondrial precursor	P47791	GVYAVGDVC$_{355/333}$GK	3dk9 (88%)41-500
Glycerol-3-phosphate dehydrogenase [NAD+], cytoplasmic	P13707	IC$_{102}$DQLKGHLK	1x0v (93%) 1-349
Guanine nucleotide-binding protein subunit beta-2-like 1	P68040	TNHIGHTGYLNTVTVSPDGSLC$_{207}$ASGGK	2zkq (99%)4-311
H-2 class II histocompatibility antigen, A beta chain precursor	P14483	TRAELDTVC$_{106/105}$RHNYEGPETHTSLR	1lnu
Heat shock protein HSP 90-beta	P11499	C$_{412}$LELFSELAEDKENYKK	3pry (95%)284-546
Heterogeneous nuclear	Q9D0E1	DKFNEC$_{675}$GHVLYADIK	2dgv (100%)651-729

ribonucleoprotein M			
Heterogeneous nuclear ribonucleoproteins C1/C2	Q9Z204	IVGC$_{46}$SVHKGFAFVQYVNER	1wf2 (94%)2-92
Histidine triad nucleotide-binding protein 1	P70349	IIFEDDRC$_{38}$LAFHDISPQAPTHFLVIPK	1kpe (94%)14-126
Histone-binding protein RBBP7	Q60973	TPSSDVLVFDYTKHPAKPDPSGEC$_{166}$NPDLR	3cfv (95%)1-410
Hydroxymethylglutaryl-CoA lyase, mitochondrial	P38060	TSSKVAQATC$_{323}$KL	2cw6 (87%) 28-323
Hypoxanthine-guanine phosphoribosyltransferase	P00493	DLNHVC$_{206/205}$VISETGK	1bzy (97%)5-218
Indolethylamine N-methyltransferase	P40936	VLRC$_{142/141}$DVTK	2a14 (57%) 6-262
Kynureninase	Q9CXF0	GVVC$_{425}$DKREPDGIR	2hzp (83%) 6-460
Lymphocyte antigen 75 precursor	Q60767	C$_{83/55}$LGLDITK	1dqg (20%)32-155
Macrophage migration inhibitory factor	P34884	LLC$_{81/80}$GLLSDRLHISPDR	2gdg
Malate dehydrogenase, cytoplasmic	P14152	SAPSIPKENFSC$_{154/153}$LTR	5mdh (94%)2-334
Malate dehydrogenase, mitochondrial precursor	P08249	EGVVEC$_{275/251}$SFVQSK	1mld (95%)25-337
Myosin light polypeptide 6	Q60605	ILYSQC$_{32/31}$GDVMR	1br1 (89%)4-151
NADPH--cytochrome P450 reductase	P37040	VHPNSVHIC$_{472}$AVAVEYEAK	1ja1 (98%)63-678
Non-POU domain-containing octamer-binding protein	Q99K48	FAC$_{147}$HSASLTVR	2cpj (68-153)
PDZ and LIM domain protein 1	O70400	GHFFVEDQIYC$_{305/65}$EKHAR	1x62 (91%)249-316
Peptidyl-prolyl cis-trans isomerase A	P17742	HTGPGILSMANAGPNTNGSQFFIC$_{115}$TAK	3k0m (96%)2-164
Peroxisomal 2,4-dienoyl-CoA reductase	Q9WV68	HGC$_{53/54}$HTVIVGR	1g0o (23%)1-273
Peroxisomal acyl-coenzyme A oxidase 1	Q9R0H0	NLC$_{559}$LLYSLYGISQK	1is2 (89%) 1-655
Peroxisomal acyl-coenzyme A oxidase 1	Q9R0H0	ASEAHC$_{531}$HYVTVK	1is2 (89%) 1-655

Phenylalanine-4-hydroxylase	P16331	VFHC$_{265}$TQYIR	1phz (96%)19-427
Profilin-1	P62962	C$_{71/70}$SVIRDSLLQDGEFTMDLR	1pne (96%)2-140
Proliferating cell nuclear antigen	P17918	C$_{62}$DRNLAMGVNLTSMSK	1vyj (97%)1-257
Proliferation-associated protein 2G4	P50580	KADVIKAAHLC$_{149}$AEAALR	2v6c
Proteasome subunit beta type-10	O35955	ATNDSVVADKSC$_{70/31}$EKIHFIAPK	1iru(57%)40-259, chain I
Protein DJ-1	Q99LX0	VTVAGLAGKDPVQC$_{46}$SR	1q2u(91%)1-189
Pyruvate dehydrogenase E1 component subunit alpha, somatic form, mitochondrial	P35486	EATKFAAAYC$_{273/244}$R	1ni4(98%)29-390
Pyruvate dehydrogenase E1 component subunit beta, mitochondrial	Q9D051	IERQGTHITVVAHSRPVGHC$_{249/219}$LEAAAVLSK	2ozl(94%)30-359
Quinone oxidoreductase	P47199	VHAC$_{45}$GVNPVETYIR	1yb5 (80%) 6-331
Ras-related protein Rab-14	Q91V41	FMADC$_{40}$PHTIGVEFGTR	1z0f (100%)7-173
Regucalcin	Q64374	VEC$_{8}$VLRENYR	3g4e (88%) 3-299
RNA-binding protein Raly	Q64012	VAGC$_{51/58}$SVHKGYAFVQYANER	1wf1 (94%)3-97
Sarcoplasmic/endoplasmic reticulum calcium ATPase 2	O55143	SMSVYC$_{498}$TPNKPSR	3ar4 (84%)1-992
Sepiapterin reductase	Q64105	LKSDGALVDC$_{235}$GTSAQK	1oaa
Serine hydroxymethyltransferase, cytosolic	P50431	LIIAGTSC$_{198/204}$YSR	1eji
Serine protease inhibitor A3K	P07759	HFRDEELSC$_{259/258}$SVLELK	1yxa (73%)48-418
Serine/threonine-protein phosphatase 2A 56 kDa regulatory subunit gamma isoform	Q60996	C$_{334/324}$VSSPHFQVAER	3fga (99%)34-436
S-formylglutathione hydrolase	Q9R0P3	C$_{11}$FGGLQK	3fcx(90%)3-281
Succinate dehydrogenase [ubiquinone] flavoprotein subunit, mitochondrial precursor	Q8K2B3	GC$_{357/315}$GPEKDHVYLQLHHLPPEQLATR	1zoy (96%)52-664
Succinyl-CoA ligase [GDP-forming] subunit alpha, mitochondrial	Q9WUM5	IIC$_{60/20}$QGFTGK	1euc (93%) 42-346
SUMO-activating enzyme subunit 1	Q9R1T2	DVIIKVDQIC$_{150/146}$HR	3kyd (87%)29-349

Superoxide dismutase [Cu-Zn]	P08228	AVC$_{7}$VLKGDGPVQGTIHFEQK	3gtt
Transcription elongation factor SPT5	O55201	VELHSTC$_{734/740}$QTISVDR	2e70 (96%) 696-751
Transitional endoplasmic reticulum ATPase	Q01853	LADDVDLEQVANETHGHVGADLAALC$_{415}$SEAALQAIR	/1e32
Transketolase	P40142	TVPFC$_{386}$STFAAFFTR	3mos (95%) 4-618
Trifunctional enzyme subunit beta, mitochondrial precursor	Q99JY0	KDGGQYALVAAC$_{459/386}$AAGGQGHAMIVEAYPK	1ulq (32%)53-473
Tubulin beta-5 chain	P99024	REIVHIQAGQC$_{12}$GNQIGAK	1tvk (97%)2-427
Ubiquitin-like modifier-activating enzyme 1	Q02053	C$_{588/556}$VYYRKPLLESGTLGTK	3cmm(51%)48-1057
UDP-glucose 6-dehydrogenase	O70475	AADLKYIEAC$_{112}$ARR	3khu (97%) 1-466
Voltage-dependent anion-selective channel protein 1	Q60932	EHINLGC$_{140/127}$DVDFDIAGPSIR	3emn
Voltage-dependent anion-selective channel protein 1	Q60932	YQVDPDAC$_{245/232}$FSAK	3emn

CHAPTER 4

STRUCTURAL CONSEQUENCES OF S-NITROSYLATION THAT INFLUENCE ACTIVITY IN VIVO

By

Jennifer L. Greene[a,b], Margarita Tenopoulou[c], Paschalis-Thomas Doulias[c], Karthik Raju[e], Roland Dunbrack, Jr.[f], and Harry Ischiropoulos[c,d]

[a]Department of Biochemistry and Biophysics, The Raymond and Ruth Perelman School of Medicine, University of Pennsylvania, Philadelphia, PA 19104, USA
[b]Graduate Group in Biochemistry and Molecular Biophysics, University of Pennsylvania, Philadelphia, PA 19104, USA
[c]Department of Pediatrics, Children's Hospital of Philadelphia Research Institute, Philadelphia, PA, 19104, USA
[d]Department of Pharmacology, The Raymond and Ruth Perelman School of Medicine, University of Pennsylvania, Philadelphia, PA 19104, USA
[e]Neuroscience Graduate Group, University of Pennsylvania, Philadelphia, PA 19104, USA
[f]Program in Molecular Medicine, Fox Chase Cancer Center, Philadelphia, PA 19111, USA

4.1 Abstract

Understanding the structural consequences of S-nitrosylation has proved to be difficult due to a lack of structures for SNO-proteins. A recent study has revealed that S-nitrosylation may regulate the function of very long chain acyl-coA dehydrogenase (VLCAD), a mitochondrial enzyme that catalyzes the first rate-limiting step in the β-oxidation of fatty acids. Upon S-nitrosylation, the K_m of the enzyme decreases by 5-fold, suggesting that the protein can bind the substrate more efficiently. Normal mode analysis was used to investigate this hypothesis and identify protein movements which might be correlated to enhanced substrate binding upon S-nitrosylation. S-nitrosylation did not induce global conformational changes in the protein. However, smaller motions were observed across four different regions in the binding site, with the most apparent movement near the VLCAD S-nitrosocysteine, Cys238. This work further supports the hypothesis that S-nitrosylation may induce protein conformational changes that influence activity.

4.2 Introduction

A global proteomic investigation into the endogenous S-nitrosoproteome of mouse liver identified 328 sites belonging to 192 proteins (Doulias, et al. 2010). Protein network mapping revealed that sixteen of the S-nitrosylated proteins were clustered around the hormone leptin (Figure 4.1). Leptin is a hormone secreted by adipose tissue which acts on the central nervous system to maintain energy homeostasis. Leptin has also been shown to play a role in liver metabolism through its repression of stearoyl-CoA desaturase-1 which is the rate limiting step in monosaturated fat biosynthesis (Cohen et

al., 2004). Mice lacking leptin (ob/ob) can be nearly triple the size of their wildtype littermates with increased adipocyte size and number (Halaas et al., 1995; Pelleymounter

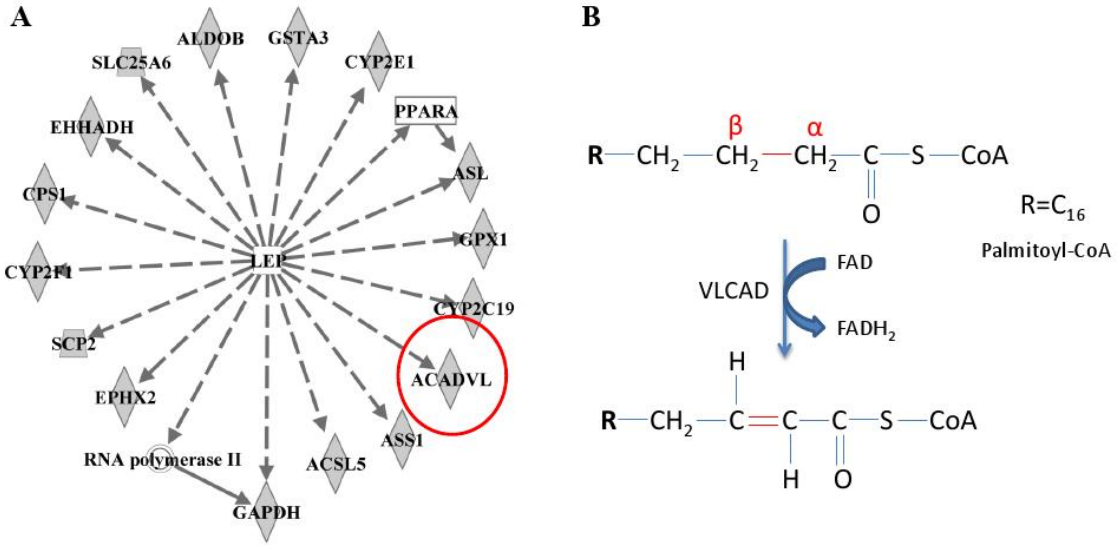

Figure 4.1: **Ingenuity pathway analysis (IPA) identifies indirect relationship between leptin and Very long chain acyl-CoA dehydrogenase** (A) Protein network mapping reveals significant clustering of 16 S-nitrosylated liver proteins around the hormone leptin. Very long chain acyl-CoA dehydrogenase (gene name: ACADVL, red circle) was revealed as indirect target (dashed line) of leptin. (B) Very long chain acyl-CoA dehydrogenase (VLCAD) catalyzes the first step in the β-oxidation of fatty acids. It oxidizes the substrate palmitoyl-CoA, forming a double bond between α and β carbons to form trans-Δ^2-Enoyl-CoA.

et al.,1995; Jackson Laboratories).

A study conducted in 2008 (Oliveira, et al. 2008) investigated the role of nitric oxide in nonalcoholic fatty liver, a disease that is characterized by an accumulation of fat deposits in the liver which can then result in impairment of its function. Administration of the S-nitrosothiol S-nitroso-N-acetylcysteine (SNAC) to ob/ob mice by gavage inhibited and reversed the phenotype. Interestingly, mice lacking endothelial nitric oxide

synthase also exhibited accumulation of lipids, further substantiating a role for nitric oxide in lipid metabolism (Schild et al. 2008).

Very long-chain specific acyl-CoA dehydrogenase (VLCAD), a mitochondrial enzyme, is one of the sixteen proteins identified as having an indirect link to leptin. VLCAD catalyzes the rate limiting first step in the β-oxidation of fatty acids in the liver (Figure 4.1). With a catalytic glutamate as its proton acceptor, VLCAD oxidizes the substrate palmitoyl-CoA, producing a double bond between its α and β carbons to form trans-Δ^2-Enoyl-CoA. Its recent identification has led to the hypothesis that S-nitrosylation of VLCAD may function as a molecular link between nitric oxide and liver metabolism. Therefore, when nitric oxide is unable to S-nitrosylate VLCAD, its function is impaired leading to the accumulation of fatty acids. Recent work within the lab has confirmed that Cys238 is S-nitrosated in ob/ob mice after GSNO treatment (Figure 4.2). Upon S-nitrosylation, the kinetics of VLCAD are altered such that its K_m is decreased by nearly 5-fold (Figure 4.2), suggesting an increased binding efficiency of its substrate palmitoyl-CoA. However, the molecular mechanism by which S-nitrosylation might alter substrate binding is largely unknown.

VLCAD consists of a 67 kiloDalton homodimer and is a member of the acyl-CoA deydrogenase (ACAD) family (McAndrew et al. 2008). Its substrate specificity is derived from a salt bridge formed between two helices which extends its binding cavity as compared to other ACADS. It also has an additional 180 residues on its carboxyl-terminal end shown to be essential in mitochondrial membrane binding (Souri et al. 1998b). Several studies have attempted to correlate VLCAD modifications with its activity. Mutation of a phosphorylation site resulted in reduced electron transfer activity

of the enzyme (Kabuyama et al. 2010). Souri et al. demonstrated abnormal K_m values for palmitoyl-CoA after mutation of an alanine to a proline near the carboxyl-terminus (Souri et al. 1998a). A more comprehensive study investigated the effect of missense mutations on substrate binding, enzyme-cofactor interaction, dimerization, & folding of the polypeptide chain (Gobin-Limballe et al. 2010). A glycine-to-alanine mutation

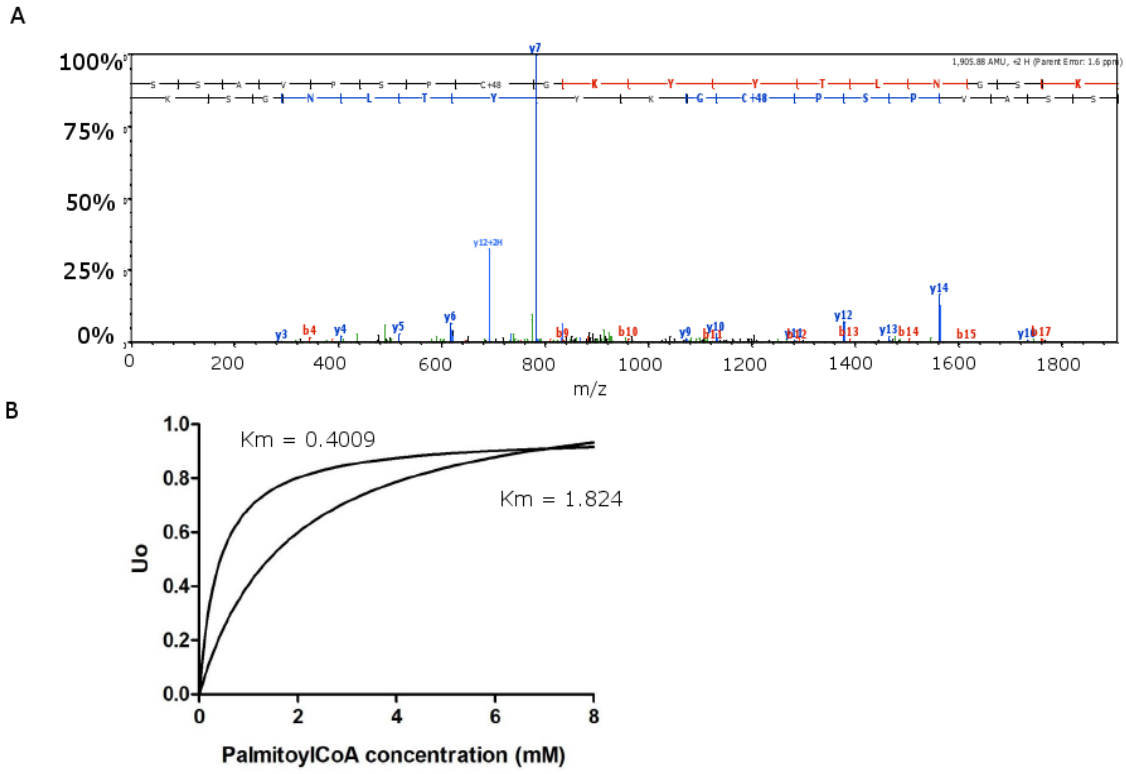

Figure 4.2: Cysteine238 confirmed as S-nitrosation site after GSNO treatment. (A) Cys238 identified as site of S-nitrosylation in VLCAD peptide sequence: SSAVPSPC_{238}GKYYTLNGSK. (B) Kinetics of VLCAD altered after GSNO treatment.

disrupted a hydrophobic pocket lining the substrate binding cavity whereas a R453Q mutation induced changes in the positioning of its catalytic glutamate.

Herein, we describe attempts to elucidate the structural consequences of S-nitrosylation for the enzyme VLCAD. We first began with an interrogation into the structures of existing S-nitrosylated cysteines to acquire favorable rotamer conformations for S-nitrosocysteine. Using normal mode analysis, we investigated the influence that introducing a nitric oxide moiety might have on protein structure in an attempt to explain our kinetic data.

4.3 Methods

Sequence conservation. Basic local alignment search tool (BLAST) was used to align the sequences of human (Uniprot Accession Number: P49748) and mouse VLCAD (Uniprot Accession Number: P50544).

Calculating bond angles and lengths. Bond angles and lengths of existing S-nitrosylated proteins were calculated by editing Perl scripts made available by the Dunbrack laboratory.

Generation of S-nitrosylated cysteine. S-nitrosocysteine was generated using the "S-nitrosator"` Python script from Timerghazin laboratory in the Molecular Modeling Toolkit. "S-nitrosator" utilizes the coordinates of thioredoxin and $\chi 3$ values calculated using from PCM-ONIOM(PBE0/def2-TZVPPD:AmberFF) calculation of an S-nitrosocysteine residue in an alpha–helix content.

Normal mode analysis using elNemo. ElNemo (Suhre et al. 2004) was used to observe the 100 lowest frequency modes and perturbed models were generated for the first five non-trivial modes of VLCAD. Residue mean square displacement (r^2) (as calculated by

elNemo) was used to identify protein movement. The substrate binding site was separated into four regions for the purpose of analysis. Region 1: 160Tyr, 163Leu, 164Val, 167Val, 174Val, 176Ile, 178Leu, 179Gly, 180Ala, 182Gln, 183Ser, and 184Ile; Region2: 214Phe, 216Leu, 217Thr, 222Gly, 223Ser, 224Asp, and 225Ala; Region3: 334Met, 337Leu, 340Gly, 341Arg, 343Gly, 344Met, and 347Ala; Region4: 458Phe, 460Ile, 461Phe, 462Glu, 463Gly, and 464Thr.

4.4 Results and Discussion

Use of existing S-nitrosylated protein structures for prediction of Cys238 side chain conformation

There is currently no published structure of mouse very long chain acyl-CoA dehydrogenase; however, the PDB contains two structures of human VLCAD. The first structure (PDB ID: 2UXW) was released in 2007. It is at 1.45 Å resolution, crystallized with trans-Δ^2-Palmitenoyl-CoA and contains residues 72-655. The second structure is at 1.91 Å resolution and contains amino acids 69-655 (PDB ID: 3B96); however, 3B96 is instead crystallized with myristoyl-CoA, a fatty acid of shorter chain length. The structure of 2UXW was selected for the purposes of this study (Figure 4.3).

Basic Local Alignment Search Tool (BLAST) was used to identify sequence homology between mouse and human VLCAD. The sequence alignment of mouse VLCAD (mVLCAD) and human VLCAD (hVLCAD) showed that the two share more than 80% sequence homology. More importantly, there was conservation of the S-nitrosylated cysteine residue (Cys238 in mouse; Cys237 in human) as well as high

conservation near the substrate binding site. In addition to being conserved between mice and humans, Cys238 is conserved across other mammalian species including rat, bovine, canine, and pig.

To investigate the influence of S-nitrosocysteine on VLCAD dynamics, it was first necessary to generate an S-nitrosylated form of the protein. The program SCWRL (Bower et al. 1997) can be used to predict the position of the cysteine side chain using a $\chi 1$-dependent rotamer library; however, because S-nitrosylation is still an emerging posttranslational modification, the library must be appended to incorporate the S-nitrosocysteine residue. The rotamer library is composed of a curated set of residues from high resolution structures in the PDB with low B-factors (Wang et al. 2008). A search of the PDB for the ligand S-nitrosocysteine (SNC) resulted in a total of 9 structures of which 6 were nonredundant: hemoglobin (1BUW), hypoxia inducible factor prolyl hydroxylase domain 2 (2Y33 and 2Y34), protein tyrosine phosphatase 1B (3EU0), blackfin tuna myoglobin (2NRM), thioredoxin (2HXK, 2IFQ, and 2IIY) and dimethylarginine dimethylaminohydrolase (2CI1).

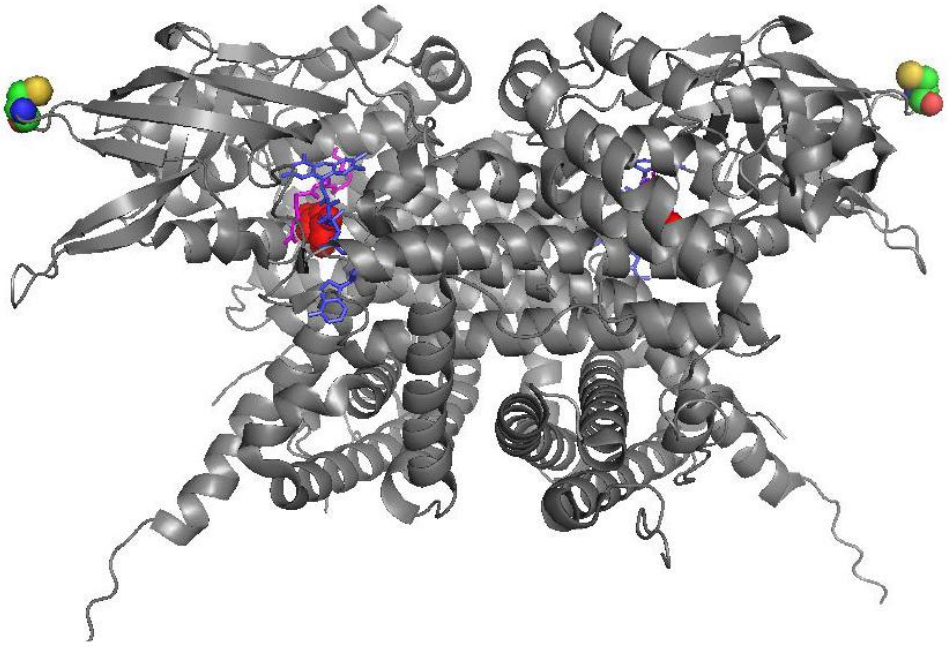

Figure 4.3: VLCAD structure 2uxw. Cysteine 238 is shown in sphere representation with coloring based upon elemental composition. Trans-Δ^2-Palmitenoyl-CoA is shown in purple in stick representation. Electron acceptor FAD is shown in blue in sticks representation. Catalytic glutamate shown in red in sphere representation.

In total, bond lengths and angles were calculated for twelve S-nitrocysteine residues across 9 different structures. The χ3 (chi3) value measures the bond angle between CB-SG-ND-OE; therefore, it is a detailed descriptor of the S-nitrosocysteine rotamer conformation. The chi3 data exhibited some variance but values for all thioredoxin S-nitrosocysteines remained fairly close to 0 (Table 4.1). Measured bond lengths of r(N-CA), r(CA-C), r(CA-CB), and r(CB-SG) remained fairly consistent across all S-nitrosocysteine residues (Table 4.2) with Cα carbon bond lengths being the most tightly distributed. Bond lengths between SG-ND and ND-OE were the most dispersed. r(SG-ND) ranged in length from 1.63 to 1.806 Å and r(ND-OE) ranged in length from 1.193 to 1.472 Å (Table 4.2). When comparing structures of hypoxia inducible factor

prolyl hydroxylase which forms S-nitrosocysteine by two different chemical reactions (GSNO soaked versus NO exposed), there is a striking difference in bond lengths for (ND-OE). The GSNO soaked structure (which would form S-nitrosocysteine through a transnitrosation reaction with a nitrosonium ion) had a measured length of 1.193 Å compared to the same protein treated with an $^{\bullet}$NO donor, which had a bond length of 1.46 Å. These data suggest that chemical species other than –Cys-S-N=O may exist. In fact, QM/MM studies conducted in the English Laboratory at Concordia University show that geometries for S-nitrosocysteine residues in published crystal structures are oftentimes more consistent with –C-S-NH-OH (personal communication).

With a total of six independent data points, these data were not incorporated into the rotamer library for side chain prediction. Additionally, the diversity of data calculated suggests that all residues classified as an S-nitrosocysteine may not be the same chemical species as an S-nitrosocysteine residue. Interestingly, that is what Chen and coworkers proposed when they published the structures of hypoxia inducible factor prolyl hydroxylase (Chen et al. 2008). They suggest that they were instead observing a reaction intermediate between nitric oxide and the cysteine residue. This again underscores that 1) the field of S-nitrosylation is in dire need of three dimensional structures of protein S-nitrosocysteine, and 2) exogenous sources of nitric oxide can result in different reaction products. Additionally, it is unfortunate that the Protein Data Bank still classifies 2Y33 and 2Y34 as containing S-nitrosocysteine residues when the authors themselves doubt its existence (Chen et al. 2008).

Table 4.1: Calculated bond angles of existing S-nitrosylated cysteines

PDBid	ResNum	Chain	phi	psi	omega	chi1	chi2	chi3
2IFQ	69	A	-88.69	3.06	178.45	-68.42	-71.19	1.22
2IFQ	69	C	-84.94	2.70	178.52	-66.26	-84.91	151.85
1BUW	93	B	-79.99	-60.79	-176.99	-54.71	-99.84	87.55
1BUW	93	D	-81.96	-70.29	-179.79	-54.16	-79.77	-75.65
2CI1	83	A	-139.30	111.23	177.56	175.12	79.42	-69.50
2HXK	62	B	-121.26	66.48	-174.47	-92.66	-156.02	-0.56
2HXK	69	B	-96.58	7.66	178.68	-63.56	-81.45	2.49
2IIY	62	A	-125.61	56.22	-161.63	-65.03	-81.52	1.30
2IIY	69	A	-82.42	-2.56	-173.57	-64.35	-71.75	0.71
2Y33	302	A	-135.82	113.66	-178.52	-168.91	-83.34	-76.06
2Y34	302	A	-128.28	117.37	176.77	178.34	-76.24	-93.49
3EU0	215	A	-138.14	-132.92	179.22	175.05	-56.03	41.08

2IFQ: S-nitroso thioredoxin (only Cys69 modified)
1BUW: S-nitroso hemoglobin
2CI1: Dimethylarginine dimethylaminohydrolase in complex with S-nitroso-L-homocysteine
2HXK: S-nitroso thioredoxin (both 62 and 69 modified)
2IIY: S-nitroso thioredoxin (both 62 and69 modified)
2Y33: S-nitrosylated hypoxia inducible factor prolyl hydroxylase domain 2 (GSNO soaked)
2Y34: S-nitrosylated hypoxia inducible factor prolyl hydroxylase domain 2 (NO exposed)
3EU0: S-nitrosylated protein tyrosine phosphatase 1B

Table 4.2: Calculated bond lengths of existing S-nitrosylated cysteines

PDBid	ResNum	Chain	r(N-CA)	r(CA-C)	r(CA-CB)	r(CB-SG)	r(SG-ND)	r(ND-OE)
2IFQ	69	A	1.458	1.533	1.532	1.764	1.783	1.196
2IFQ	69	C	1.469	1.506	1.532	1.795	1.797	1.188
1BUW	93	B	1.466	1.514	1.566	1.839	1.757	1.202
1BUW	93	D	1.478	1.522	1.557	1.855	1.762	1.209
2CI1	83	A	1.455	1.526	1.519	1.787	1.646	1.472
2HXK	62	B	1.485	1.523	1.567	1.787	1.806	1.205
2HXK	69	B	1.479	1.525	1.535	1.779	1.804	1.199
2IIY	62	A	1.437	1.509	1.535	1.768	1.759	1.193
2IIY	69	A	1.483	1.538	1.519	1.785	1.803	1.207
2Y33	302	A	1.432	1.512	1.522	1.778	1.788	1.193
2Y34	302	A	1.47	1.53	1.53	1.83	1.63	1.46
3EU0	215	A	1.454	1.524	1.53	1.8	1.665	1.308

Normal mode analysis reveals movement near S-nitrosylated cysteine

QM/MM calculations were used to generate an S-nitrosocysteine residue within the protein structure of VLCAD (2UXW). VLCAD was modified at Cysteine238 to form SNO-Cysteine (SNC) using the Python script "S-nitrosator" developed by the Timerghazin Laboratory. Using the program elNemo: The Elastic Network Model, low frequency vibrational modes of the protein were calculated (Suhre and Sanejouand, et al.

2004). The lowest frequency normal modes (modes 7-10) were initially examined to determine if S-nitrosylation induced large

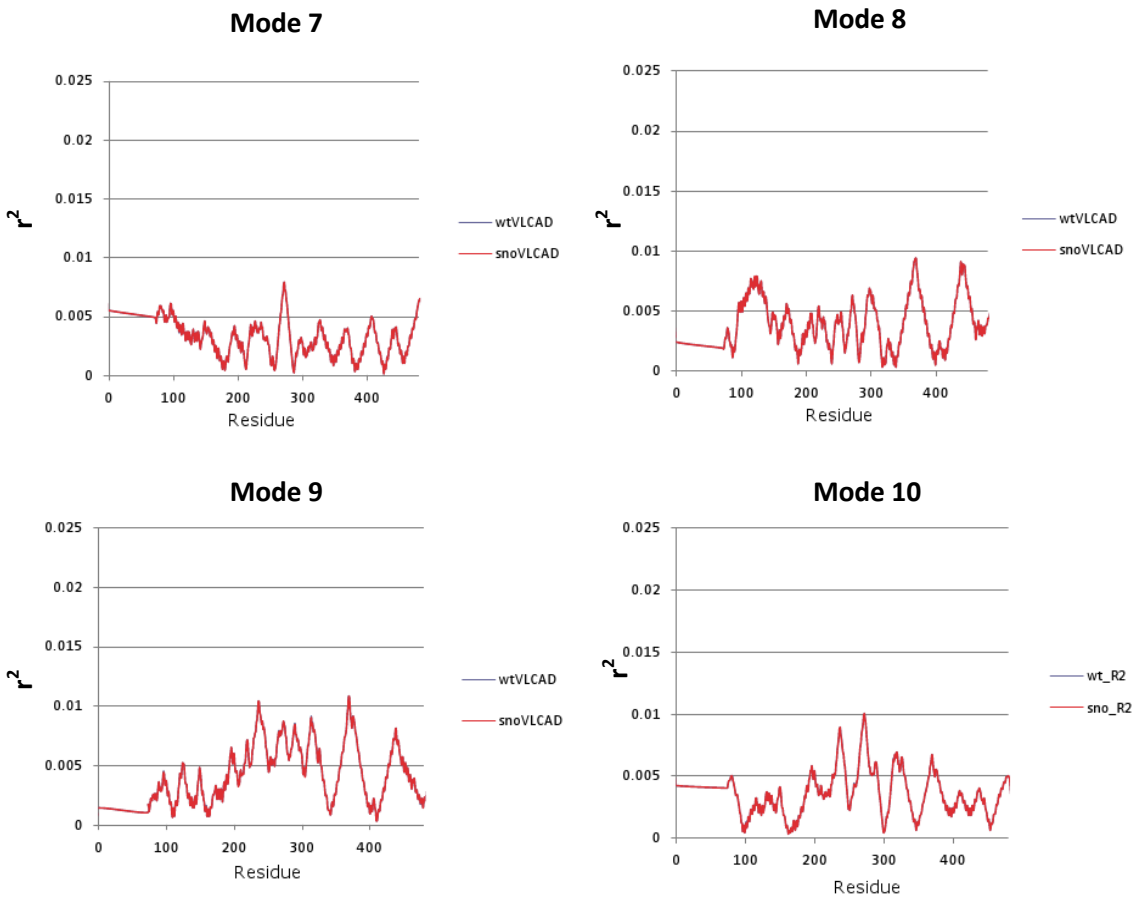

Figure 4.4: S-nitrosylation does not induce large scale motions in VLCAD. Residue mean square displacement values were examined for lower frequency normal modes before and after S-nitrosylation.

conformational changes. Large global or collective motions of a protein are described using low-frequency modes. Examination of Modes 7, 8, 9, and 10 revealed no global motions which may have been induced by S-nitrosylation of Cys238. In these modes, residue mean square displacement (r^2) remained consistent between wildtype and SNO-VLCAD (Figure 4.4).

The binding site of palmitoyl-CoA was next examined to determine if S-nitrosylation induced any quantifiable structural changes. Although Uniprot identifies the substrate binding pocket as 338-341 and 462-463, viewing the three dimensional structure of VLCAD in PyMol

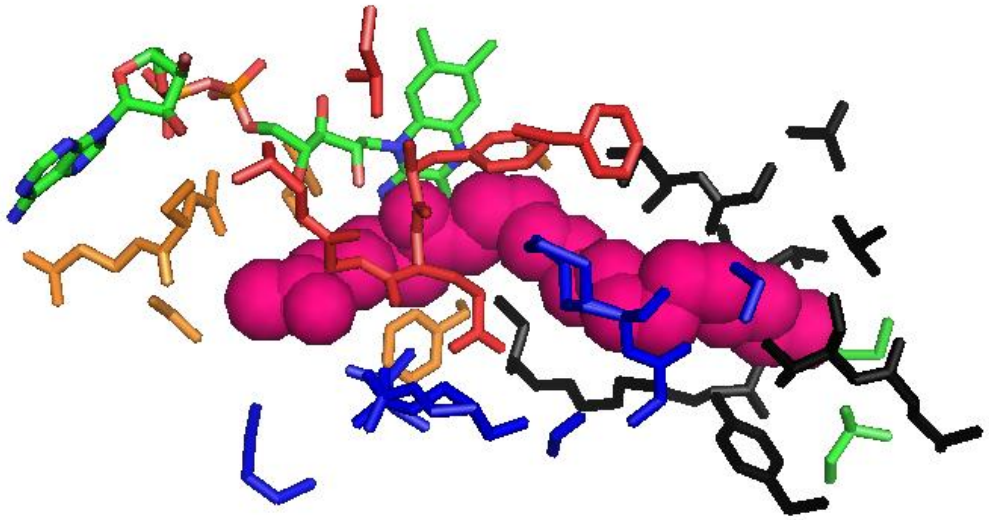

Figure 4.5: Binding site of trans-Δ^2-Palmitenoyl-CoA in VLCAD. Binding site is composed of 35 residues divided into 4 different regions: Region 1 (in black), Region 2 (orange); Region 3 (blue); Region 4 (red). Image generated in PyMol Viewer.

revealed that the substrate is in close proximity of 35 residues when bound (Figure 4.5). To better characterize the entire substrate binding site, it was grouped into 4 different regions based upon its neighboring residues (Figure 4.5). Residues comprising each region are previously described in Materials and Methods section. Region 4 (in red) included the catalytic glutamate residue 462.

The higher frequency modes 45 through 50 were examined to investigate smaller local motions which might occur near the binding site. Examination of Modes 49 & 50 in particular revealed the greatest difference in the movement of atoms in response to S-

nitrosylation. Region 4 consists of 214Phe, 216Leu, 217Thr, 222Gly, 223Ser, 224Asp, and 225Ala. Upon S-nitrosylation, these residues within the binding site do not show much movement (Figure 4.6); however, examination of residues surrounding Cys238 shows a large difference in residue displacement (r^2) upon S-nitrosylation. The region displaying the most movement (Residues 232-240) is composed of the cysteine-containing loop as well as an adjacent beta sheet. Preservation of the shape upon S-nitrosylation also suggests a correlated movement of these flanking amino acids. Region 4 also appears to display movement; however, these motions are an artifact since these residues are involved in membrane anchoring in the mitochondria and are not contained within the structure.

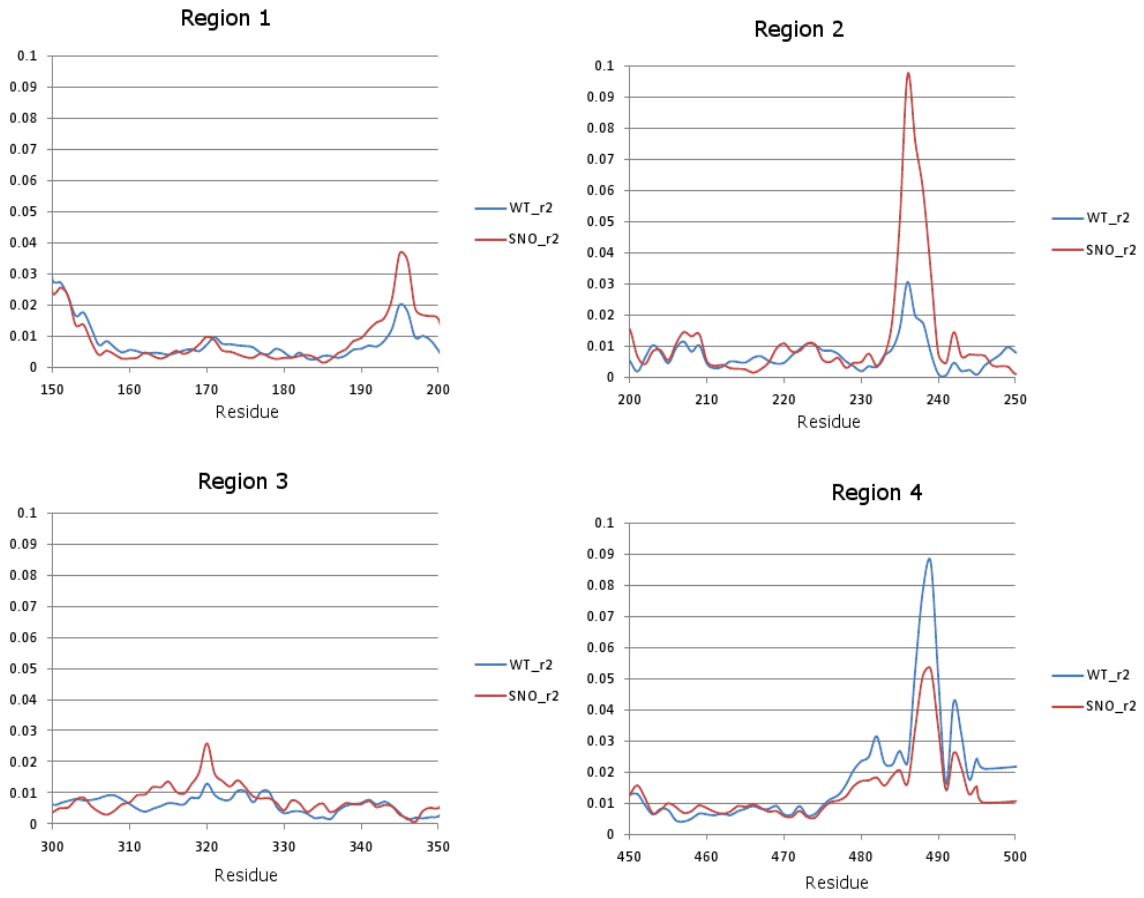

Figure 4.6: Higher frequency mode indicates extensive movement of Cys238 upon S-nitrosylation. Mode 49 is examined across the four different regions of the binding site with Region 1. Mode 49 is also representative of Mode 50.

Collectively, these data suggest that the loop region containing Cys238 may be involved in enhancing the enzymatic activity of very long chain acyl-CoA dehydrogenase. Interestingly, Cys238 is measured to be ≥ 30 Angstroms from the substrate binding site, suggesting that longer range motions can influence the ability of the enzyme to bind substrate. After S-nitrosylation inhibited the activity of the protein methionine adenosyltransferase, Perez-Mato et al. concluded that S-nitrosylation of cysteine in a flexible loop changed its conformation and did not allow access of the

substrate to its binding site (Perez-Mato et al. 1999). In the case of VLCAD, S-nitrosylation instead appears to make the loop even more flexible (Figure 4.6). This is a particularly intriguing finding since the ligand that VLCAD is crystallized with is the product and not the substrate. Trans-Δ^2-Palmitenoyl-CoA is the product that is formed upon oxidation of palmitoyl-coA. This suggests that S-nitrosylation may play a role in helping to release the product once it is formed. However, additional experiments, possibly molecular dynamics simulations, are necessary to fully elucidate these local protein motions.

CHAPTER FIVE: SUMMARY AND GENERAL DISCUSSION

5.1 Summary

S-nitrosylation is an emerging posttranslational modification (PTM) by which nitric oxide can exert its biological function. However, gaps in knowledge regarding its mechanism of formation, the specificity of its targets, and the molecular mechanism by which S-nitrosylation can alter protein function remain resolved. This thesis aimed to address each one of these questions with the use of a global proteomic method for the identification of endogenous protein S-nitrosocysteine residues.

5.2 Proteomic techniques are essential for characterization of the endogenous S-nitrosoproteome

While there are still large gaps in knowledge regarding S-nitrosylation, many cysteines have been and continue to be identified as being S-nitrosylated in vivo. Initial investigations into the identification of S-nitrosocysteine protein residues began with techniques which did not allow for a priori hypotheses regarding the identity of the protein. Sample preparations mandated that the protein either be in isolation or that an antibody must be available to validate its identification.

The application of tandem mass spectrometry allowed for proteins to be identified in complex solutions when coupled to chromatographic separation techniques. The advent of this technology helped to test hypotheses on a much larger scale. For S-nitrosylation, many answers to the gaps in knowledge lie in the identification of its

targets. While LC-MS/MS is a powerful tool, it is useless without a method upstream that is sensitive enough to enrich for endogenous protein S-nitrosocysteine. To that end we developed a complementary mercury-based mass spectrometric approach for the identification of endogenous S-nitrosoproteomes. Without the development of this global unbiased enrichment technique, the data would not have as effortlessly revealed a population of cysteines which has yet to be described.

While cysteine residues are not one of the most frequently occurring amino acids, they are highly conserved, suggesting an important role in biochemical processes. Cysteines are known to be highly reactive; therefore it was a surprising finding that identification of S-nitrosylated cysteines resulted in the characterization of an entirely unique population of cysteine residues. Cysteines identified using our global proteomic approach were not predicted or experimentally shown to be redox active, engaged in disulfide bonds, coordinated to metals, glutathionylated, or alkylated. The identification of this unique population of cysteine residues underscores their biological importance.

Although our proteomic tool does provide a robust proteomic tool for interrogating an endogenous S-nitrosoproteome, it does have some limitations. By applying our stringent criteria (i.e. 2 unique protein peptides as well as 1 cysteic acid containing peptide), the sites of identification may not always be consistent with those previously found to be S-nitrosylated by others. In addition, because S-nitrosylation is an emerging signaling mechanism that has been shown to be regulated, the dynamic nature of SNO may not always allow for the capture of the protein in its S-nitrosylated state.

Identification of the wildtype liver SNO-proteome resulted in nearly 50% complementary between both the MRC and mPEG-biotin approach with 25% being unique to either method. Consequently, when only a single method is used as with the GSNOR$^{-/-}$ proteome, a fraction of the proteome may be unaccounted for. To be consistent, the same approach should be employed when making comparisons between different proteomes.

5.3 Transnitrosation by GSNO is a precisely controlled and targeted mechanism

After identifying that multiple mechanisms of S-nitrosocysteine formation could be taking place in vivo in Chapter 2, Chapter 3 sought to delve further into the mechanism by which GSNO can modify protein cysteine residues. Using a knockout of the enzyme responsible for in vivo metabolism of GSNO, we were able to identify a subset of cysteine residues which may form S-nitrosocysteine using this GSNO-mediated mechanism of transnitrosation. When biochemically/biophysically characterizing the cysteine residues, there were two novel findings within the GSNOR$^{-/-}$ unique SNO-proteome. The first was that cysteine residues were surrounded by charged residues. Only 2 out of 111 cysteines with structures did not have a single charged residue within 6 Angstroms. This is not a completely surprising finding, since the presence of charged residues near cysteines in the wildtype liver proteome supported our hypothesis regarding a GSNO-mediated mechanism. However, there does seem to be enrichment for charged residues within this population since all but 2% fall into this category.

The second finding is regarding the presence of cysteines in their surrounding secondary structure. The data revealed that these GSNOR$^{-/-}$ unique cysteines were more frequently in coils than cysteine within the previously published wildtype proteome (Doulias et al.). Our initial hypothesis was that S-nitrosylated cysteines lie in these more flexible regions of the protein in order to accommodate whatever their mechanism of S-nitrosocysteine formation might be. This suggests that cysteines targeted by GSNO may need to exist in these flexible regions to accommodate the tripeptide. This claim is further supported when examining the relative residue surface accessibility of the cysteines. With the majority of cysteines classified as being buried, it only underscores that the protein needs to be flexible to allow access to the residue.

Chapter 3 also presented a novel mechanism of GSNO mediated transnitrosation. Previous data has posited the idea that the process of transnitrosation is an acid-base catalysis. Using mutational analysis, Perez-Mato et al. (Perez-Mato et al. 1999) demonstrate that an acidic residue is somehow involved in the formation of protein S-nitrosocysteine. They propose that the acidic residue promotes the leaving of a nitrosonium ion from GSNO by promoting GSH formation and that basic residues are involved in increasing the nucleophilicity of the cysteine residue through its deprotonation.

However, our data support the idea of a base catalysis mechanism of GSNO-mediated transnitrosation. Using a model protein which was identified in the GSNOR$^{-/-}$ unique dataset, the data show that coordination of a basic residue (Arg) to the sulfur atom of the CYG intermediate can promote the formation of S-nitrosocysteine to the opposing

cysteine residue. Therefore, coordination of a basic residue to the SG of GSNO would result in formation of protein S-nitrosocysteine. In addition, coordination of this same basic residue to other atoms such as N or O had the opposite effect and did not form protein S-nitrosocysteine. These findings illustrate how the protein environment can tightly regulate the reactivity of the transnitrosating agent (GSNO) and promote the formation of specific reaction products. Initially these findings seem to conflict with what was previously suggested for the push/pull or acid-base catalyzed mechanism of GSNO transnitrosation; however, as the QM/MM calculations illustrate, the coordination of the residue to a specific atom in the S-nitrosothiol is really what drives its reactivity. Previous calculations conducted by the Timerghazin Laboratory have illustrated how coordination of acidic residues to atoms other than S (O, N) can actually promote nitrosonium formation as well.

Collectively, these findings imply that ex vivo supplementation with GSNO does not faithfully replicate in vivo transnitrosation. Cellular processes are in place to readily metabolize GSNO when it is in a cellular environment (i.e. GSNOR, reactivity with other molecules). However, when samples such as cell lysates are treated with GSNO, it can result in an uncontrolled and non-specific manner. While this is concentration-dependent, data within our own lab has shown this to be the case (data not shown).

Another important fact to consider is the population of $GSNOR^{-/-}$ unique cysteines that are identified by comparison between the $GSNOR^{-/-}$ and wildtype proteomes. S-nitrosylated cysteines shared between both proteomes were removed to enrich for the population of cysteines targeted by GSNO-mediated mechanisms of transnitrosation. By

deriving this unique population of GSNOR$^{-/-}$ cysteines in this way, the data may be skewed toward more extreme examples of GSNO-mediation. Because our previous wildtype data suggested that multiple mechanisms may be occurring in vivo, it is likely that stable GSNO-targeted cysteines would also exist within this population. However, by subtracting out those cysteines which belong to both groups, this population is not included in the bioinformatics analysis.

5.4 Implications of this work

Collectively, this body of work illustrates how a global tool can be used to generate testable hypotheses leading to more targeted investigations regarding cellular processes. This thesis begins which a global investigation into the identification of an S-nitrosoproteome containing over 300 proteins and ends with an investigation into the S-nitrosylation induced structural consequences of a single protein. Existing knowledge in the field of S-nitrosylation can be broadly divided into 5 categories (in decreasing order of knowledge): 1) identification of S-nitrosylated proteins, 2) alteration in protein functionality, 3) dependency of target on a specific NOS isoform, 4) regulation of the signal by denitrosylation, and 5) structural consequences. The data described herein have contributed in some form to each one of these five categories.

The identification of many proteins as being S-nitrosylated has resulted in the development of several predictive tools (Lee et al. 2011; Xue et al. 2010). For S-nitrosylation, this still remains a challenge due to the fact that there are not specific motifs which are required for S-nitrosylation. This is largely due to the fact that unlike

other posttranslational modifications such as acetylation or phosphorylation, no specific group of proteins has been identified as mediators in the process of S-nitrosylation. Therefore, protein-protein interactions which have helped to derive motifs and predictive tools for other PTMs, do not appear to be essential for all S-nitrosocysteine formation. While several proteins have been shown to transfer nitrosonium ion to another protein, there is no general category of "S-nitrosyl"-ases. Those tools which do exist often use data which have been obtained using exogenous sources before. As was described previously, exogenous forms of nitric oxide can result in a myriad of different chemical species. Therefore, it does not accurately describe endogenous mechanisms of S-nitrosocysteine formation.

REFERENCES

Ascenzi, P., Colasanti, M., Persichini, T., Muolo, M., Polticelli, F., Venturini, G., Bordo, D., Bolognesi, M. (2000) Re-Evaluation of Amino Acid Sequence and Structural Consensus Rules for Cysteine-Nitric Oxide Reactivity. *Biol Chem* **381**, 623-627.

Al-Sa'doni, HH, & Ferro, A. (2000) S-nitrosothiols: a class of nitric oxide-donor drugs. *Clin Sci (Lond)* **98**(5), 407-20.

Al-Shahrour, F., Díaz-Uriarte, R., Dopazo, J. (2004) FatiGO: A web tool for finding significant associations of Gene Ontology terms with groups of genes. *Bioinformatics* **20**,578–580.

Arnold, W.P., Mittal, C.K., Katsuki, S., Murad, F. (1977) Nitric oxide activates guanylate cyclase and increases guanosine 3'5'-cyclic monophosphate levels in various tissue preparations. *Proc Natl Acad Sci U S A* **74**, 3203-3207.

Asada, K., Kurokawa, J., and Furukawa, T. (2009) Redox- and calmodulin-dependent S-nitrosylation of the KCNQ1 channel. *J Biol Chem* **284**, 6014-20.

Balbatun, A., Louka. F.R., & Malinski, T. (2003) Dynamics of nitric oxide release in the cardiovascular system. *Acta Biochimica Polonica* **50**(1), 61-68.

Beckman, J.S., Beckman, T.W., Chen, J., Marshall, P.A., Freeman, B.A. (1990) Apparent hydroxyl radical production by peroxynitrite implications for endothelial, *Proc Natl Acad Sci U S A* **87**(4), 1620-4.

Benhar, M., Forrester, M.T., Hess, D.T., Stamler, J.S. (2008) Regulated protein denitrosylation
by cytosolic and mitochondrial thioredoxins. *Science* **320**, 1050–1054.

Boese, M., Mordvintcev, P.I., Vanin, A.F., Busse, R. & Mulsch, A. (1995) S-nitrosation of serum albumin by dinitrosyl iron complex. *J. Biol. Chem.* **270**, 29244-29249.

Bosworth, C.A., Toledo, J.C., Zmijewski, J.W., Li, Q., Lancaster Jr., J.R. (2009). Dinitrosyliron complexes and the mechanism(s) of cellular protein nitrosothiol formation from nitric oxide. *Proc Natl Acad Sci U S A* **106**(12), 4671-4676.

Bredt, D.S., Hwang, P.M., Glatt, C.E., Lowenstein, C., Reed, R.R. and Snyder, S.H. (1991)
Nature **351**, 714-718.

Bredt, D.S., Snyder, S.H. (1990) Isolation of nitric oxide synthetase, a calmodulin-requiring enzyme. *Proc Natl Acad Sci U S A* **87**, 682-685.

Britto, P.J., Knipling, L., Wolff, J. (2002) The Local Electrostatic Environment Determines Cysteine Reactivity of Tubulin. *J Biol Chem* **277**, 29018-29027.

Broillet, M. C. (2000) A single intracellular cysteine residue is responsible for the activation of the olfactory cyclic nucleotide-gated channel by NO. *J Biol Chem* **275**, 15135-41.

Brown G.C., Cooper, C.E. (1994) Nanomolar concentrations of nitric oxide reversibly inhibit synaptosomal respiration by competing with oxygen at cytochrome oxidase. *FEBS Lett* **356**, 295–298.

Brunton T.L.. (1867) On the use of nitrite of amyl in angina pectoris. *Lancet* **2,** 97–8.

Butler, A. R. (2006) Pharmacological preparations in which NO was the active agent have been used for over 1000 years, although this fact was not appreciated at the time. *J. R Coll. Physicians Edinb.* **36,** 185–189.

Chalker, J.M., Bernardes, G.J.L., Lin, Y.A., Davis, B.G. (2009) Chemical modification of proteins at cysteine: opportunities in chemistry and biology. *Chem. Asian J.* **4**, 630-640.

Chen, Y.-ju, Ku, W.-chi, Lin, P.-yi, Chou, H.-chiao, Khoo, K.-hooi, Chen, Y.-ju. (2010) S-Alkylating Labeling Strategy for Site-Specific Identification of the S-Nitrosoproteome research articles, *J Prot Res* **9**, 6417-6439.

Chen, C-A., Wang, T-Y., Varadharaj, S. (2010) S-glutathionylation uncouples eNOS and regulates its cellular and vascular function. *Nature* **468**, 1115-1120.

Chen, Y., Irie, Y., Keung, W. M., Maret, W. (2002) S-nitrosothiols react preferentially with zinc thiolate clusters of metallothione in III through transnitrosation. *Biochemistry* **41**, 8360-7.

Chen, Y-Y., Chu, H-M., Pan, K-T., Teng, C.H., Wang, D.L., Wang, A.H., Khoo, K.H., Meng, T.C. (2008) Cysteine S-nitrosylation protects protein-tyrosine phosphatase 1B against oxidation-induced permanent inactivation. *J Biol Chem* **283**(50), 35265-35272.

Cho, D.-H., Nakamura, T., Fang, J., Cieplak, P., Godzik, A., Gu, Z., and Lipton, S. A. (2009) S-nitrosylation of Drp1 mediates beta-amyloid-related mitochondrial fission and neuronal injury. *Science* **324**, 102-5.

Cho, H., Mu, J., Kim, J.K. (2001) Insulin resistance and a diabetes mellitus-like syndrome in mice lacking the protein kinase Akt2 (PKB beta). *Science* **292**, 1728-1731.

Choi, Y. B., Tenneti, L., Le, D. a, Ortiz, J., Bai, G., Chen, H. S., and Lipton, S. A. (2000) Molecular basis of NMDA receptor-coupled ion channel modulation by S-nitrosylation. *Nat Neurosci* **3**, 15-21.

Choudhary, C., Kumar, C., Gnad, F., Nielsen, M.L., Rehman, M., Walther, T.C., Olsen, J.V., Mann, M. (2009) Lysine acetylation targets protein complexes and coregulates major cellular functions. *Science* **325**, 834–840.

Chowdhury, R., Flashman, E., Mecinović, J., et al. (2011) Studies on the reaction of nitric oxide with the hypoxia-inducible factor prolyl hydroxylase domain 2 (EGLN1). *J Mol Biol* **410**, 268-279.

Cohen, P., Friedman, J.M. (2004) Leptin and the control of metabolism: Role for stearoyl-CoA desaturase-1 (SCD-1). *J Nutr* **134**, 2455S–2463S.

Dastoor, Z. & Dreyer, J.L. (2001) Potential role of nuclear translocation of glyceraldehyde-3-phosphate dehydrogenase in apoptosis and oxidative stress. *J. Cell Sci*. **114**, 1643-1653.

de Oliveira CP, de Lima, V.M., Simplicio, F.I., Soriano, F.G., de Mello, E.S., de Souza, H.P., Alves, V.A., Laurindo, F.R., Carrilho, F.J., de Oliveira, M.G. (2008) Prevention and reversion of nonalcoholic steatohepatitis in OB/OB mice by S-nitroso-N-acetylcysteine treatment. *J Am Coll Nutr* **27**, 299–305.

delaTorre, A., Schroeder, R.A., Kuo, P.C. (1997) Alteration of NF-KB p50 DNA binding kineticts by S-nitrosylation. *Biochem Biophys Res Commun*. **238**(3), 73-6.

Derakhshan B, Wille PC, Gross SS (2007) Unbiased identification of cysteine S-nitrosylation sites on proteins. *Nat Protoc* **2**, 1685–1691.

Doulias, P.-T., Greene, J. L., Greco, T. M., Tenopoulou, M., Seeholzer, S. H., Dunbrack, R. L., and Ischiropoulos, H. (2010) Structural profiling of endogenous S-nitrosocysteine residues reveals unique features that accommodate diverse mechanisms for protein S-nitrosylation. *Proc Natl Acad Sci U S A* **107**, 16958-16963.

Dosztanyi, Z., Csizmok, V., Tompa, P., and Simon, I. (2005) IUPred: web server for the prediction of intrinsically unstructured regions of proteins based on estimated energy content. *Bioinformatics*, **21**(16),3433-3434.

Dudzinski, D.M., & Michel, T. (2007) Life history of eNOS: partners and pathways. *Cardiovasc. Res.* **75**, 247-260.

Dupradeau, F.Y., Pigache, A., Zaffran, T., Savineau, C., Lelong, R., Grivel, N., Lelong, D., Rosanski, W., Cieplak, P. (2010) The R.E.D. tools: Advances in RESP and ESP charge derivation and force field library building. *Phys. Chem. Chem. Phys.* **12**, 7821-7839.

Erwin, P.A., Mitchell, D.A., Sartoretto, J., Marletta, M.A. & Michel, T. (2006). Subcellular Targeting and Differential S-nitrosylation of Endothelial Nitric-oxide Synthase. *J. Biol. Chem.* **281**, 151-7.

Eu, J.P., Sun, J., Xu, L., Stamler, J.S. & Meissner, G. (2000) The skeletal muscle calcium release channel: coupled O_2 sensor and NO signaling functions. *Cell* **102**, 499-509.

Faccenda A., Bonham, C.A., Vacratsis, P.O., Zhang, X., & Mutus, B. (2010) Gold nanoparticle enrichment method for identifying S-nitrosylation and S-glutathionylation sites in proteins. *J. Am. Chem. Soc.* **132**, 11392-11394.

Fomenko, D.E., Xing, W., Adair, B.M., Thomas, D.J., & Gladyshev, V.N. (2007) High-Throughput Identification of Catalytic Redox-Active Cysteine Residues. *Science* **315**, 387-389.

Fomenko, D.E., Marino, S.M., & Gladyshev, V.N. (2008) Functional diversity of cysteine residues in proteins and unique features of catalytic redox-active cysteines in thiol oxidoreductases. *Mol Cells* **26**(3), 228-235.

Forrester MT, Foster MW, Stamler JS (2007) Assessment and application of the biotin switch technique for examining protein S-nitrosylation under conditions of pharmacologically induced oxidative stress. *J Biol Chem* **282**, 13977–13983.

Forrester, M.T., Seth, D., Hausladen, A., et al. (2009) Thioredoxin-interactiving Protein (Txnip) is a feedback regulator of S-nitrosylation. *J. Biol. Chem.* **284**(52), 36160-36166.

Frank, S., Kampfer, H., Wetzler, C., Pfeilschifter, J. (2002) Nitric oxide drives skin repair: novel functions of an established mediator. *Kidney Int* **61**, 882-888.

Furchgott, R.F., Zawadzki, J.V. (1980) The obligatory role of endothelial cells in the relaxation of arterial smooth muscle by acetylcholine. *Nature* **288**, 373-6.

Gamgee A. (1868) Researches on the blood – on the action of nitrites on blood. *Phil Tran Roy Soc* **158**, 589–96.

Garcia-Cardena, G., Fan, R., Shah, V., et al. (1998) Dynamic activation of endothelial nitric oxide synthase by Hsp90. *Nature* **392**, 821-4.

Garcin, E. D., Bruns, C. M., Lloyd, S. J., Hosfield, D. J., Tiso, M., Gachhui, R., Stuehr, D. J., Tainer, J. A., and Getzoff, E. D. (2004) Structural basis for isozyme-specific regulation of electron transfer in nitric-oxide synthase. *J. Biol. Chem.* **279**, 37918–37927.

Ghosh, D.K., & Stuehr, D.J. (1995) Macrophage NO synthase: characterization of isolated oxygenase and reductase domains reveals a head-to-head subunit interaction. *Biochemistry* **34**, 801-807.

Giustarini, D., Milzani, A., Aldini, G., et al. (2005) S-Nitrosation versus S-Glutathionylation of Protein Sulfhydryl Groups by S-nitrosogluathione. *Antioxidants & Redox Signaling* **7**(7-8), 930-9.

Giustarini, D., Dalle-Donne, I., Colombo, R., Milzani, A., & Rossi, R. (2008) Is ascorbate able to reduce disulfide bridges? A cautionary note. *Nitric Oxide* **19**, 252-258.

Gobin-Limballe, S., McAndrew, R.P., Djouadi, F., Kim, J.-J., & Bastin, J. (2010) Compared effects of missense mutations in Very-Long-Chain Acyl-CoA Dehydrogenase deficiency: Combined analysis by structural, functional, and pharmacological approaches. *Bioch Biophys Acta* **1802**, 478-484.

Gow, A.J., Buerk, D.G. & Ischiropoulos, H. (1997) A novel reaction mechanism for the formation of S-nitrosothiol in vivo. *J. Biol. Chem*. **272**, 2841-2845

Green, L.C., Ruiz de Luzuriaga, K., Wagner, D.A., Rand, W., Istfan, N., Young, V.R. & Tannenbaum, S.R. (1981) Nitrate biosynthesis in man. *PNAS USA*, 78, 7764-8.

Greco, T.M., Hodara, R., Parastatidis, I., Heijnen, H.F.G., Dennehy, M.K., Liebler, D.C., & Ischiropoulos, H. (2006) Identification of S-nitrosylation motifs by site-specific mapping of the S-nitrosocysteine proteome in human vascular smooth muscle cells. *PNAS* **103**(19), 7420-7425.

Gregersen, N., Andresen, B.S., Pedersen, C.B., Olsen, R.K., Corydon, T.J., Bross, P. (2008) Mitochondrial fatty acid oxidation defects – remaining challenges. *J. Inherit. Metab. Dis*. **31**, 643-657.

Gruetter, C.A., Barry, B.K., McManara, D.B., Gruetter, D.Y., Kadowitz, P.J., & Ignarro, L.J. (1979) Relaxation of bovine coronary artery and activation of coronary arterial guanylate cyclase by nitric oxide, nitroprusside and a carcinogenic nitrosamine. *J Cycl Nucl Res* **5**, 211-24.

Guo, C.J., Atochina-Vasserman, E.N., Abramova, E., Foley, J.P., Zaman, A., Crouch, E., Beers, M.F., Savani, R.C., Gow, A.J. (2008) S-nitrosylation of surfactant protein-D controls inflammatory function. *PLoS Biol* **6**, 2414-2423.

Halaas, J.L., Gajiwala, K.S., Maffei, M., Cohen, S.L., Chait, B.T., Rabinowitz, D., Lallone, R.L., Burley, S.K., Friedman, J.M. (1995) Weight-reducing effects of the plasma protein encoded by the obese gene. *Science* **269**, 543–546.

Hao G, Derakhshan B, Shi L, Campagne F, Gross SS (2006) SNOSID, a proteomic method for identification of cysteine S-nitrosylation sites in complex protein mixtures. *Proc Natl Acad Sci USA* **103**, 1012–1017.

Hao G, Xie L, Gross SS (2004) Argininosuccinate synthetase is reversibly inactivated by S-nitrosylation in vitro and in vivo. *J Biol Chem* **279**, 36192–36200.

Hara, M.R., Agrawal, N., Kim, S.F. et al. (2005) S-nitrosylated GAPDH initiates apoptotic cell death by nuclear translocation following Siah1 binding. *Nat Cell Biol* **7**(7), 665-674.

Harrison, DG., Kurz, MA., Quillen, JE., Sellke, FW, Mugge, A. (1992) Normal and pathophysiologic considerations of endothelial regulation of vascular tone and their relevance to nitrate therapy. *Am J Cardiol* **70**,11B-17B.

Hashemy, S.I. & Holmgren, A. (2008) Regulation of the catalytic activity and structure of human thioredoxin 1 via oxidation and S-nitrosylation of cysteine residues. *J Biol Chem* **283**(32), 21890-21898.

Henry, Y., Lepoivre, M., Drapier, J.C., Ducrocq, C., Boucher, J.L. & Giussani, A. (1993) EPR characterization of molecular targets for NO in mammalian cells and organelles. *FASEB Journal*, **7**, 1124-34.

Hess, D.T., Matsumoto, A., Kim, S.O., Marshall, H.E. & Stamler, J.S. (2005). Protein S-nitrosylation: purview and parameters. *Nat. Rev. Mol. Cell Biol*. **6**, 150-166.

Hess, D. T., Matsumoto, A., Nudelman, R., and Stamler, J. S. (2001) S-nitrosylation: spectrum and specificity. *Nat Cell Biol* **3**, E46-9.

Hibbs Jr., J.B., Taintor, R.R., Vavrin, V., Granger, D.L., Drapier, J.-C., Amber, I.J., & Lancaster Jr., J.R. (1990) Synthesis of nitric oxide from a guanidino nitrogen of L-arginine: a molecular mechanism that targets intracellular iron. Nitric Oxide from L-arginine: A Bioregulatory System (Moncada, S. and E.A. Higgs, eds.) pp. 189-223.

Hibbs, J.B., Jr., Taintor, R.R., and Vavrin, Z. (1987) Macrophage cytotoxicity: role for L-arginine deiminase and imino nitrogen oxidation to nitrite. *Science* **235**, 473-476.

Hibbs, J.B., Jr., Taintor, R.R., Vavrin, Z., and Rachlin, E.M. (1989) Nitric oxide: a cytotoxic activated macrophage effector molecule. *Biochem. Biophys. Res. Commun.* **157**, 87-94.

Hill, B.G., Dranka, B.P., Bailey, S.M., Lancaster Jr., J.R. & Darley-Usmar, V.M. (2010) What Part of NO Don't You Understand? Some Answers to the Cardinal Questions in Nitric Oxide Biology. *J. Biol. Chem.* **285**, 19699-19704.

Hou, Y., Guo, Z., Li, J., & Wang, P.G. (1996) Seleno compounds and glutathione peroxidase catalyzed decomposition of S-nitrosothiols. *Biochem. Biophys. Res. Commun*. **228**, 88-93.

Houk, K. N., Hietbrink, B. N., Bartberger, M. D., McCarren, P. R., Choi, B. Y., Voyksner, R. D., Stamler, J. S., and Toone, E. J. (2003) Nitroxyl disulfides, novel intermediates in transnitrosation reactions. *J. Am Chem Soc* **125**, 6972-6976.

Ignarro LJ, Buga GM, Wood KS, Byrns RE, Chaudhuri G. (1987) Endothelium-derived relaxing factor produced and released from artery and vein is nitric oxide. *Proc Natl Acad Sci USA* **84**, 9265-9269.

Ignarro, L.J., Byrns, R.E., Buga, G.M. & Wood, K.S. (1987b). Endothelium-derived relaxing factor from pulmonary artery and vein possesses pharmacologic and chemical properties identical to those of nitric oxide radical. *Circ Res* **61**, 866-79.

Ip, YT & Davis, RJ. (1998) Signal transduction by the c-Jun N-terminal kinase (JNK) – from inflammation to development. *Curr Opin Cell Biol.* **10**(2), 205-19.

Ishitani, R., Tanaka, M., Sunaga, K., Katsube, N. & Chuang, D.M. (1998) Nuclear localization of overexpressed glyceraldehyde-3-phosphate dehydrogenase in cultured cerebellar neurons undergoing apoptosis. *Mol. Pharmacol.* **53**, 701-707.

Iyengar, R., Stuehr, D.J., & Marletta, M.A. (1987) Macrophage synthesis of nitrite, nitrate, and N-nitrosoamines: precursors and role of the respiratory burst. *Proc Natl Acad Sci USA* **84**, 6369-73.

Jaffrey SR, Erdjument-Bromage H, Ferris CD, Tempst P, Snyder SH (2001) Protein S-nitrosylation: A physiological signal for neuronal nitric oxide. *Nat Cell Biol* **3**, 193–197.

Jao, S-C., Ospina, S.M.E., Berdis, A.J., Starke, D.W., Post, C.B., and Mieyal, J.J. (2006) Computational and Mutational Analysis of Human Glutaredoxin (Thioltransferase): Probing the molecular basis of the Low pK_a of Cysteine 22 and Its Role in Catalysis. *Biochemistry* **45**, 4785-4796.

Jia, L., Bonaventura, C., and Stamler, J. S. (1996) S-nitrosohaemoglobin: a dynamic activity of blood involved in vascular control. *Nature* **380**, 221-226.

Jiang, Z.Y., Zhou, Q.L., Colemna, K.A., Chouinard, M., Boese, Q., and Czech, M.P. (2003) Insulin signaling through Akt/protein kinase B analyzed by small interfering RNA-mediated gene silencing. *Proc Natl Acad Sci USA* **100**, 7569-7574.

Jourd'heuil, D., Laroux, F.S., Miles, A.M., Wink, D.A., & Grisham, M.B. (1999) Effect of superoxide dismutase on the stability of S-nitrosothiols. *Arch. Biochem. Biophys.* **361**, 323-330.

Johnson, M.A., Macdonald, T.L., Mannick, J.B., Conaway, M.R., & Gaston, B. (2001) Accelerated S-nitrosothiol breakdown by amyotrophic lateral sclerosis mutant copper, zinc-superoxide dismutase. *J. Biol. Chem.* **276**, 39872-39878.

Kabuyama, Y., Suzuki, T., Nakazawa, N., Yamaki, J., Homma, M.K., & Homma, Y. (2010) Dysregulation of very long chain acyl-CoA dehydrogenase coupled with lipid peroxidation. *Am J Physiol Cell Physiol* **298**, 107-113.

Katsuki, S., Arnold, W., Mittal, C., Murad, F. (1977) Stimulation of guanylate cyclase by sodium nitroprusside, nitroglycerin, and nitric oxide in various tissue preparations and comparison to the effects of sodium azide and hydroxylamine. *J. Cyclic Nucleotide Res.* **3**, 23-35.

Kendrew, J.C., Bodo, G., Dintzis, H.M., et al. (1958) A three-dimensional model of the myoglobin molecule obtained by X-ray analysis. *Nature* **181**, 662-6.

Kharitonov, V.G., Sundquist, A.R. & Sharma, V.S. (1995) Kinetics of nitrosation of thiols by nitric oxide in the presence of oxygen. *J. Biol. Chem.* **270**, 28158-28164.

Kim, S. O., Merchant, K., Nudelman, R., Beyer Jr., W. F., Keng, T., DeAngelo, J., Hausladen, A., and Stamler, J. S. (2002) OxyR: A Molecular Code for Redox-Related Signaling, Cell 109, 383-396.

Kim, Y.J., Pannell, L.K., Sackett, D.L. (2004) Mass spectrometric measurement of differential reactivity of cysteine to localize protein-ligand binding sites. Application to tubulin-binding drugs. *Anal Biochem* **332**, 376–83.

Kinsella, JP, Abman SH. (2007) Inhaled nitric oxide in the premature newborn. *J. Pediatrics* **151**, 10-15.

Knipp, M., Braun, O., et al. (2003) Zn(II)-free dimethylarginase-1 (DDAH-1) is inhibited upon specific Cys-S-nitrosylation. *J. Biol. Chem.* **278**, 3410-3416

Kohr, M. J., Aponte, A. M., Sun, J., Wang, G., Murphy, E., Gucek, M., and Steenbergen, C. (2011) Characterization of potential S-nitrosylation sites in the myocardium. *Am J Phys* **300**, H1327-35.

Koppenol, W. H. (2001) 100 years of peroxynitrite chemistry and 11 years of peroxynitrite biochemistry. *Redox Rep.* **6**, 339–341.

Kornberg, M.D., Sen, N., Hara, M.R., et al. (2010) GAPDH mediates nitrosylation of nuclear proteins. *Nat Cell Biol* **12**(11), 1094-1100.

Krissinel E, Henrick K (2007) Inference of macromolecular assemblies from crystalline state. *J Mol Biol* **372**, 774–797.

Lam, Y. W., Yuan, Y., Isaac, J., Babu, C. V. S., Meller, J., and Ho, S.-M. (2010) Comprehensive identification and modified-site mapping of S-nitrosylated targets in prostate epithelial cells. *PloS One* **5**, e9075.

Lander, H. M., Hajjar, D. P., Hempstead, B. L., Mirza, U. a, Chait, B. T., Campbell, S., and Quilliam, L. a. (1997) A molecular redox switch on p21(ras). Structural basis for the nitric oxide-p21(ras) interaction. *J. Biol Chem* **272**, 4323-6.

Lee B, Richards FM (1971) The interpretation of protein structures: Estimation of static accessibility. *J Mol Biol* **55**, 379–400.

Lee, T.-Y., Chen, Y.-J., Lu, T.-C., Huang, H.-D., and Chen, Y.-J. (2011) SNOSite: Exploiting Maximal Dependence Decomposition to Identify Cysteine S-Nitrosylation with Substrate Site Specificity. *PLoS ONE* **6**, e21849.

Lei, SZ, Pan, ZH, Aggarwal, SK, Chen, HS, Hartman, J, Sucher, NJ, & Lipton, SA. (1992) Effect of nitric oxide production on the redox modulatory site of the NMDA receptor-channel complex. *Neuron* **8**, 1087-99.

Lepoivre, M., Fieschi, F., Coves, J., Thelander, L., and Fonrecave, M. (1991) Inactivation of ribonucleotide reductase by nitric oxide. *Biochem. Biophys. Res. Commun*. **179**, 442-448.

Li H, Robertson AD, Jensen JH (2005) Very fast empirical prediction and rationalization of protein pKa values. *Proteins* **61**, 704–721.

Liu, M., Hou, J., Huang, L., Huang, X., Heibeck, T. H., Zhao, R., Pasa-Tolic, L., Smith, R. D., Li, Y., Fu, K., Zhang, Z., Hinrichs, S. H., and Ding, S.-J. (2010) Site-specific proteomics approach for study protein S-nitrosylation. *Anal. Chem.* **82**, 7160-8.

Liu, X., Miller, M.J., Joshi, M.S., Thomas, D.D., & Lancaster Jr., J.R. (1998) Accelerated reaction of nitric oxide with O_2 within the hydrophobic interior of biological membranes. *Proc Natl Acad Sci USA* **95**, 2175-9.

López-Sánchez LM, et al. (2008) Alteration of S-nitrosothiol homeostasis and targets for protein S-nitrosation in human hepatocytes. *Proteomics* **8**, 4709–4720.

MackMicking, J.D., Nathan, C., Hom, G., Chartrain, N., Fletcher, D.S., Trumbauer, M., Stevens, K., Xie, Q-W., Sokoi, K., Hutchinson, N., Chen, H., & Mudgett, J.S. (1995). Altered responses to bacterial infection and endotoxic shock in mice lacking inducible nitric oxide synthase. *Cell* **81**, 641-50.

Mannick, J.B., Hausladen, A., Liu, L., Hess, D.T., Zeng, M., Miao, QX, Kane, L.S., Gow, A.J., & Stamler, J.S. (1999) Fas-induced caspase denitrosylation. *Science* **284**, 651-654.

Marino, S.M., & Gladyshev, V.N. (2010) Structural analysis of cysteine S-nitrosylation: a modified acid-based motif and the emerging role of trans-nitrosylation. *J. Mol. Biol*. **395**, 844-859.

Marino, S.M. & Gladyshev, V.N. (2009). A Structure-Based Approach for Detection of Thiol Oxidoreductases and Their Catalytic Redox-Active Cysteine Residues. *PLoS Comp. Biol*. **5**, 1-13.

Marcineck, D.J., Bonaventura, J., Wittenberg, J.B., & Block, B.A. (2001) Oxygen affinity and amino acid sequence of myoglobins from endothermic and ectothermic fish. *Am. J. Physiol*. **280** (4), R1123-R1133.

Marletta, MA, Yoon PS, Iyengar R, et al. (1988) Macrophage oxidation of L-arginine to nitrite and nitrate: nitric oxide is an intermediate. *Biochemistry* **27**, 8706-11.

Marletta, M.A., Yoon, P.S., Iyengar, R., Leaf, C.D., and Wishnok, J.S. (1988) Macrophage oxidation of L-arginine to nitrite and nitrate: nitric oxide in an intermediate. *Biochemistry* **21**, 8706-8711.

Maseri, A. (1991) Coronary vasoconstriction: visible and invisible. *N. Engl J Med* **325**, 1579-1580.

Matthews JR., Botting CH, Panico M, Morris HR, Hay RT. (1996) Inhibition of NF-kappaB DNA binding by nitric oxide. *Nucleic Acids Res*, **24**(12), 2236-42.

McAndrew, R.P., Wang, Y., Mohsen, A.-W., He, M., Vockley, J. & Kim, J.-J. (2008) Structural basis for substrate fatty acyl chain specificity: crystal structure of human very-long-chain acyl-coA dehydrogenase. *J. Biol. Chem.*, **283**(14), 9435-9443.

Mcdonagh, J., Waggoner, W.G., Hamilton, E.G., Hindenbach, B. & Mcdonagh, R.P. (1976)
Affinity chromatography of human plasma and platelet factor XIII on organomercurial agarose. *Biochim Biophys Acta* **446**, 345–357.

Medina I, Carbonell J, Pulido L, Madeira S, Goetz S, Conesa A, Tárraga J, Pascual-Montano A, Nogales-Cadenas R, Santoyo J, García F, Marbà M, Montaner D and Dopazo J (2010). Babelomics: an integrative platform for the analysis of transcriptomics, proteomics and genomic data with advanced functional profiling. *Nucleic Acids Res* **38**, W210-3.

Mitchell, D. a, Morton, S. U., Fernhoff, N. B., and Marletta, M. A. (2007) Thioredoxin is required for S-nitrosation of procaspase-3 and the inhibition of apoptosis in Jurkat cells. *Proc Natl Acad Sci USA* **104**, 11609-14.

Mitchell, H.H., Shonle, H.A. & Grindley, H.S. (1916). The origin of the nitrates in the urine. *J Biol Chem* **24**, 461-90.

Mitchell, D.A. & Marletta, M.A. (2005) Thioredoxin catalyzes the S-nitrosation of the caspase-3 active site cysteine. *Nat Chem Biol* **1**(3), 154-158.

Mitchell DA, Morton SU, Fernhoff NB, Marletta MA (2007) Thioredoxin is required for S-nitrosation of procaspase-3 and the inhibition of apoptosis in Jurkat cells. *Proc Natl Acad Sci* USA **104**, 11609–11614.

Mohan S, Reddick, R.L., Musi, N., Horn, D.A., Yan, B., Prihoda, T.J., Natarajan, M., Abboud-Werner, S.L. (2008) Diabetic eNOS knockout mice develop distinct macro- and microvascular complications. *Lab Invest* **88**, 515–528.

Moller, M.N., Li, Q., Vitturi, D.A., Robinson, J.M., Lancaster Jr., J.R., & Denicola, A. (2007) Membrane "lens" effect: focusing the formation of reactive nitrogen oxides from the *NO/O2 reaction. *Chem. Res. Toxicol.* **20**, 709-714.

Moller, MN, Li, Q., Lancaser JR, Jr., Denicola, A. (2007) Acceleration of nitric oxide autoxidation and nitrosation by membranes. *IUBMB Life* **59**, 243-248.

Moncada, S., Palmer, R.M., Higgs, E.A. (1988) The discovery of nitric oxide as the endogenous nitrovasodilator. *Hypertension* **12**, 365-372.

Mugge, A., Forestermann, U., Lichtlen, PR. (1991) Platelets, endothelium-dependent responses and atherosclerosis. *Ann Med* **23**, 545-550.

Murad, F., Mittal, C.K., Arnold, W.P., Katsuki, S., & Kimura, H. (1978) Guanylate cyclase: activation by azide, nitro compounds, nitric oxide, and hydroxyl radical and inhibition by hemoglobin and myoglobin. *Adv Cycl Nucl Res* **9**, 145-58.

Nakane, M., Schmidt, H.H.H.W., Pollock, J.S., Fostermann, U., & Murad, F. (1993) Cloned human brain nitric oxide synthase is highly expressed in skeletal muscle. *FEBS Lett.* **316**, 175-180.

Naor, MM, & Jan H. Jensen. (2004) Determinants of cysteine pKa values in creatine kinase and alpha 1antitrypsin. *Proteins* **57**(4), 799-803.

Nathan, C. (1992) Nitric oxide as a secretory product of mammalian cells. *FASEB* **6**, 3051-3064.

Nedospasov, A., Rafikov, R., Beda, N. et al. (2000) An autocatalytic mechanism of protein nitrosylation. *Proc Nat. Acad Sci USA* **97**, 13543-13548.

Nguyen, T; Brunson D, Crespi CL, Penman BW, Wishnok JS, Tannenbaum SR (1992) DNA damage and mutation in human cells exposed to nitric oxide in vitro. *Proc Natl Acad Sci USA* **89** (7), 3030–4.

Nikitovic, D., & Holmgren, A. (1996) S-nitrosoglutathione is cleaved by the thioredoxin system with liberation of glutathione and redox regulating nitric oxide. *J Biol Chem* **271**, 19180-19185.

Nisoli E, et al. (2004) Mitochondrial biogenesis by NO yields functionally active mitochondria in mammals. *Proc Natl Acad Sci USA* **101**, 16507–16512.

Nogales E, Whittaker M, Milligan RA, Downing KH (1999) High-resolution model of the microtubule. *Cell* **96**, 79–88.

Nott, A., Watson, P.M., Robinson, JD, Crepaldi, L., & Riccio, A. (2008) S-nitrosylation of histone deacetylase 2 induces chromatin remodelling in neurons. *Nature* **455**(18), 411-6.

O'Donnell VB, Chumley PH, Hogg N, Bloodsworth A, Darley-Usmar VM, Freeman BA. (1999) Nitric oxide inhibition of lipid peroxidation: kinetics of reaction with lipid peroxyl radicals and comparison with a-tocopherol. *Biochemistry* **36**, 15216 –15223.

Olsen, J.V., Blagoev, B., Gnad, F., Macek, B., Kumar, C., Mortensen, P., Mann, M. (2006) Global, in vivo, and site-specific phosphorylation dynamics in signaling networks. *Cell* **127**, 635–648.

Pacher, P., Beckman, J. S., and Liaudet, L. (2007) Nitric oxide and peroxynitrite in health and disease. *Physiol. Rev.* **87**, 315–424

Paige, J.S., Xu, G., Stancevic, B., & Jaffrey, S.R. (2008). Nitrosothiol Reactivity Profiling Identifies S-nitrosylated Proteins with Unexpected Stability. *Chemistry & Biology* **15**, 1307-1316.

Palmer, R.M.J., Ferrige, A.G. & Moncada, S. (1987). Nitric oxide release accounts for the biological activity of endothelium-derived relaxing factor. *Nature*, **327**, 524-6.

Palmer, R.M.J., Ashton, D.S., & Moncada, S. (1988) Vascular endothelial cells synthesize nitric oxide from L-arginine. *Nature* **333**, 664-6.

Park, H.S., Huh, S.H., Kim, M.S., et al. (2000) Nitric oxide negatively regulates c-Jun N-terminal kinase/stress-activated protein kinase by means of S-nitrosylation. *Proc. Natl Acad. Sci. USA* **97**, 14382-14387.

Pelleymounter M.A., Cullen, M.J., Baker, M.B., Hecht, R., Winters, D., Boone, T., Collins, F. (1995) Effects of the obese gene product on body weight regulation in ob/ob mice. *Science* **269**, 540–543.

Perez-Mato, I., Castro, C., Ruiz, F.A., Corrales, F.J., Mato, J.M. (1999) Methionine Adenosyltransferase S-nitrosylation is regulated by the basic and acidic amino acids surrounding the target thiol. *J. Biol. Chem.* **274**(24), 17075-17079.

Pesavento JJ, Garcia BA, Streeky JA, Kelleher NL, Mizzen CA (2007) Mild performic acid oxidation enhances chromatographic and top down mass spectrometric analyses of histones. *Mol Cell Proteomics* **6**, 1510–1526.

Petersen, M.T.N., Jonson, P.H., & Petersen, S.B. (1999) Amino acid neighbours and detailed conformational analysis of cysteines in proteins. *Protein Engineering* **12**(7):535-548.

Petros, A, Bennet, D., Vallance, P. (1991) Effect of nitric oxide synthase inhibitors on hypotension in patients with septic shock. *Lancet* **338**, 1557-8.

Rahman, M.A., Senga, T., Ito, S., Hyodo, T., Hasegawa, H., & Hamaguchi, M. (2010) S-nitrosylation at Cysteine 498 of c-Src Tyrosine Kinase regulates nitric oxide-mediated cell invasion. *J. Biol. Chem.* **285**(6), 3806-3814.

Rayner, B.S., Wu, B.J., Raferty, M., et al. (2005) Human S-nitroso oxymyoglobin is a store of vasoactive nitric oxide. *J. Biol. Chem.* **280**(11), 9985-93.

Reif, D.W., and Simmons, R.D. (1990) Nitric oxide mediates iron release from ferritin. *Arch. Biochem. Biophys.* **283**, 537-541.

Reynaert, N.L., Ckless, K., Korn, S.H. et al. (2004) Nitric oxide represses inhibitory KB kinase through S-nitrosylation. *Proc. Natl Acad. Sci. USA* **101**(24), 8945-8950.

Rigsby, R. E., Brown, D. W., Dawson, E., Lybrand, T. P., and Armstrong, R. N. (2007) A model for glutathione binding and activation in the fosfomycin resistance protein, FosA. *Arch Biochem Biophys* **464**, 277-83.

Rizzo MA, Piston DW (2003) Regulation of beta cell glucokinase by S-nitrosylation and association with nitric oxide synthase. *J Cell Biol* **161**, 243–248.

Romero, J.M. & Bizzozero, O.A. (2009). Intracellular glutathione mediates the denitrosylation of protein nitrosothiols in the rat spinal cord. *J. Neur. Res.* **87**, 701-709.

Rosenfeld, R.J. et al. (2010) Nitric-oxide Synthase Forms N-NO-pterin and S-NO-Cys. *J. Biol. Chem.* **285**(41), 31581–31589.

Roychowdhury M, Sarkar N, Manna T, Bhattacharyya S, Sarkar T, Basusarkar P, Roy S,Bhattacharyya B. (2000) Sulfhydryls of tubulin. A probe to detect conformational changes of tubulin. *Eur J Biochem* **267**, 3469–76.

Rubanyi, G.M. (1993) The role of the endothelium in cardiovascular homeostasis and disease. *J Card Pharm* **22**(Suppl 4), S1-14.

Salter, M., Knowles, R.G. and Moncada, S. (1991) Widespread tissue distribution, species distribution and changes in activity of Ca(2+)-dependent and Ca(2+)-independent nitric oxide synthases. *FEBS Lett.* **291**, 145-149.

Sanchez R, Riddle M, Woo J, Momand J (2008) Prediction of reversibly oxidized protein cysteine thiols using protein structure properties. *Protein Sci* **17**, 473–481.

Saville B (1958) A scheme for the colorimetric determination of microgram amounts of thiols. *Analyst (Lond)* **83**, 670–672.

Sawa, A., Khan, A.A., Hester, L.D. & Snyder, S.H. (1997) Glyceraldehyde—phosphate dehydrogenase: nuclear translocation participates in neuronal and nonneuronal cell death. *Proc. Natl Acad. Sci. USA* **94**, 11669-11674.

Schild L, Dombrowski, F., Lendeckel, U., Schulz, C., Gardemann, A., Keilhoff, G. (2008) Impairment of endothelial nitric oxide synthase causes abnormal fat and glycogen deposition in liver. *Biochim Biophys Acta* **1782**, 180–187.

Schwartz D, Gygi SP (2005) An iterative statistical approach to the identification of protein phosphorylation motifs from large-scale data sets. *Nat Biotechnol* **23**, 1391–1398.

Schreiter, E. R., Rodríguez, M. M., Weichsel, A., Montfort, W. R., and Bonaventura, J. (2007) S-nitrosylation-induced conformational change in blackfin tuna myoglobin. *J Biol Chem.* **282**, 19773-80.

Sen, N., Hara, M.R., Kornberg, M.D., et al. (2008) Nitric oxide-induced nuclear GAPDH activates p300/CBP and mediates apoptosis. *Nat Cell Biol* **10**(7), 866-873.

Sen, N., Hara, M.R., Ahmad, A.S. et al. (2009) GOSPEL: A neuroprotective protein that binds to GAPDH upon S-nitrosylation. *Neuron* **63**, 81-91.

Sengupta, R., Ryter, S.W., Zuckerbraun, B.S., et al. (2007) Thioredoxin catalyzes the denitrosation of low-molecular mass and protein S-nitrosothiols. *Biochemistry* **46**, 8472-8483.

Shi, H.P., Efron, D.T., Most, D., Tantry, U.S., Barbul, A. (2000) Supplemental dietary arginine enhances wound healing in normal but not inducible nitric oxide synthase knockout mice. *Surgery* **128**, 374-378.

Singh A, et al. (2009) Leptin-mediated changes in hepatic mitochondrial metabolism, structure, and protein levels. *Proc Natl Acad Sci USA* **106**,13100–13105.

Sliskovic, I., Raturi, A., & Mutus, B. (2005) Characterization of the S-denitrosation activity of protein disulfide isomerase. *J. Biol. Chem*. **280**, 8733-8741.

Souri, M., Aoyama, T., Yamaguchi, S., & Hashimoto, T. (1998a) Relationship between structure and substrate-chain-length specificity of mitochondrial very-long-chain acyl-coenzyme A dehydrogenase. *Eur J. Biochem*. **257**, 592-598.

Souri, M., Aoyama, T., Hoganson, G., & Hashimoto, T. (1998b) Very-long-chain acyl-CoA dehydrogenase subunit assembles to the dimer form on mitochondrial inner membrane. *FEBS Letters* **426**, 187-190.

Staab, C.A., Hartmanova, T., et al. (2011) Studies on reduction of S-nitrosoglutathione by human carbonyl reductases 1 and 3. *Chem-Biol Int* **191** (1-3), 95-103.

Stamler, J. S. (1994) Redox signaling: Nitrosylation and related target interactions of nitric oxide, *Cell* **78**, 931-936.

Stamler, J. S., Toone, E. J., Lipton, S. A., and Sucher, N. J. (1997) (S)NO Signals: Translocation, Regulation, and a Consensus Motif. *Neuron* **18**, 691-696.

Stamler, J. S., Jia, L., Eu, J. P., McMahon, T. J., Demchenko, I. T., Bonaventura, J., Gernert, K., and Piantadosi, C. A. (1997) Blood flow regulation by S-nitrosohemoglobin in the physiological oxygen gradient. *Science* **276**, 2034-7.

Stamler, J.S., Simon, D.I., Osborne, J.A., Mullins, M.E., Jaraki, O., Michel, T., Singel, D.J., Loscalzo, J. (1992) S-nitrosylation of proteins with nitric oxide: synthesis and characterization of biologically active compounds. *Proc. Natl Acad. Sci. USA* **89**, 444-448.

Stamler, JS, Jaraki, O., Osborne, J., Simon, D.I., Keaney, J., Vita JXSD, Valeri C.R., Loscalzo, J. (1992). Nitric oxide circulates in mammalian plasma primarily as an S-nitroso adduct of serum albumin. *Proc. Natl Acad. Sci. USA* **89**, 7674-7677.

Stamler JS, Toone EJ, Lipton SA, et al. (1997) (S)NO signals: translocation, regulation, and a consensus motif. *Neuron* **18**(5), 691-9.

Star, R.A. (1993) Southwestern Internal Medicine Conference: Nitric Oxide. *Am J Med Sci*, **306**(5).

Stoyanovsky, DA, Tyurina, YY, Tuyurin, VA, Anand, D., Mandavia, D.N., Gius, D., Ivanova, J., Pitt, B., Billiar, T.R., and Kaga, V.E. (2005) Thioredoxin and lipoic acid

catalyze the denitrosation of low molecular weight and protein S-nitrosothiols. *J. Am. Chem. Soc.* **127**, 15815-15823.

Stuehr, D.J. & Marletta, M.A. (1985). Mammalian nitrate biosynthesis: mouse macrophages produce nitrite and nitrate in response to Escherichia coli lipopolysaccharide. *Proc. Natl Acad. Sci. USA* **82**, 7738-42.

Stuehr, D.J. and Nathan, C.F. (1989) Nitric oxide: a macrophage product responsible for cytostasis and respiratory inhibition in tumor target cells. *J. Exp. Med*. **169**, 1543-1545.

Sun, J., Xin, C., Eu, J.P., Stamler, J.S., & Meissner, G. (2001) Cysteine-3635 is responsible for skeletal muscle ryanodine receptor modulation by NO. *Proc. Natl Acad. Sci. USA* **98**(20), 11158-62.

Sun, J., Xu, L., Eu, J.P., Stamler, J.S., & Meissner, G. (2003) Nitric Oxide, NOC-12, and S-Nitrosoglutathione Modulate the Skeletal Muscle Calcium Release Channel/Ryanodine Receptor by Different Mechanisms. *J Biol Chem* **278**(10):8184-8189.

Tannenbaum, S.R., Fett, D., Young, V.R., Land, P.D., & Bruce, W.R. (1978). Nitrite and nitrate are formed by endogenous synthesis in the human intestine. *Science* **200**, 1487-9.

Tao, L. & English, AM. (2004) Protein S-glutathionylation triggered by decomposed S-nitrosoglutathione. *Biochemistry* **43**(13):4028-38.

Thiermermann, C., Szabo, C., Mitchell, J.A., Vane, J.R. (1993) Vascular hyporeactivity to vasoconstrictor agents and hemodynamic decompensation in hemorrhagic shock is mediated by nitric oxide. *Proc. Natl Acad. Sci. USA* **90**, 267-271.

Thibeault, S., Rautureau, Y., Oubaha M., Faubert, D., Wilkes B.C., Delisle, C. & Gratton, J-P. (2010). S-nitrosylation of β-Catenin by eNOS-Derived NO Promotes VEGF-Induced Endothelial Cell Permeability. *Mol. Cell* **39**, 468-476.

Thomas, J.A., Poland, B., & Honzatko, R. (1995) Protein Sulfhydryls and Their Role in the Antioxidant Function of Protein S-Thiolation. *Arch Biochem Biophys* **319**(1),1-9.

Thomas, D. D., Liu, X., Kantrow, S. P., and Lancaster, J. R., Jr. (2001) The biological lifetime of nitric oxide: implications for the perivascular dynamics of NO and O2. *Proc. Natl. Acad. Sci. U.S.A.* **98**, 355–360.

Timerghazin, Q.K., Peslherbe, G.H. & English, A.M. (2007). Resonance Description of S-Nitrosothiols: Insights into Reactivity. *Organic Letters* **9**, 3049-3052.

Torta, F., Elviri, A., & Bachi, A. (2010) Direct and indirect detection methods for the analysis of S-nitrosylated peptides and proteins. *Methods Enzymol.* **473**, 265-280.

Trujillo, M., Alvarez, M.N., Peluffo, G., Freeman, B.A. & Radi, R. (1998) Xanthine oxidase-mediated decomposition of S-nitrosothiols. *J. Biol. Chem.* **273**, 7828-7834.

Tullett, J.M., Rees, D.D., Shuker, D.E.G. et al. (2001) Lack of correlation between the observed stability and pharmacological properties of S-nitroso derivatives of glutathione and cysteine-related peptides. *Biochem Pharm* **62**, 1239-1247.

Tummala, M., Ryzhov, V., et al. (2008) Identification of the cysteine nitrosylation sites in human endothelial nitric oxide synthase. *DNA and Cell Biology* **27** (1), 25-33.

Venema, R.C., Sayegh, H.S., Kent, J.D., et al. (1996) Identification, characterization, and comparison of the calmodulin-binding domains of the endothelial and inducible nitric oxide synthases. *J. Biol. Chem.* **271**, 6435-40.

Villén J, Gygi SP (2008) The SCX/IMAC enrichment approach for global phosphorylation analysis by mass spectrometry. *Nat Protoc* **3**, 1630–1638.

Wade, R. & Castro, C. (1990) Redox reactivity of iron(III) porphyrins and heme proteins with nitric oxide. Nitrosyl transfer to carbon, oxygen, nitrogen, & sulfur. *Chem. Res. Toxicol.* **3**(4), 289-29.

Wang, Y., Liu, T., Wu, C., & Li, H. (2008) A strategy for direct identification of protein S-nitrosylation sites by quadrupole time-of-flight mass spectrometry. *J. Am. Soc. Mass Spectrom.* **19**, 1353-1360.

Wang, Q., Canutescu, AA, Dunbrack, Jr., RL. (2008) SCWRL and MOlIDE: computer programs for side-chain conformation prediction and homology modeling. *Nature Protocols* **3**(12), 1832-1847.

Watson, W.H., Pohl, J., Montfort, W.R., Stuchlik, O., Reed, M.S., Powis, G., & Jones, D.P. (2003) Redox potential of human thioredoxin 1 and identification of a second dithiol/disulfide motif. *J. Biol. Chem.* **278**, 33408-33415.

Wei, X., Charles, I.G., Smith, A., Ure, J., Feng, G., Huang, F., Xu, D., Muller, W., Moncada, S., & Liew, F.Y. (1995). Altered immune responses in mice lacking inducible nitric oxide synthase. *Nature* **375**, 408-11.

Weichsel, A., Brailey, J.L., & Montfort, W.R. (2007) Buried S-Nitrosocysteine revealed in crystal structures of human thioredoxin. *Biochemistry* **46** (5), 1219-1227.

Weichsel A, et al. (2005) Heme-assisted S-nitrosation of a proximal thiolate in a nitric oxide transport protein. *Proc Natl Acad Sci USA* **102,** 594–599.

Weischel, A., Gasdaska, J.R., Powis, G., & Montfort, W.R. (1996) Crystal structures of reduced, oxidized, and mutated human thioredoxins: Evidence for a regulatory homodimer. *Structure* **4**, 735-751.

Whalen EJ, et al. (2007) Regulation of beta-adrenergic receptor signaling by S-nitrosylation of G-protein-coupled receptor kinase 2. *Cell* **129**, 511–522.

Wink, D.A., Nims, R.W., Darbyshire, J.F., Christodolou, D., Hanbauer, I., Cox, G.W., et al. (1994) Reaction kinetics for nitrosation of cysteine and glutathione in aerobic nitric oxide solutions at neutral pH. Insights into the fate and physiological effects of intermediates generated in the NO/O2 reaction. *Chem Res Toxicol*. **7**, 519-525.

Wink, DA; et.al. (1991). DNA deaminating ability and genotoxicity of nitric oxide and its progenitors. *Science* **254** (5034), 1001–3.

Witting, P.K., Douglas, D.J., and Mauk, A.G. (2001) Reaction of human myoglobin and nitric oxide. Heme iron or protein sulfhydryl (s) nitrosation dependence on the absence or presence of oxygen. *J. Biol. Chem*. **276** (6), 3991-8.

Xie, Q-W., et al. (1992) Cloning and characterization of inducible nitric oxide synthase from mouse macrophages. *Science* **256**, 225-228.

Xue, Y., Liu, Z., Gao, X., Jin, C., Wen, L., Yao, X., and Ren, J. (2010) GPS-SNO: computational prediction of protein S-nitrosylation sites with a modified GPS algorithm. *PloS One* **5**, e11290.

Yao, D. et al. (2004) Nitrosative stress linked to sporadic Parkinson's disease: S-nitrosylation of Parkin regulates its E3 ubiquitin ligase activity. *Proc Natl Acad Sci USA* **101**, 10810-10814.

Yasukawa, T., Tokunaga, E.,et al. (2005) S-nitrosylation-dependent inactivation of Akt/Protein Kinase B in Insulin resistance. *J Biol Chem* **280** (9), 7511-7518.

Zhang, Y., Keszler, A., Broniowska, K.A., & Hogg, N. (2005) Characterization and application of the biotin-switch assay for the identification of S-nitrosated proteins. *Free Radic. Biol. Med.* **38**, 874-881.

Zhang, J., Li, S., Zhang, D., Wang, H., Whorton, A.R., Xian, M. (2010) Reductive ligation mediated one-step disulfide formation of S-nitrosothiols. *Org. Lett.* **12**, 4208-4211.

Zhang Y, Hogg N (2005) S-Nitrosothiols: Cellular formation and transport. *Free Radic Biol Med* **38**, 831–838.